University of Nevada, Reno

Design, Modeling, and Testing of Microstrip Patch Antenna Arrays for Vertical Takeoff & Landing Aircraft

A thesis submitted in partial fulfillment of the requirements for the degree of Master of Science in Electrical Engineering

By

Stephanie A. Luongo

Dr. Indira Chatterjee/Thesis Advisor

December 2009

THE GRADUATE SCHOOL

We recommend that the thesis
prepared under our supervision by

STEPHANIE A. LUONGO

entitled

Design, Modeling, and Testing Of Microstrip Patch Antenna Arrays for Vertical Takeoff & Landing Aircraft

be accepted in partial fulfillment of the
requirements for the degree of

MASTER OF SCIENCE

Indira Chatterjee, PhD., Advisor

Roy Adams, Committee Member

Pete Mastin, PhD., Committee Member

Jim Henson, PhD., Committee Member

Dave Bennum, PhD., Grad School Representative

Marsha H. Read, PhD., Associate Dean, Graduate School

December, 2009

ABSTRACT

A major shortcoming of aircraft antennas for autonomous landing systems is the acquisition and tracking errors resulting because of the illumination of the airframe components by the 360° azimuth beamwidth of a low gain omni-directional antenna. Also, existing low and high gain antennas currently found in the marketplace are both expensive and time-consuming to manufacture.

The purpose of this thesis is twofold: to develop a low gain omni-directional antenna that radiates only in the forward direction and to develop a high gain antenna that is less expensive compared to antennas currently found in landing systems. Microstrip patch antenna arrays are selected due to their light weight and low cost.

The design, numerical modeling, and experimental characterization of two types of microstrip patch antenna arrays are described. CST's Microwave Studio, a three-dimensional electromagnetic simulator, is used to model, simulate, and optimize the performance of the antennas. The antennas have been fabricated and the return loss and radiation patterns were measured. Return loss comparisons between the simulated and measured antennas show a difference of nearly 500 MHz in the resonance frequency for both the low and high gain arrays. Simulated and measured peak directivities differ by as much as 1.7 dB. These differences between the simulated and measured results are believed to be caused by manufacturing tolerance uncertainties as well as by some design details that were intentionally not accounted for in the modeled antennas.

ACKNOWLEDGEMENTS

I would like to thank Dr. Indira Chatterjee for being an excellent advisor for the last four years. She showed patience and understanding while I worked full-time, yet she was still able to tactfully keep my progress moving along. Her edits and suggestions have significantly improved the quality of this thesis. I would also like to thank Roy Adams, Dr. Pete Mastin, Dr. Jim Henson, and Dr. Dave Bennum for serving on my thesis committee.

My mother, Gloria, and aunt, Barbara, also deserve thanks for their love and support and for their astounding efforts at the "Proofreading Party" which kept me motivated and focused. I am grateful for their patience while I worked every weekend and had to neglect many of my daughter/niece responsibilities. I would also like to thank T.J. Dobson for his timely assistance with the antenna mounting fixture.

TABLE OF CONTENTS

ABSTRACT i

ACKNOWLEDGEMENTS ii

TABLE OF CONTENTS iii

1 INTRODUCTION 1

1.1 System Description 1

1.2 Background Information 1

1.2.1 Microstrip Patch Antenna Theory of Operation 3

1.3 Design Criteria 5

1.3.1 Size 5

1.3.2 Complexity of High Volume Production 5

1.3.3 Low Gain Antenna Beam Pattern and Directivity 5

1.3.4 High Gain Antenna Beam Pattern and Directivity 6

1.3.5 Voltage Standing Wave Ratio (VSWR) 6

1.4 Thesis Overview 7

1.5 References 7

2 DESIGN AND MODELING OF A TWO-ELEMENT MICROSTRIP PATCH ARRAY 8

2.1 Introduction 8

2.2 Methodology 8

2.2.1 Antenna Desired Performance 8

2.2.2 Substrate Selection 9

2.2.3 Resonant Microstrip Patch Design 10

2.2.3.1 Coordinate System 15

2.2.3.2 Pattern Calculation of a Single Patch Antenna 16
2.2.3.3 Directivity of a Single Patch Antenna 17
2.2.3.4 Feed Design 18
2.2.3.5 Input Impedance of a Single Patch Antenna 19
2.2.4 Modeling a Single Patch Antenna 19
2.2.4.1 Simulation Parameters 20
2.2.4.2 Model Iterations 23
2.2.5 Two-element Array Design 30
2.2.5.1 Initial Designs – Corporate Feed Network 32
2.2.5.2 Design Change to a Series-Fed Array 46
2.3 Conclusion 59
2.4 References 60
3 DESIGN AND MODELING OF AN EIGHT-ELEMENT MICROSTRIP PATCH ARRAY 61
3.1 Introduction 61
3.2 Methodology 61
3.2.1 Antenna Desired Performance 61
3.2.2 Substrate Selection 62
3.2.3 Coordinate System 62
3.2.4 Determining the Number of Array Elements 62
3.2.4.1 Six-element Array Directivity Verification 69
3.2.4.2 Eight-element Array 70
3.2.5 Feed Methods 73
3.2.6 Modeling of the Eight-element Array 74
3.2.6.1 Simulation Parameters 74

3.2.6.2 Model Iterations 75
3.2.6.3 Increasing the Directivity 90
3.3 Conclusion 98
3.4 References 98
4 THE EXPERIMENTAL CHARACTERIZATION OF PERFORMANCE OF THE TWO-ELEMENT AND EIGHT-ELEMENT PATCH ANTENNA ARRAYS 100
4.1 Introduction 100
4.2 Test Philosophy 100
4.2.1 Variation of Resonant Frequency of the Two-element Array 100
4.2.1.1 Variation of Patch Length 100
4.2.1.2 Variation of Dielectric Constant 105
4.2.2 Eight-element Array Variations 109
4.2.3 Experimental Characterization of the Antennas 117
4.3 Fabricated Antennas and Test Equipment 118
4.4 Return Loss Measurements 119
4.4.1 Two-element Array Return Loss Measurement (No Solder) 121
4.4.2 Eight-element Array Return Loss Measurement (No Solder) 126
4.5 Far-field Radiation Pattern Measurements 128
4.5.1 Calculation of the Far-field 131
4.5.2 Two-element Array Far-field Radiation Pattern Measurement 132
4.5.3 Eight-element Array Far-field Radiation Pattern Measurement 135
4.6 The Effects of Solder on Return Loss Measurements 139
4.7 Conclusion 143
4.8 References 144
5 CONCLUSIONS 145

5.1 Low Gain Antenna 145

5.2 High Gain Antenna 146

6 FUTURE WORK 148

6.1 Introduction 148

6.2 Patch Length Tolerance Verification 148

6.3 Dielectric Permittivity Measurement Capability 148

6.4 Method of Board Stiffening 149

6.5 Integration into the Aircraft 149

LIST OF FIGURES

Figure 1-1. Typical Antenna Mounting Location on a VTOL Aircraft 2

Figure 1-2. Microstrip Patch Electric Field Lines 180º Out-of-Phase 4

Figure 2-1. Microstrip Patch Structure Dimensions 11

Figure 2-2. Patch Geometry Showing the Effective Length due to Fringing Fields 12

Figure 2-3. TM_{10} and TM_{02} Mode Configurations for a Patch of Effective Length 0.0985 inch and Width 0.160 inch 14

Figure 2-4. Coordinate System for the Patch Antenna 15

Figure 2-5. Calculated Principal Plane Radiation Patterns (E- and H-plane) obtained from Equations (2-7) and (2-8), respectively 17

Figure 2-6. Microstrip Patch Fed by an (a) Inset-feed and (b) Quarter-wave Transformer 18

Figure 2-7. Modeled Patch Antenna with Calculated Dimensions 20

Figure 2-8. Simulated Electric Field at the Excitation Port 21

Figure 2-9. Example of CST's "Open (Add Space)" Boundary Condition 22

Figure 2-10. Return Loss for a Patch of Length 0.093 inch (Figure 2-7) 24

Figure 2-11. Radiation Pattern for a Patch of Length 0.093 inch (Figure 2-7)..... 24

Figure 2-12. E-plane Pattern for a Patch of Length 0.093 inch (Figure 2-7),..... 25

Figure 2-13. H-plane Pattern for a Patch of Length 0.093 inch (Figure 2-7), ... 25

Figure 2-14. Return Loss for the Patch of Length 0.089 inch with a Resonant Frequency of 34.965 GHz..... 27

Figure 2-15. Radiation Pattern for a Patch of Length 0.089 inch with a Resonant Frequency of 34.965 GHz..... 28

Figure 2-16. E-plane Pattern for a Patch of Length 0.089 inch with a Resonant Frequency of 34.965 GHz,..... 29

Figure 2-17. H-plane Pattern for a Patch of Length 0.089 inch with a Resonant Frequency of 34.965 GHz,..... 29

Figure 2-18. (a) Normalized Element Pattern (E-plane) and (b) Array Factor of a Two-element Array Consisting of Isotropic Sources of Equal Amplitude and Phase Currents Spaced Half a Wavelength Apart..... 31

Figure 2-19. Normalized E-plane Pattern (Element Pattern x Array Factor) for a Two-element Array of Microstrip Patches 31

Figure 2-20. Two-element Array with a T-junction Corporate Feed and 0.169 inch Patch-to-Patch Spacing 33

Figure 2-21. Radiation Pattern for a Two-element Array with a T-junction Corporate Feed and 0.169 inch Patch-to-Patch Spacing..... 34

Figure 2-22. Two-element Array with a T-junction Corporate Feed and 0.160 inch Patch-to-Patch Spacing 36

Figure 2-23. Radiation Pattern for a Two-element Array with a T-junction Corporate Feed and 0.160 inch Patch-to-Patch Spacing..... 36

Figure 2-24. Two-element Array with a T-junction Corporate Feed and 0.181 inch Patch-to-Patch Spacing 37

Figure 2-25. Radiation Pattern for a Two-element Array with a T-junction Corporate Feed and 0.181 inch Patch-to-Patch Spacing..... 38

Figure 2-26. Two-element Array with a T-junction Corporate Feed and 50 Ω Bend Moved Further Away from the Array..... 39

Figure 2-27. Radiation Pattern for a Two-element Array with a T-junction Corporate Feed and 50 Ω Bend Moved Further Away from the Array 40

Figure 2-28. Two-element Array with the T-junction Moved Closer to Array Elements by 0.050 inch (0.170 inch Spacing to Patches) 41

Figure 2-29. Radiation Pattern for a Two-element Array with the T-junction Moved Closer to Array Elements by 0.050 inch (0.170 inch Spacing to Patches) 42

Figure 2-30. Radiation Pattern for a Two-element Array with the T-junction Moved Closer to Array Elements by 0.075 inch (0.145 inch Spacing to Patches) 43

Figure 2-31. Radiation Pattern for a Two-element Array with the T-junction Moved Closer to Array Elements by 0.100 inch (0.120 inch Spacing to Patches) 43

Figure 2-32. Two-element Array with the Y-junction Located 0.145 inch Away from the Array Elements 45

Figure 2-33. Radiation Pattern for a Two-element Array with the Y-junction Located 0.145 inch Away from the Array Elements 45

Figure 2-34. Radiation Pattern for a Two-element Array with the Y-junction Located 0.120 inch Away from the Array Elements 46

Figure 2-35. Two-element Array with a Series Feed 47

Figure 2-36. Return Loss for the Two-element Array with a Series Feed 48

Figure 2-37. Radiation Pattern for the Two-element Array with a Series Feed 49

Figure 2-38. End Launch Connector, Model # 1492-03-5 [12] 50

Figure 2-39. Two-element Array with a Series Feed and the 1492-03-5 Connector 51

Figure 2-40. Radiation Pattern for the Two-element Array with a Series Feed and the 1492-03-5 Connector 51

Figure 2-41. E-plane Pattern for the Two-element Array with a Series Feed and the 1492-03-5 Connector 52

Figure 2-42. Two-element Array with a Series Feed and Low Profile Connector 54

Figure 2-43. Radiation Pattern for the Two-element Array with a Series Feed and Low Profile Connector 54

Figure 2-44. E-plane Pattern for the Two-element Array with a Series Feed and Low Profile Connector 55

Figure 2-45. Final Geometry of the Two-element Array with a Series Feed, Low Profile Connector, and Board Launch Design 56

Figure 2-46. Radiation Pattern for the Final Geometry of the Two-element Array with a Series Feed, Low Profile Connector, and Board Launch Design 57

Figure 2-47. E-plane Pattern for the Final Geometry of the Two-element Array with a Series Feed, Low Profile Connector, and Board Launch Design 58

Figure 2-48. H-plane Pattern for the Final Geometry of the Two-element Array with a Series Feed, Low Profile Connector, and Board Launch Design 58

Figure 2-49. Return Loss for the Final Geometry of the Two-element Array with a Series Feed, Low Profile Connector, and Board Launch Design 59

Figure 3-1. Calculated E- and H-plane Radiation Patterns for a Single-element Patch obtained from Equations (3-1) and (3-2), respectively 63

Figure 3-2. Two-dimensional Array with Three Elements in the E-plane and Two Elements in the H-Plane 65

Figure 3-3. (a) Normalized Element Pattern (H-plane) and (b) Array Factor of a Two-element Array Consisting of Isotropic Sources of Equal Amplitude and Phase Currents Spaced Half a Wavelength Apart 66

Figure 3-4. Normalized H-plane Pattern (Element Pattern x Array Factor) for a Two-element Array of Microstrip Patches 67

Figure 3-5. (a) Normalized Element Pattern (E-plane) and (b) Array Factor for a Three-element Array Consisting of Isotropic Sources of Equal Amplitude and Phase Currents Spaced Half a Wavelength Apart 68

Figure 3-6. Normalized E-plane Pattern (Element Pattern x Array Factor) for a Three-element Array of Microstrip Patches 69

Figure 3-7 . Two-dimensional Array with Four Elements in the E-plane and Two Elements in the H-Plane 71

Figure 3-8. (a) Normalized Element Pattern (E-plane) and (b) Array Factor for a Four-element Array Consisting of Isotropic Sources of Equal Amplitude and Phase Currents Spaced Half a Wavelength Apart 72

Figure 3-9. Normalized E-plane Pattern (Element Pattern x Array Factor) for a Four-element Array of Microstrip Patches 72

Figure 3-10 . Antenna from [3] Showing a Two-way Splitter and Two Series-fed Columns 74

Figure 3-11. Eight-element Array of Microstrip Patches with a Horizontal and Vertical Patch-to-Patch Spacing of 0.169 inch 76

Figure 3-12. Radiation Pattern for an Eight-element Array of Microstrip Patches with a Horizontal and Vertical Patch-to-Patch Spacing of 0.169 inch 77

Figure 3-13. E-plane Pattern for an Eight-element Array of Microstrip Patches with a Horizontal and Vertical Patch-to-Patch Spacing of 0.169 inch 78

Figure 3-14. H-plane Pattern for an Eight-element Array of Microstrip Patches with a Horizontal and Vertical Patch-to-Patch Spacing of 0.169 inch 78

Figure 3-15. Eight-element Array of Microstrip Patches with a Horizontal and Vertical Patch-to-Patch Spacing of 0.169 inch and 0.160 inch, respectively 79

Figure 3-16. E-plane Pattern for an Eight-element Array with a Horizontal and Vertical Patch-to-Patch Spacing of 0.169 inch and 0.160 inch, respectively 80

Figure 3-17. Eight-element Array Geometry from Figure 3-15 with a Low Profile Connector 81

Figure 3-18. Radiation Pattern for the Eight-element Array of Figure 3-17 82

Figure 3-19. E-plane Pattern for the Eight-element Array of Figure 3-17 82

Figure 3-20. Eight-element Two-dimensional Microstrip Patch Array with Series Line Path Lengths of 0.097 inch 84

Figure 3-21. Radiation Pattern for the Eight-element Array shown in Figure 3-20 with Series Line Path Lengths of 0.097 inch 84

Figure 3-22. E-plane Pattern for the Eight-element Array with Series Line Path Lengths of 0.097 inch 85

Figure 3-23. Four-element Array Used in [6] to Reduce SLL by Decreasing *l* 86

Figure 3-24. Eight-element Two-dimensional Array of Microstrip Patches with Meandered Quarter-wave Transformers 87

Figure 3-25. Radiation Pattern for the Eight-element Array of Microstrip Patches with Meandered Quarter-wave Transformers shown in Figure 3-24 88

Figure 3-26. E-plane Pattern for the Eight-element Array of Microstrip Patches with Meandered Quarter-wave Transformers shown in Figure 3-24 88

Figure 3-27. H-plane Pattern for the Eight-element Array of Microstrip Patches with Meandered Quarter-wave Transformers shown in Figure 3-24 89

Figure 3-28. Eight-element Array of Microstrip Patches with Horizontal Spacing Increased to 0.184 inch 91

Figure 3-29. E-plane Pattern for an Eight-element Array of Microstrip Patches with Horizontal Spacing Increased to 0.184 inch 92

Figure 3-30. H-plane Pattern for an Eight-element Array of Microstrip Patches with Horizontal Spacing Increased to 0.184 inch 92

Figure 3-31. Eight-element Array of Microstrip Patches with Horizontal Spacing Increased to 0.200 inch 93

Figure 3-32. E-plane Pattern for an Eight-element Array of Microstrip Patches with Horizontal Spacing Increased to 0.200 inch 94

Figure 3-33. H-plane Pattern for an Eight-element Array of Microstrip Patches with Horizontal Spacing Increased to 0.200 inch 94

Figure 3-34. Final Geometry of the Eight-element Array of Microstrip Patches with 0.200 inch Horizontal Spacing, Low Profile Connector, and Board Launch Design 95

Figure 3-35. Radiation Pattern for the Final Geometry of the Eight-element Planar Microstrip Array with 0.200 inch Horizontal Spacing, Low Profile Connector, and Board Launch Design 96

Figure 3-36. E-plane Pattern for the Final Geometry of the Eight-element Planar Microstrip Array with 0.200 inch Horizontal Spacing, Low Profile Connector, and Board Launch Design 96

Figure 3-37. H-plane Pattern for the Final Geometry of the Eight-element Planar Microstrip Array with 0.200 inch Horizontal Spacing, Low Profile Connector, and Board Launch Design 97

Figure 3-38. Return Loss for the Final Geometry of the Eight-element Planar Microstrip Array with 0.200 inch Horizontal Spacing, Low Profile Connector, and Board Launch Design 97

Figure 4-1. Geometry of a Two-element Array with Patches of Length 0.091 inch 101

Figure 4-2. Return Loss for a Two-element Array with Patches of Length 0.091 inch . 102

Figure 4-3. Geometry for a Two-element Array with Patches of Length 0.093 inch..... 103

Figure 4-4. Return Loss for a Two-element Array with Patches of Length 0.093 inch . 103

Figure 4-5. Return Loss for the Two-element Array Geometry with $\boldsymbol{\varepsilon r}$ = 2.90..... 105

Figure 4-6. Return Loss for Final Two-element Array Geometry with $\boldsymbol{\varepsilon r}$ = 2.94 106

Figure 4-7. Return Loss for Final Two-element Array Geometry with $\boldsymbol{\varepsilon r}$ = 2.98 106

Figure 4-8. Simulated Return Loss for the Eight-element Array Geometry with $\boldsymbol{\varepsilon r}$ = 2.90 109

Figure 4-9. Simulated Return Loss for the Eight-element Array Geometry with $\boldsymbol{\varepsilon r}$ = 2.94 110

Figure 4-10. Simulated Return Loss for the Eight-element Array Geometry with $\boldsymbol{\varepsilon r}$ = 2.98..... 110

Figure 4-11. Geometry for a Planar Eight-element Array of Microstrip Patches with Series Line Path Lengths of 0.094 inch 112

Figure 4-12. Return Loss for an Eight-element Array with Series Line Path Lengths of 0.094 inch and with the Top Ground Launch and Via Structures Removed 113

Figure 4-13. Geometry for an Eight-element Array with Series Line Path Lengths of 0.100 inch..... 114

Figure 4-14. Return Loss for an Eight-element Array with Series Line Path Lengths of 0.100 inch..... 114

Figure 4-15. Fabricated Low and High Gain Antennas Adjacent to a Quarter 118

Figure 4-16. Return Loss Test Setup Showing the Network Analyzer, Coaxial Cable, and Antenna 120

Figure 4-17. Coaxial Connecter Launch to Microstrip Line with No Solder 121

Figure 4-18. Measured Return Loss for 12 Two-element Arrays (No Solder)..... 122

Figure 4-19. Comparison of Simulated and Measured Return Loss for Two-element Arrays (No Solder)..... 123

Figure 4-20. Microscope View of the Non-Uniform Plating on Top Layer Copper Structures 124

Figure 4-21. Return Loss for a Two-element Array with Thicker Copper (0.0014 inch) Layers and Patches of Length 0.093 inch 125

Figure 4-22. Measured Return Loss for 4 Instances of Two-element Arrays with Patches of Length 0.093 inch (No Solder) 126

Figure 4-23. Measured Return Loss for Eight-element Arrays (No Solder) 127

Figure 4-24. Measured Return Loss for 4 Instances of Eight-element Arrays (No Solder) Compared with Simulated Results..... 128

Figure 4-25. Radiation Pattern Test Setup Showing the Source Antenna, Antenna Under Test, and Antenna Positioner 129

Figure 4-26. Source Antenna Mounted on the Wooden Arch at $\theta = 60^{\circ}$..... 129

Figure 4-27. Antenna Under Test Held in Position by the Antenna Mounting Fixture.. 130

Figure 4-28. Radiation Pattern Test Block Diagram 130

Figure 4-29. Maximum Dimension Used in Far-field Calculation..... 131

Figure 4-30. Simulated 3-D Far-field Radiation Pattern at 35.0 GHz for the Two-element Array with Patches of Length 0.093 inch 132

Figure 4-31. Measured 3-D Far-field Radiation Patterns at 35.0 GHz for the Two-element Arrays with Patches of Length 0.093 inch..... 132

Figure 4-32. Simulated versus Measured E-plane Pattern at 35 GHz for the Two-element Arrays with Patches of Length 0.093 inch..... 133

Figure 4-33. Simulated versus Measured H-plane Pattern at 35 GHz for the Two-element Array with Patches of Length 0.093 inch 134

Figure 4-34. Simulated 3-D Far-field Radiation Pattern at 35 GHz for the Eight-element Array with Series Line Path Lengths of 0.097 inch..... 136

Figure 4-35. Measured 3-D Far-field Radiation Patterns at 35 GHz for the Eight-element Array with Series Line Path Lengths of 0.097 inch 136

Figure 4-36. Simulated versus Measured E-plane Pattern at 35 GHz for the Eight-element Array with Series Line Path Lengths of 0.097 inch 137

Figure 4-37. Simulated versus Measured H-plane Pattern at 35 GHz for the Eight-element Array with Series Line Path Lengths of 0.097 inch 138

Figure 4-38. Antenna with Center Tab Soldered to the Input Feed Line 140

Figure 4-39. Measured Return Loss for the 93-1 Two-element Array (Before and After Soldering of the Connector to the Feed Line) 141

Figure 4-40. Measured Return Loss for the 93-2 Two-element Array (Before and After Soldering of the Connector to the Feed Line) 141

Figure 4-41. Measured Return Loss for the 97-1 Eight-element Array (Before and After Soldering of the Connector to the Feed Line) 142

Figure 4-42. Measured Return Loss for the 97-3 Eight-element Array (Before and After Soldering of the Connector to the Feed Line) 142

LIST OF TABLES

Table 1-1. Desired Low Gain Antenna Beam Pattern Performance 6

Table 1-2. Desired High Gain Antenna Beam Pattern Performance 6

Table 2-1. Low Gain Array Desired Performance 9

Table 2-2. $\boldsymbol{\varepsilon_{eff}}$, $\boldsymbol{NLE}$, and Patch Length for Various Patch Widths 13

Table 2-3. Theoretical versus Simulated Patch Characteristics for a Single Patch of Length 0.093 inch 26

Table 2-4. Comparison of the Two-element Array Calculated versus Simulated Characteristics 57

Table 3-1. High Gain Array Desired Performance 62

Table 3-2. Comparison of the Theoretical versus Simulated Characteristics for the Eight-element Array shown in Figure 3-24 89

Table 4-1. Resonant Frequency for the Two-element Array as Patch Length Varies 104

Table 4-2. Radiation Pattern Characteristics at 34.965 GHz for the Two-element Array as Patch Length Varies 104

Table 4-3. Two-element Array Resonant Frequencies for Low, Median, and High Values of $\boldsymbol{\varepsilon_r}$ 107

Table 4-4. Two-element Array Radiation Pattern Characteristics at 34.965 GHz for Low, Median, and High Values of $\boldsymbol{\varepsilon_r}$ 107

Table 4-5. List of Fabricated Two-element Arrays 108

Table 4-6. Eight-element Array Resonant Frequencies for Low, Median, and High Values of $\boldsymbol{\varepsilon_r}$ 111

Table 4-7. Eight-element Array Radiation Pattern Characteristics at 34.965 GHz for Low, Median, and High Values of $\boldsymbol{\varepsilon_r}$ 111

Table 4-8. Resonant Frequencies for the Eight-element Array as Series Line Path Length is Varied 115

Table 4-9. Eight-element Array Radiation Pattern Characteristics at 34.965 GHz as Series Line Path Length Varies 116

Table 4-10. List of Fabricated Eight-element Arrays 117

Table 4-11. Test Equipment and Software List 118

Table 4-12. Simulated and Measured Half Power Beamwidths at 35.0 GHz for the Low Gain Antenna 135

Table 4-13. Simulated and Measured Half Power Beamwidths for the High Gain Antenna 139

Table 5-1. Low Gain Array Measured Results 146

Table 5-2. High Gain Array Measured Results 147

1 INTRODUCTION

The design of the aircraft-mounted antennas for autonomous landing systems using microstrip patch arrays is presented. The objective of this design is to eliminate reflections from adjacent payload or fuselage surfaces. Additionally, there is a need to minimize weight, cost, and manufacturing touch labor in any new designs. The theory, design, modeling, fabrication, testing, and results for two prototype microstrip patch antenna arrays are discussed.

1.1 System Description

A typical radar-based autonomous landing system consists of a low gain and high gain antenna mounted on the aircraft and a radar tracking system located on the ground. The aircraft antenna provides a point source on the air vehicle to aid in aircraft detection and accurate position sensing. A typical tracking system provides air vehicle to touchdown point relative position data to generate guidance and landing control commands.

1.2 Background Information

A typical radar-based autonomous landing system antenna assembly consists of two antennas: a high gain directional antenna and a low gain omni-directional antenna. The directional antenna is used to acquire and track the aircraft at long range. The omni-directional antenna is used to track the aircraft at close range and provides the capability for a wide variation in approach angle relative to the ground-based tracking subsystem.

The antenna assembly is typically mounted on a Vertical Takeoff and Land (VTOL) aircraft near the underside of the nose as shown in Figure 1-1.

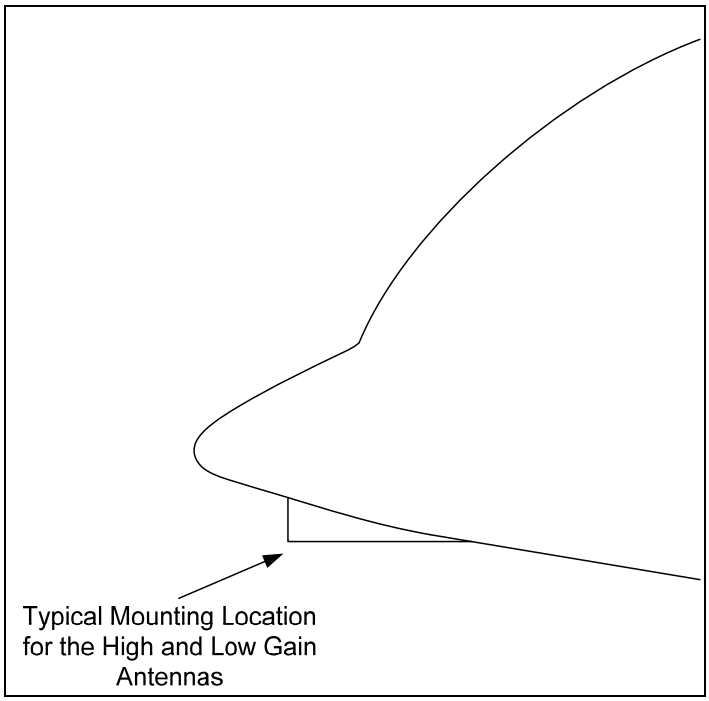

Figure 1-1. Typical Antenna Mounting Location on a VTOL Aircraft

It is known that multipath resulting from RF energy illuminating the airframe components can lead to problems with aircraft acquisition and cause inaccurate position sensing when at close range. This problem is ubiquitous to VTOL aircraft because a typical low gain antenna has a 360° azimuth beamwidth which illuminates the aircraft.

There are two primary goals of this project: (1) develop a low gain antenna that radiates only in the forward direction and (2) develop both a low gain and high gain antenna using microstrip patch arrays to minimize cost. A microstrip antenna is chosen for this application because of its thin profile, light weight, ease of fabrication, and low cost [1] when compared to antenna structures in existing autonomous landing systems.

A typical low gain antenna is a bicone structure which requires meticulous hand assembly and tuning for each antenna. A typical high gain antenna is a pyramidal horn structure. Both antennas can be replaced by microstrip patch arrays to reduce weight as well as cost.

1.2.1 Microstrip Patch Antenna Theory of Operation

Though there are many papers and textbooks explaining the basic operation of microstrip patch antennas, a brief summary is provided in this chapter for completeness.

Similar to a microstrip transmission line, a microstrip patch consists of a metallic (usually copper) patch over a ground plane. The patch and the ground plane are separated by a dielectric medium of thickness much less than a wavelength. For a resonant patch, the electric field lines are 180º apart in phase at each edge of the patch and because of the finite dimensions of the patch, fringing fields result at the edges, as shown in Figure 1-2. Though out-of-phase in the x-direction, the fringing fields at the edges are in-phase in the z-direction. The equal magnitude and phases of the z-components of the fringing fields are the mechanism by which a broadside radiation pattern results [2].

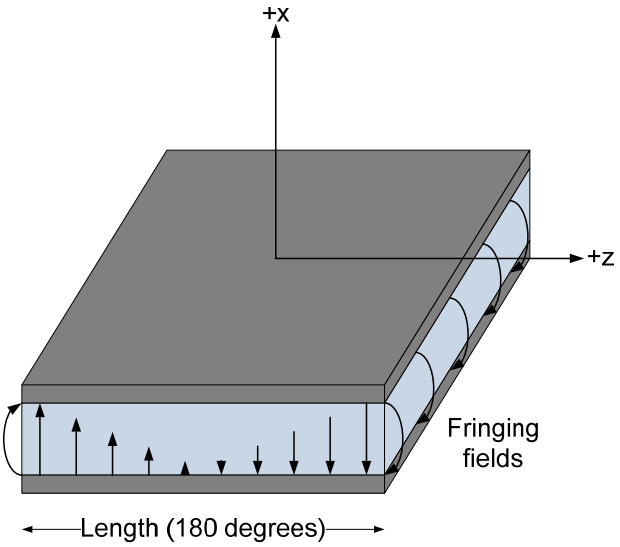

Figure 1-2. Microstrip Patch Electric Field Lines 180º Out-of-Phase

The far-field radiation pattern is the sum of the fields from the two radiating slots of the patch. The radiation pattern for one slot is first derived; because the patch has two radiating slots, an array factor can be applied, modeling the patch as a two-element array. Typical values for the azimuth beamwidth and directivity of a patch antenna are 65º and 8 dBi, respectively. More details on the radiation pattern, beamwidth, and directivity calculations for a single patch are provided in Chapter 2.

The dimensions of the patch are what determine the resonant frequency and input impedance. The resonant length of a patch is slightly less than a half-wavelength in the substrate dielectric material for a rectangular patch due to length extension caused by the fringing fields. Other parameters that can influence the resonant frequency are the ground plane size, the copper thickness, and the patch width. For a resonant edge-fed patch, the input impedance is purely resistive and is dependent on the patch length, patch width, and dielectric constant [2].

1.3 Design Criteria

The following criteria are taken into account in the design solutions for both the low gain and high gain antennas: size, complexity of high volume production, beam pattern and directivity, and Voltage Standing Wave Ratio (VSWR).

1.3.1 Size

The goal of the antenna design is to design electrical structures that do not exceed the mechanical envelope of 2 cubic inches per antenna.

1.3.2 Complexity of High Volume Production

The fabrication, assembly, and testing of the antennas when in production are important factors to be considered in the design. Performance that can be repeated without requiring individual touch labor and tuning of the units is desired.

1.3.3 Low Gain Antenna Beam Pattern and Directivity

The desired pattern is defined using estimated geometries of VTOL aircraft and the expected placement of the antenna assembly on the aircraft. The operational envelope of the aircraft relative to the tracking system at various positions (e.g., touchdown point) is also considered.

The desired beam pattern for the low gain antenna is defined in terms of azimuth and elevation angles. Table 1-1 lists the desired pattern characteristics.

Table 1-1. Desired Low Gain Antenna Beam Pattern Performance

Azimuth	Half power beamwidth greater than 60º (±30º)
	Side lobe level: At least -20 dB
Elevation	Half power beamwidth greater than 30º (±15º) but less than 60º (±30º)
	Side lobe level: At least -20 dB

The desired gain of the modified antenna is greater than 4 dBi at 34.965 GHz.

1.3.4 High Gain Antenna Beam Pattern and Directivity

The desired beam pattern of the high gain antenna is defined in terms of azimuth and elevation angles. Table 1-2 lists the desired pattern characteristics.

Table 1-2. Desired High Gain Antenna Beam Pattern Performance

Azimuth	Half power beamwidth greater than 40º (±20º) but less than 50º (±25º)
	Side lobe level: At least -20 dB
Elevation	Half power beamwidth greater than 20º (±10º) but less than 40º (±20º)
	Side lobe level: At least -13 dB

The desired gain of the modified antenna is greater than 14.0 dBi at 34.965 GHz.

1.3.5 Voltage Standing Wave Ratio (VSWR)

The desired VSWR for both the low gain and high gain antennas is less than 1.5 to 1 at 34.965 GHz.

1.4 Thesis Overview

Chapter 2 describes the theory, design, and Computer Aided Design (CAD) modeling of the low gain patch antenna array. Chapter 3 includes similar design procedures and details for the high gain patch array. The prototype development, methodology, and testing results are given in Chapter 4. A summary and conclusions of the project are given in Chapter 5. Chapter 6 briefly describes future work and necessary design improvements.

1.5 References

[1] J.R. James, and P.S. Hall, *Handbook of Microstrip Antennas*, Vols. 1 and 2, Peter Peregrinus, London, UK, 1989, pp. 1-7.

[2] W. L. Stutzman and G. A. Thiele, *Antenna Theory and Design*, 2nd ed., John Wiley & Sons, New York, 1998, pp. 210-216.

2 DESIGN AND MODELING OF A TWO-ELEMENT MICROSTRIP PATCH ARRAY

2.1 Introduction

A typical low gain, omni-directional antenna structure used in radar-based autonomous landing systems is a bicone structure with a full-coverage 360° azimuth beam pattern. However, due to placement, system performance can be degraded as a result of the antenna radiating directly towards the body of the aircraft, causing tracking of unwanted "multipath" signals, or a loss of tracking as a result of phase cancellations of the reflected signals with the incident signal. To eliminate this negative effect, a patch antenna has been considered as an alternative structure for a low gain antenna. The patch antenna is designed to have a similar radiation pattern as that of the forward pointing half of a bicone antenna, but eliminates the aft radiation directed towards the body of the aircraft. A two-element microstrip patch antenna array is designed and modeled. The return loss, when matched to 50 Ω, is less than -20 dB at the center frequency. The radiation pattern meets the design objectives. The simulated peak directivity is 10.7 dBi. The design procedure is described along with modeling results.

2.2 Methodology

2.2.1 Antenna Desired Performance

The desired performance of the low gain antenna is provided in Table 2-1.

Table 2-1. Low Gain Array Desired Performance

Center frequency, f_r:	34.965 GHz
Bandwidth:	±185 MHz
Polarization:	linear, vertical
RF feed characteristic impedance:	50 Ω
RF feed VSWR:	1.5:1 maximum
Gain at 0° azimuth, 0° elevation:	greater than 4 dBi
H-plane half power beamwidth (azimuth cut):	greater than 60º (±30º)
E-plane half power beamwidth (elevation cut):	greater than 30º (±15º) but less than 60º (±30º)
Side lobe level (SLL):	less than -20 dB

2.2.2 Substrate Selection

When selecting a substrate for a rectangular patch, there are many tradeoffs such as radiation efficiency, dielectric loss, surface wave behavior, and temperature stability [1]. The two parameters that have the most impact on performance are the relative permittivity and thickness of the substrate. Laminates from Rogers Corporation are evaluated for the substrate material. Materials having a low relative dielectric constant are considered in order to improve radiation efficiency and reduce surface wave effects. The RT/duroid® 6002 High Frequency Laminate is chosen as the dielectric. The dielectric constant is 2.94 ±0.04, the thermal coefficients of the dielectric constant and expansion are low, and the material is proven reliable in harsh environmental extremes in patch antenna applications [2].

A thickness of 0.010 inch is chosen for the substrate. A thin substrate height alleviates surface wave interference and minimizes dielectric loss [3].

According to Carver and Mink, an extremely critical parameter of the substrate is the tolerance of the relative dielectric constant, ε_r. The tolerance quoted by the manufacturer for the selected substrate is ±0.04. An approximation of the relative frequency change based on the above tolerance is shown in Equation (2-1) [4]:

$$\delta f = f_r \frac{\delta \varepsilon_r}{2\varepsilon_r} \tag{2-1}$$

where f_r is the center frequency equal to 34.965 GHz, $\delta\varepsilon_r$ is the tolerance of the dielectric constant, and ε_r is the relative dielectric constant. The potential shift in the resonant frequency for a substrate with a dielectric constant of 2.94 and tolerance of ±0.04 is calculated to be approximately ±240 MHz.

2.2.3 Resonant Microstrip Patch Design

The microstrip patch dimensions are identified in Figure 2-1. The feed line runs along the +z axis and terminates into the patch edge. The patch is oriented so that the width dimension is along the y-axis and the length dimension is along the z-axis.

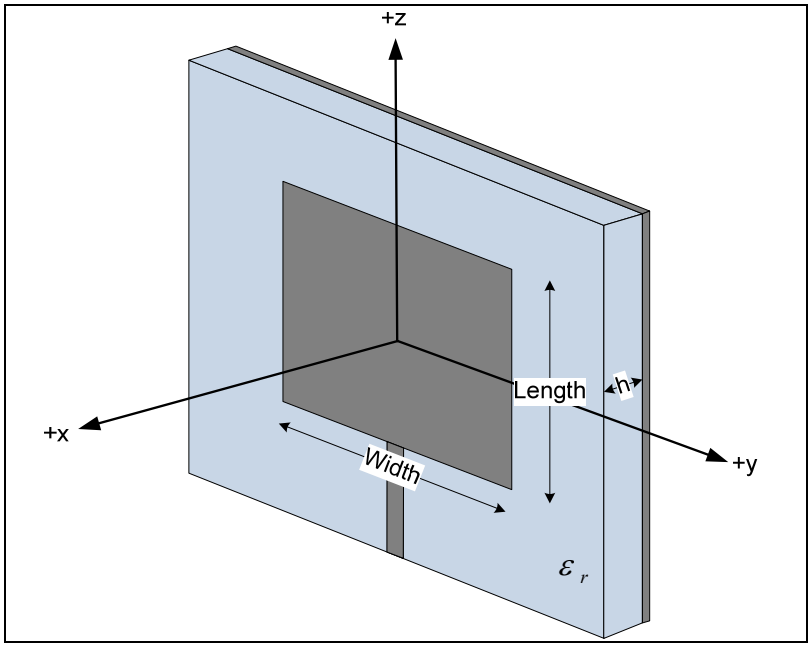

Figure 2-1. Microstrip Patch Structure Dimensions

Very simple formulas are used to calculate patch dimensions if the transmission line model is applied, however it is well known that this model is less accurate compared to other models [5]. In order to obtain accurate patch dimensions, formulas presented in [6] are evaluated as functions of width. Equations (2-2) through (2-4) are used to calculate the effective dielectric constant, ε_{eff}, the Normalized Line Extension, NLE, and the patch length:

$$\varepsilon_{eff}(Width) = \frac{\varepsilon_r + 1}{2} + \frac{\varepsilon_r - 1}{2}\left(\frac{1}{\sqrt{1 + \frac{12h}{Width}}}\right) \tag{2-2}$$

$$NLE(Width) = 0.412\frac{\left[\varepsilon_{eff}(Width) + 0.3\right]\left[\frac{Width}{h} + 0.264\right]}{\left[\varepsilon_{eff}(Width) - 0.258\right]\left[\frac{Width}{h} + 0.8\right]} \tag{2-3}$$

$$Length(Width) = \frac{c}{2f_r\sqrt{\varepsilon_{eff}(Width)}} - 2h * NLE(Width) \tag{2-4}$$

where h is the substrate thickness, 0.010 inch, and f_r is the center design frequency equal to 34.965 GHz. The effective dielectric constant takes into account the electric field lines inside the substrate in addition to the parts of the electric field lines that exist in air. The Normalized Line Extension is the added length resulting from the fringing fields; the fringing fields make the patch electrically longer than its physical length (Figure 2-2). The calculated results of Equations (2-2) through (2-4) for various widths are given in Table 2-2.

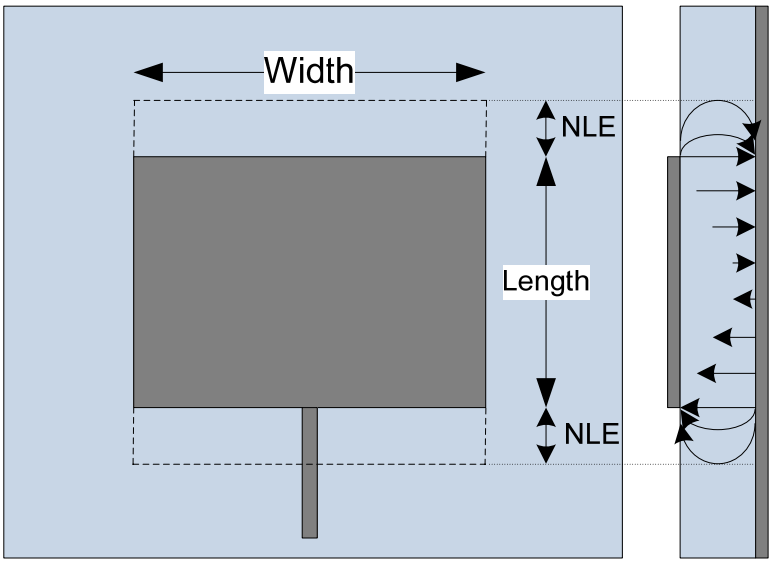

Figure 2-2. Patch Geometry Showing the Effective Length due to Fringing Fields

Table 2-2. ε_{eff}, NLE, and Patch Length for Various Patch Widths

Width (inches)	ε_{eff}	NLE	Length (inches)
0.100	2.624	0.484	0.0946
0.110	2.641	0.485	0.0942
0.120	2.656	0.487	0.0939
0.130	2.669	0.488	0.0936
0.140	2.682	0.488	0.0934
0.150	2.693	0.489	0.0931
0.160	2.703	0.470	0.0929
0.170	2.713	0.490	0.0927
0.180	2.721	0.491	0.0926
0.190	2.729	0.491	0.0924
0.200	2.737	0.492	0.0923

Larger widths result in greater radiation efficiencies; however, widths too large may cause higher order modes and cross-polarization [6]. Using the cavity model, the resonant frequencies for various modes of the patch structure are given by Equation (2-5):

$$f_{r(mn)} = \frac{c}{2\pi\sqrt{\varepsilon_r}}\sqrt{\left(\frac{m\pi}{Length}\right)^2 + \left(\frac{n\pi}{Width}\right)^2} \tag{2-5}$$

where m and n are the number of half-cycle field variations along the $Length$ and $Width$ dimensions, respectively, and $Length$ is one-half wavelength in the dielectric (0.0985 inch). The resonant frequencies for the TM_{10} and TM_{20} modes are independent

of width and are calculated to be 34.94 GHz and 69.88 GHz, respectively. To prevent higher order modes from being excited, the width must be kept smaller than a wavelength in the dielectric (0.197 inch) [7]. A width of 0.160 inch is chosen as a tradeoff between obtaining good efficiency and the excitation of higher order modes. The resonant frequencies for the TM_{01} and TM_{02} modes are calculated to be 21.51 GHz and 43.02 GHz, respectively. For a patch operating in the TM_{10} mode (Figure 2-3), the next higher mode is TM_{02} and its resonant frequency (43.02 GHz) is almost 8 GHz higher than the designed operational bandwidth of the patch (f_{max} = 35.15 GHz). Therefore the dimensions of the structure will not excite higher order modes within the bandwidth of 34.965 ±185 GHz.

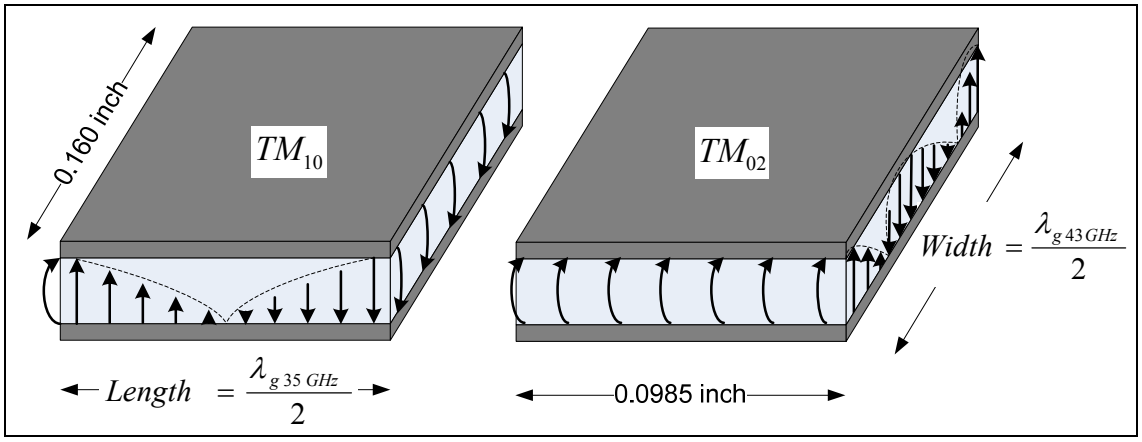

Figure 2-3. TM_{10} and TM_{02} Mode Configurations for a Patch of Effective Length 0.0985 inch and Width 0.160 inch

The resonant frequencies for patches of widths greater than 0.160 inch in the TM_{02} mode are closer to the operational bandwidths and are not considered. The corresponding length from Table 2-2 is rounded to 0.093 inch for a patch width chosen to be 0.160 inch.

2.2.3.1 Coordinate System

The spherical coordinate system shown in Figure 2-4 is used for the design and modeling of the patch antenna.

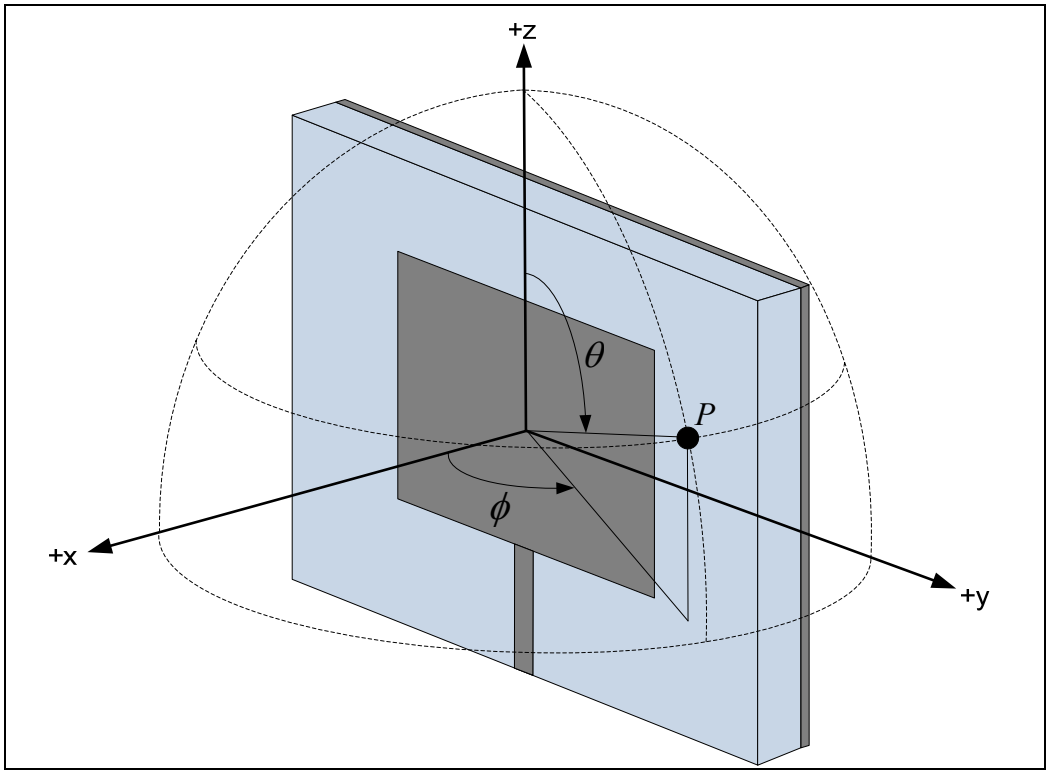

Figure 2-4. Coordinate System for the Patch Antenna

The patch lies in the y-z plane and is fed along the z-axis with radiation being normal to the patch in the x-direction. The zenith (elevation) angle θ is defined as the angle between the +z-direction and the line formed between the origin and point P. The azimuth angle ϕ is defined as the angle between the +x-direction and the line from the origin to the projection of point P on the x-y plane. The coordinate system is intentionally chosen to allow for a direct comparison of simulated versus measured vertically polarized radiation patterns.

2.2.3.2 Pattern Calculation of a Single Patch Antenna

The far-field radiation pattern of the single patch antenna is the sum of the two radiating slots as discussed in Chapter 1. The radiation pattern for one slot is first derived by creating a uniform magnetic line source from the electric field across the slot. An array factor is then applied, modeling the patch as a two-element array, where each element represents a slot. The normalized electric field radiation pattern is presented in Equation (2-6):

$$Pattern(\theta,\phi) = \frac{sin\left[\frac{\beta h}{2}cos\,(\theta)sin\left(\phi+\frac{\pi}{2}\right)\right]}{\frac{\beta h}{2}cos\,(\theta)sin\left(\phi+\frac{\pi}{2}\right)}cos\left[\frac{\beta Length}{2}cos(\theta)\right]sin\left(\phi+\frac{\pi}{2}\right)\frac{sin\left[\frac{\beta Width}{2}cos\left(\phi+\frac{\pi}{2}\right)\right]}{\frac{\beta Width}{2}cos\left(\phi+\frac{\pi}{2}\right)} \tag{2-6}$$

where $0 < \theta < \pi$, $-\frac{\pi}{2} < \phi < \frac{\pi}{2}$, β is the wave number, $\frac{2\pi}{\lambda_0}$, and h is the substrate thickness. The expressions for the principal plane patterns reduce to Equations (2-7) and (2-8) for the E- and H-plane, respectively [6]:

$$E(\theta) = \frac{sin\left[\frac{\beta h}{2}cos\,(\theta)\right]}{\frac{\beta h}{2}cos\,(\theta)}cos\left[\frac{\beta Length}{2}cos(\theta)\right], \phi = 0° \tag{2-7}$$

$$H(\phi) = sin\left(\phi+\frac{\pi}{2}\right)\frac{sin\left[\frac{\beta Width}{2}cos\left(\phi+\frac{\pi}{2}\right)\right]}{\frac{\beta Width}{2}cos\left(\phi+\frac{\pi}{2}\right)}, \theta = 90° \tag{2-8}$$

Because the coordinate system used in [6] is not the same as the coordinate system shown in Figure 2-4, Equations (2-6) through (2-8) are modified to represent

consistent patch orientation and broadside radiation in the x-direction. Figure 2-5(a) and Figure 2-5(b) illustrate the E- and H-plane patterns, respectively.

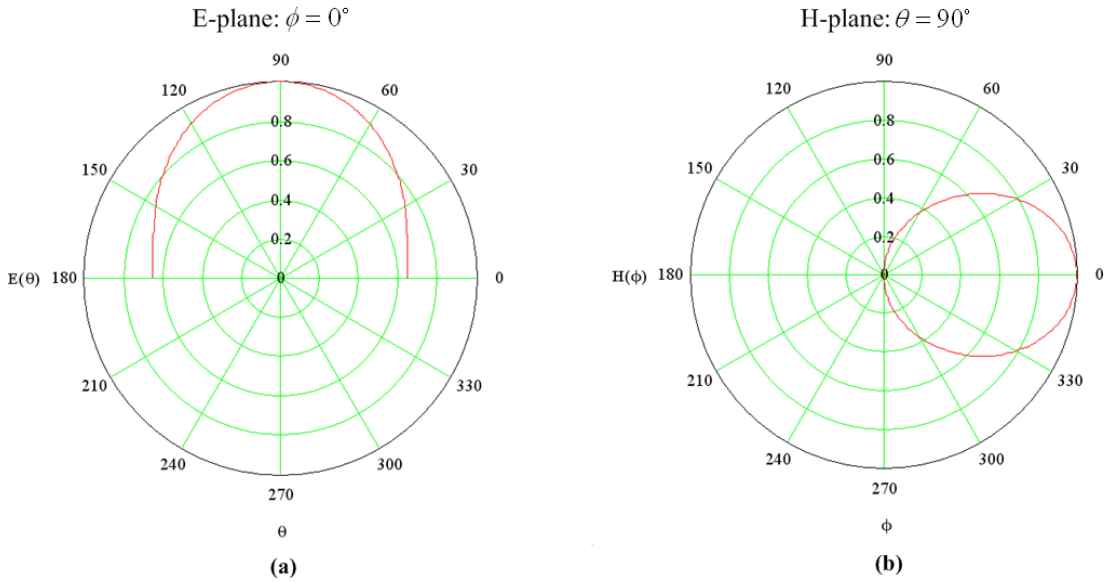

Figure 2-5. Calculated Principal Plane Radiation Patterns (E- and H-plane) obtained from Equations (2-7) and (2-8), respectively

2.2.3.3 Directivity of a Single Patch Antenna

The directivity of a single patch is defined as the ratio of the radiation intensity in a certain direction to the average radiation intensity [8]. It is calculated by Equation (2-9):

$$Directivity = \frac{4\pi}{\Omega_A} \tag{2-9}$$

where Ω_A is the beam solid angle given by:

$$\Omega_A = \int_{-\frac{\pi}{2}}^{\frac{\pi}{2}} \int_{0}^{\pi} |Pattern(\theta, \phi)|^2 \, sin(\theta) \, d\theta d\phi \tag{2-10}$$

Evaluating the above equations for a patch width of 0.160 inch, a length of 0.093 inch, and a substrate thickness of 0.010 inch yields a directivity of 6.065 or 7.829 dB.

2.2.3.4 Feed Design

A microstrip line feed is used because it is easy to fabricate and simple to match. It is also a design goal to use a single layer board for simplicity and to reduce manufacturing cost. Both an inset-feed and a quarter-wave transformer are considered for matching the 50 Ω impedance line to the patch. Illustrations of each feed method are showed in Figure 2-6.

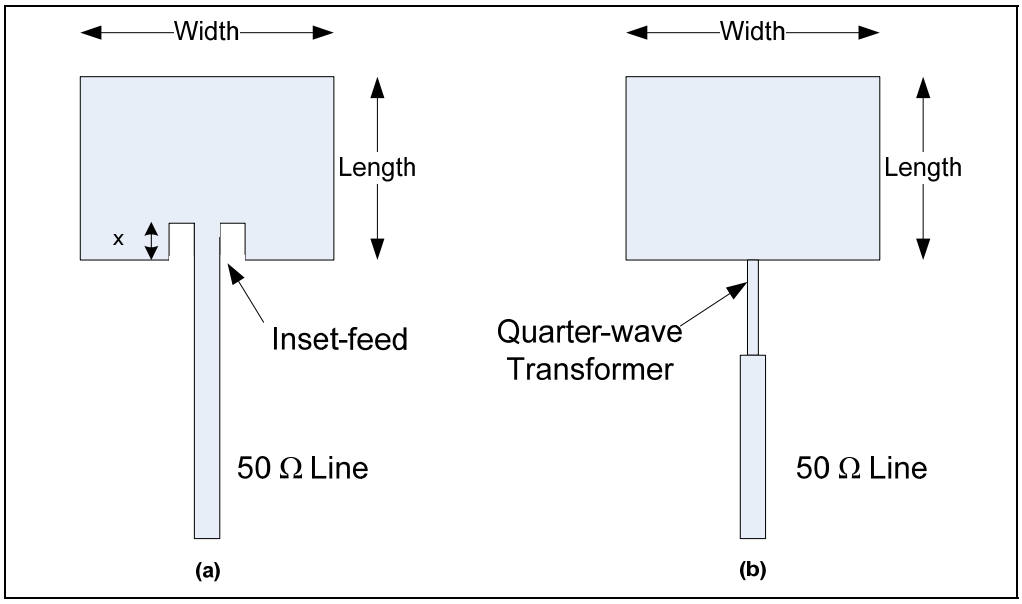

Figure 2-6. Microstrip Patch Fed by an (a) Inset-feed and (b) Quarter-wave Transformer

The advantage of using an inset-feed is that there exists an inset distance, x, which yields a 50 Ω patch input impedance, hence the patch can be directly fed by a 50 Ω line. However, the physical notches introduced by the inset-feed require a tight tolerance in order to maintain input impedance accuracy; these notches also cause cross polarization

and affect radiation pattern shape [8]. On the other hand, the quarter-wave transformer matches the patch input impedance to 50 Ω with minimal effects on the patch geometry. Use of a quarter-wave transformer maintains continuity along the width of the patch (no notches) and is therefore chosen instead of the inset-feed method.

2.2.3.5 Input Impedance of a Single Patch Antenna

In order to properly match a transmission line to the patch, its input impedance, Z_{in}, must be known. An approximate formula is given by Equation (2-11) [8].

$$Z_{in} = 90\left(\frac{\varepsilon_r^2}{\varepsilon_r - 1}\right)\left(\frac{Length}{Width}\right)^2 \tag{2-11}$$

where ε_r is 2.94, $Length$ is 0.093 inch, and $Width$ is 0.160 inch. Z_{in} is calculated to be 135.5 Ω.

Once a value for Z_{in} is obtained, the characteristic impedance of the quarter-wave transformer, Z_{qtr}, is easily calculated using Equation (2-12):

$$Z_{qtr} = \sqrt{Z_{in}Z_0} \tag{2-12}$$

where the input characteristic impedance, Z_0, is 50 Ω. A value of 82.3 Ω is obtained for Z_{qtr}.

2.2.4 Modeling a Single Patch Antenna

A single patch is modeled using Microwave Studio® Version 2009.07 (CST, Massachusetts). The dimensions of the substrate and ground plane are arbitrarily chosen to be 1 inch by 1 inch. The center of the patch is placed at the center of the board. The appropriate line widths for both the quarter-wave transformer and the 50 Ω transmission

line are calculated based on the material used and the thickness of the dielectric. The line widths of the transformer and the 50 Ω transmission line are 0.010 inch and 0.025 inch, respectively. Dimensions of the patch structure are shown in Figure 2-7.

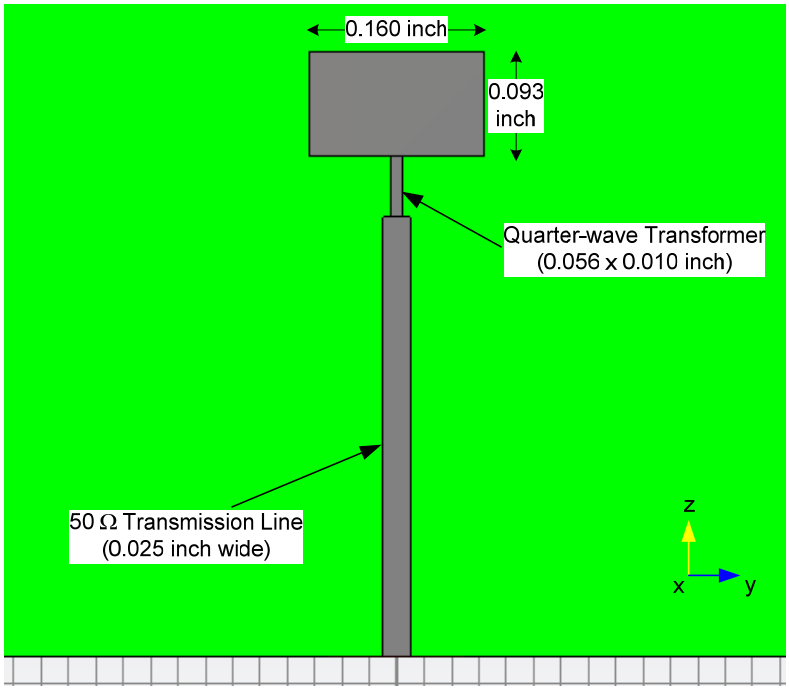

Figure 2-7. Modeled Patch Antenna with Calculated Dimensions

2.2.4.1 Simulation Parameters

A copper thickness of 0.0007 inch is used for the ground plane and patch top layer conductors in the real antenna. However, the modeled material definition used in CST Microwave Studio® is "Perfect Electric Conductor." The reason for not modeling the conductor losses is to reduce simulation times. For the substrate, RT/duroid®6002 material from Rogers Corporation is used from the CST predefined material library package.

The method of excitation is chosen to be a waveguide port. Waveguide ports are used to feed power and to absorb the returning power. Proper excitation is verified by viewing the two-dimensional electric field below the microstrip as shown in Figure 2-8.

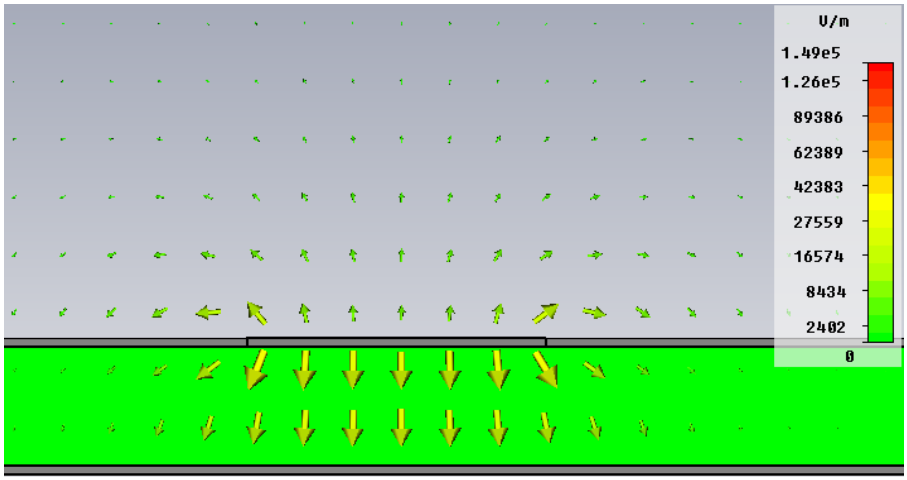

Figure 2-8. Simulated Electric Field at the Excitation Port

The electric field lines behave as expected for a microstrip transmission line, therefore successful port excitation has been accomplished.

In order to perform simulations, CST requires the selection of boundary conditions to create a finite geometry. The boundary conditions recommended for antenna simulations are "open (add space)." This boundary behaves similar to that of free space, where waves pass through with minimal reflections. The added space is used for far-field calculations. An example of the "open (add space)" boundary type is shown in Figure 2-9.

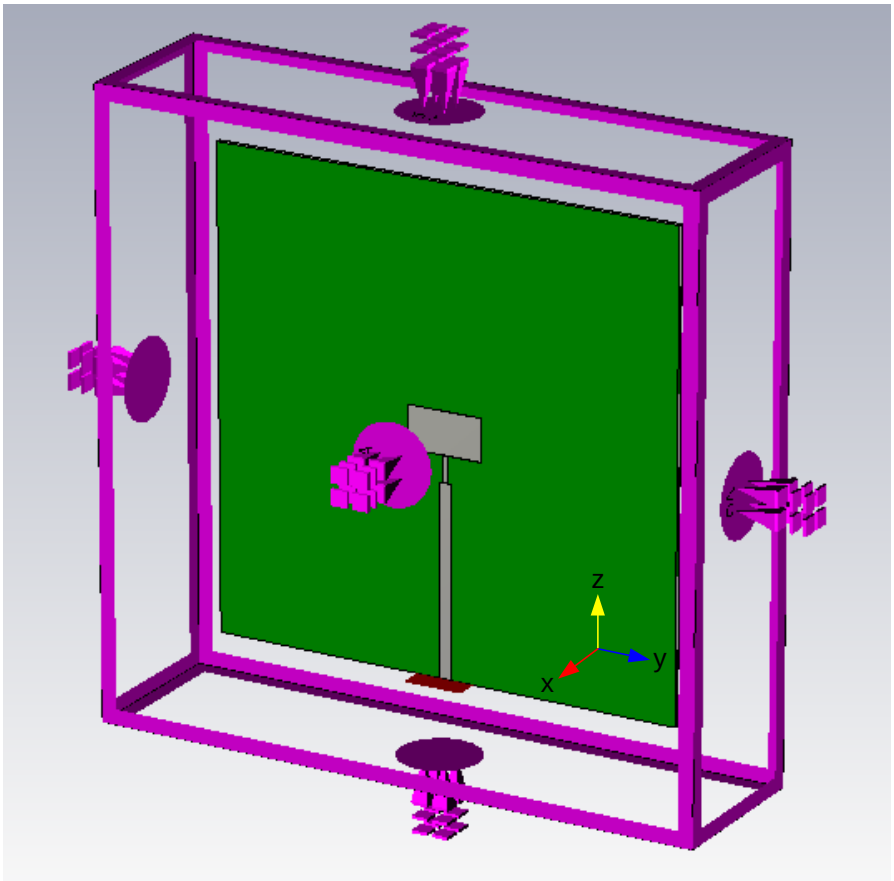

Figure 2-9. Example of CST's "Open (Add Space)" Boundary Condition

A transient solver is used because it can perform broadband simulations much faster than the frequency domain solver; the reason for this is the frequency solver requires a new simulation run for each frequency sample whereas the transient solver stimulates the structure using a broadband signal [9]. The transient solver calculates the development of fields through time at discrete locations and time samples. In addition to being able to solve for S-parameters, the electromagnetic field patterns at various desired frequencies are obtained from only one calculation run.

Another feature of the software is the use of adaptive mesh refinement. For each simulation, multiple passes are performed with each pass having an increasing number of

mesh cells. The mesh refinement strategy used is energy based; the energy density distribution within the structure from a pass is used to refine the mesh in regions with high energy density for the following pass. The factor for mesh cell increases is set by the user and determines how many new cells are introduced between two subsequent passes. The value of this factor used for the patch antenna simulations is 0.7, hence the number of mesh cells increases by 70% from pass to pass. Though accuracy improves with increasing number of mesh cells, the solver time also increases.

2.2.4.2 Model Iterations

For all model iterations, two significant performance results are considered: the return loss to ensure a good match and the far-field radiation pattern to ensure acceptable half power beamwidths. Figure 2-10 shows the return loss for the antenna shown in Figure 2-7. The adaptive meshing feature is used, and convergence is reached by pass 6. The return loss of the antenna reveals a good match (less than -20 dB at resonance); however, the resonance is at a lower frequency than desired, 33.67 GHz versus the design frequency of 34.965 GHz. The shift of about 1.3 GHz in resonant frequency is perhaps due to fringing fields increasing the length of the patch more than the approximation taken into account in Equation (2-4).

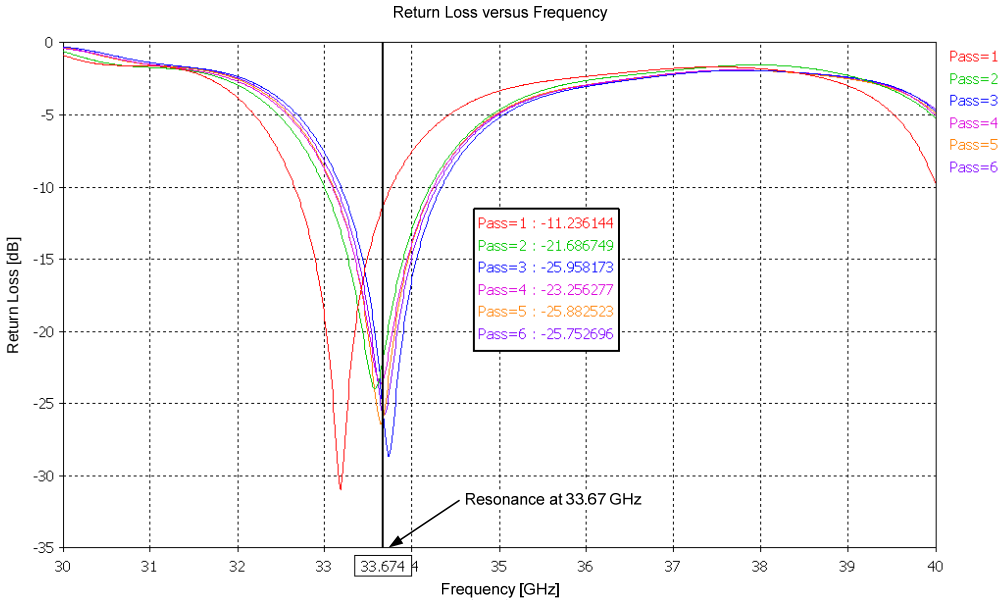

Figure 2-10. Return Loss for a Patch of Length 0.093 inch (Figure 2-7)

The resulting radiation pattern shown in Figure 2-11 is a 3-dimensional visualization of the far-field pattern for the antenna at the design frequency of 34.965 GHz; two-dimensional E- and H-plane cross-sectional patterns are shown in Figure 2-12 and Figure 2-13, respectively.

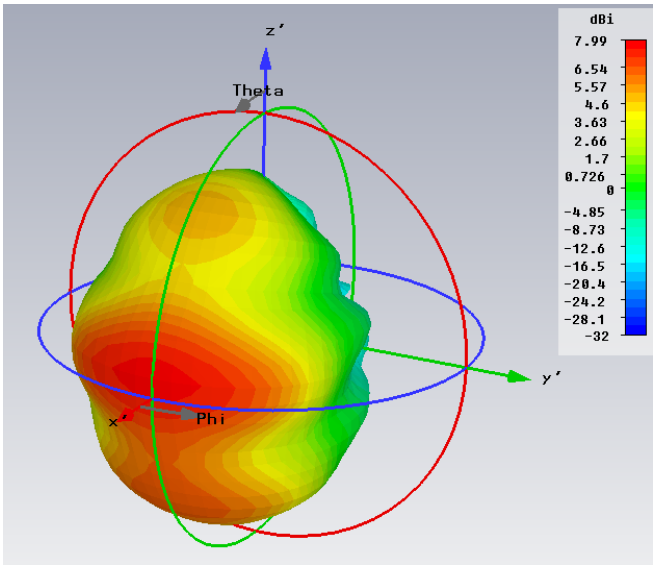

Figure 2-11. Radiation Pattern for a Patch of Length 0.093 inch (Figure 2-7)

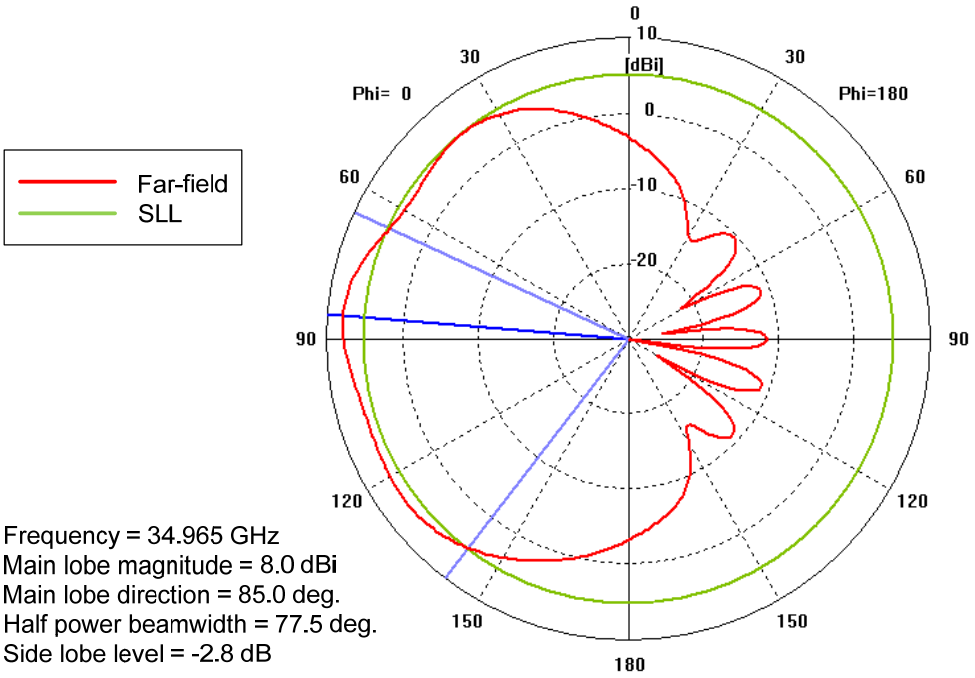

Frequency = 34.965 GHz
Main lobe magnitude = 8.0 dBi
Main lobe direction = 85.0 deg.
Half power beamwidth = 77.5 deg.
Side lobe level = -2.8 dB

Figure 2-12. E-plane Pattern for a Patch of Length 0.093 inch (Figure 2-7),

$$\phi=0°,\ 0° < \theta < 180°$$

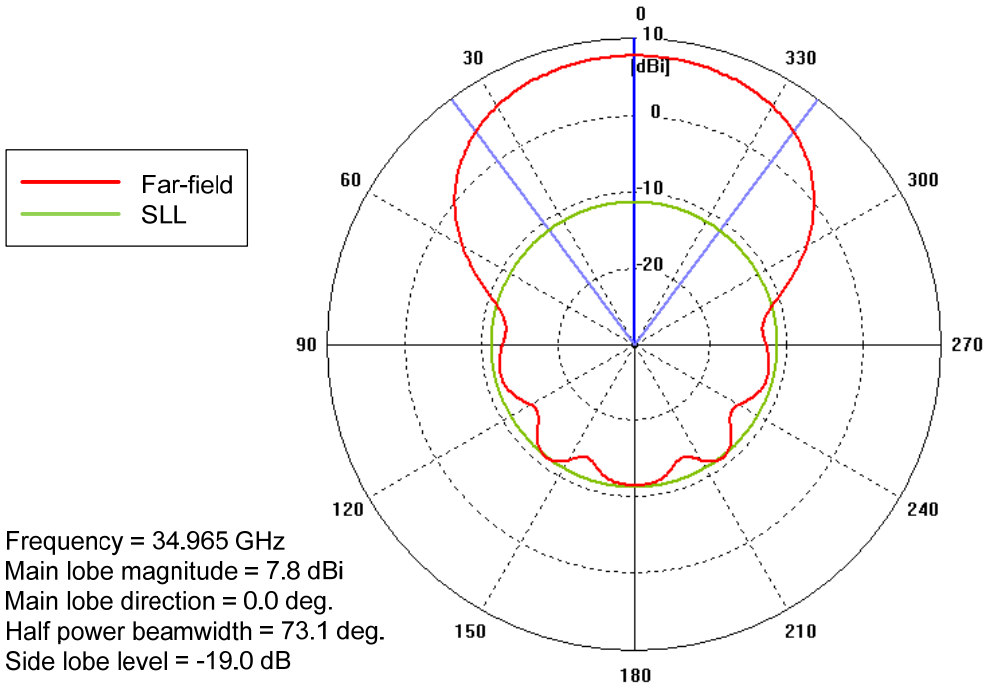

Frequency = 34.965 GHz
Main lobe magnitude = 7.8 dBi
Main lobe direction = 0.0 deg.
Half power beamwidth = 73.1 deg.
Side lobe level = -19.0 dB

Figure 2-13. H-plane Pattern for a Patch of Length 0.093 inch (Figure 2-7),

$$0° < \phi < 360°,\ \theta = 90°$$

The peak directivity of 8 dBi is in agreement with well known values for thin substrates with low relative permittivity [3] and is also very close to the theoretical directivity obtained from Equation (2-9). The E-plane pattern shape shows a very subtle ripple, which is believed to be caused by the input microstrip feed line. Besides the ripple, the principal plane patterns agree with the calculated E- and H-plane patterns shown in Figure 2-5. Table 2-3 is a comparison between the patch theoretical and simulated characteristics.

Table 2-3. Theoretical versus Simulated Patch Characteristics for a Single Patch of Length 0.093 inch

	Calculated	Simulated	% Difference
Peak directivity (dBi)	7.8	8.0	4.6%
E-plane half power beamwidth	128º	77.5º	50%
H-plane half power beamwidth	73º	73.1º	0.1%

The main reason for the large difference between the calculated E-plane half power beamwidth and the simulated result is due to the subtle ripple in the E-plane pattern curve. This results in a half power level at an angle of 65º instead of 40º. Because the H-plane pattern behaves so closely to the theoretical value, the distortion in the E-plane pattern (ripple) is most likely caused by the microstrip feed line which runs directly along the E-plane. This speculation is confirmed after a quick simulation was executed with a reduced feed line length.

Because the initial computation of patch resonance frequency is inaccurate (required design value of 34.965 GHz), adjustments are made to the model. The length

of the patch is reduced in order to move the resonant frequency to a center frequency of 34.965 GHz. While maintaining all other dimensions constant, the patch length is iteratively reduced until resonance is achieved at the center frequency. The final acceptable length is 0.089 inch and the resulting return loss is shown in Figure 2-14 along with markers at the minimum and maximum edges of the frequency band. The return loss over the desired bandwidth is less than -20 dB.

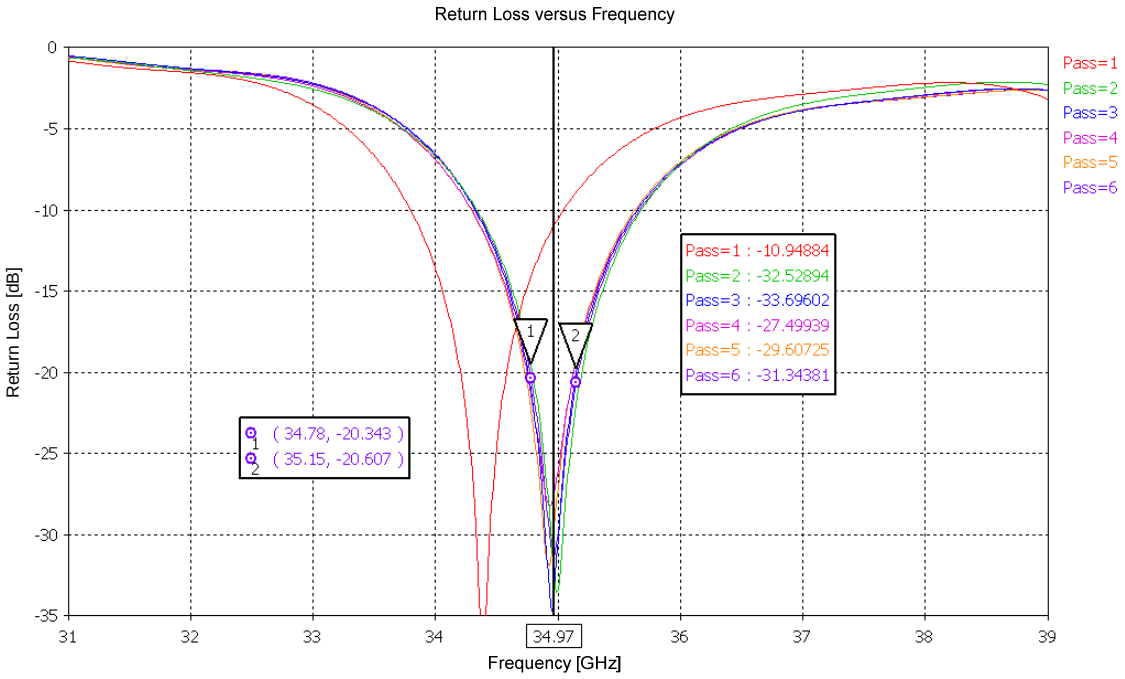

Figure 2-14. Return Loss for the Patch of Length 0.089 inch with a Resonant Frequency of 34.965 GHz

Comparing the corresponding far-field radiation pattern of Figure 2-15 to the pattern for the 0.093 inch patch (Figure 2-11) shows that there is no difference in the peak directivity of a single patch as the resonant length is varied slightly. E- and H-plane patterns are provided in Figure 2-16 and Figure 2-17, respectively.

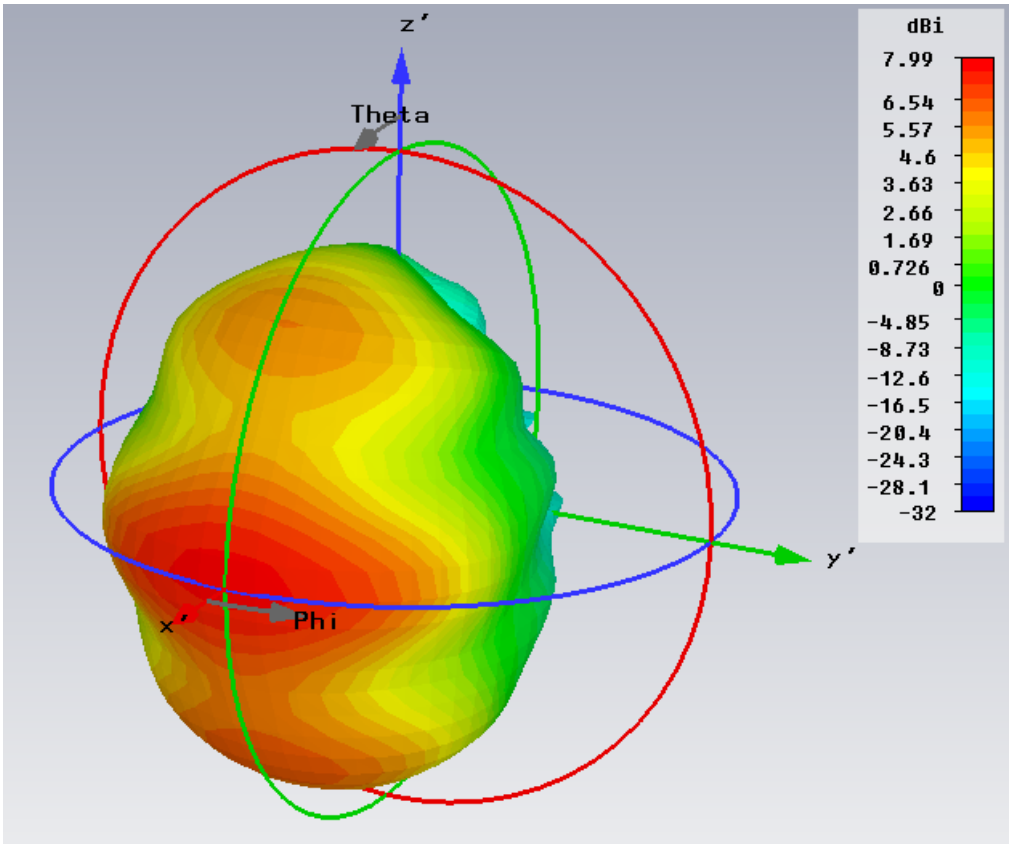

Figure 2-15. Radiation Pattern for a Patch of Length 0.089 inch with a Resonant Frequency of 34.965 GHz

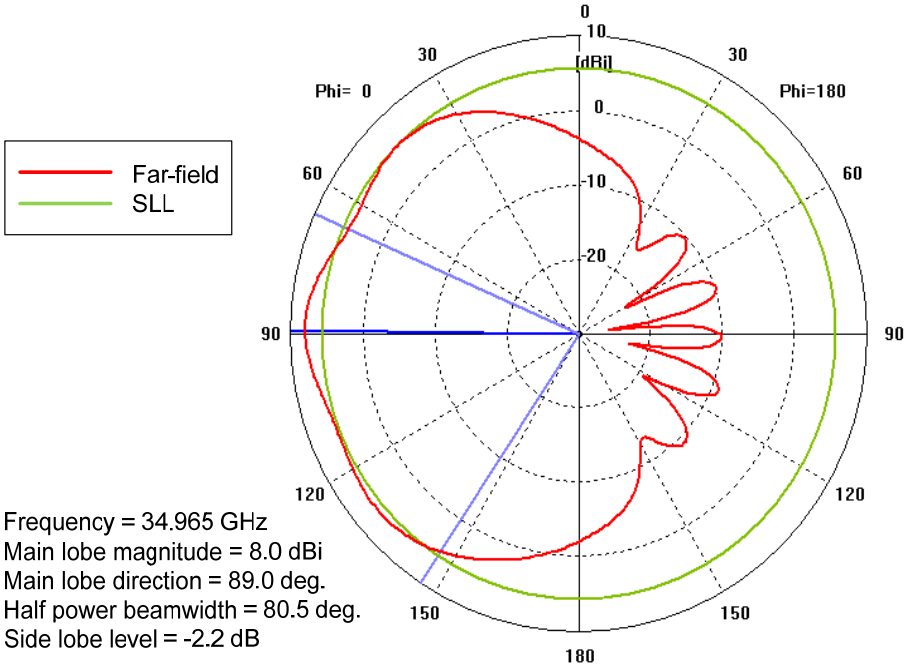

Figure 2-16. E-plane Pattern for a Patch of Length 0.089 inch with a Resonant Frequency of 34.965 GHz,

$\phi=0°, 0° < \theta < 180°$

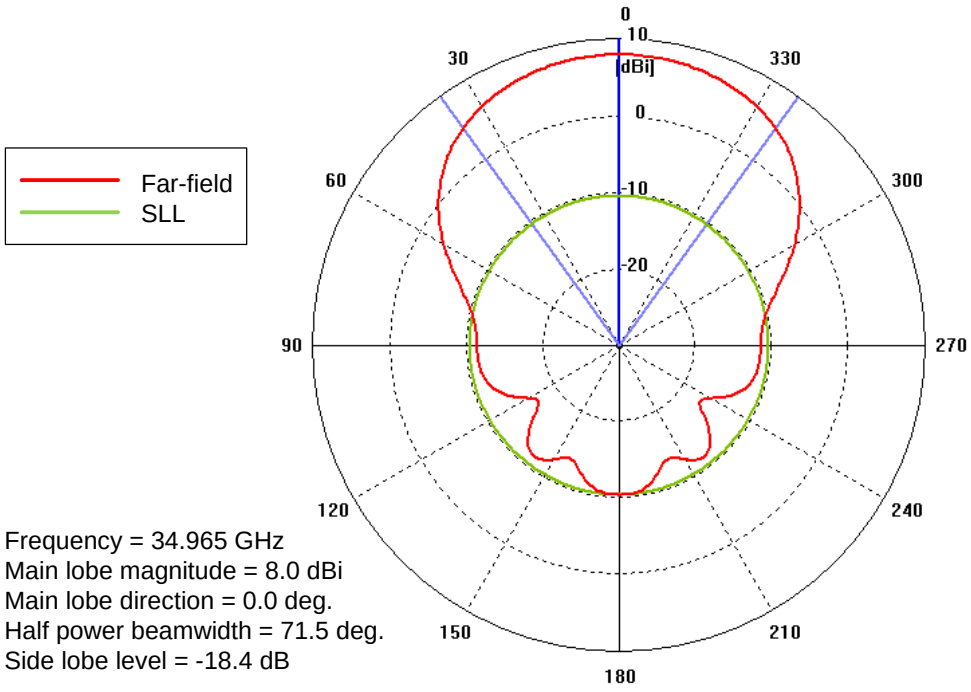

Figure 2-17. H-plane Pattern for a Patch of Length 0.089 inch with a Resonant Frequency of 34.965 GHz,

$0° < \phi < 360°, \theta = 90°$

2.2.5 Two-element Array Design

The broad beam pattern of the single patch in the H-plane has a 3 dB beamwidth of 73.1º (simulated) and achieves the desired performance (greater than 60º). The beamwidth in the E-plane (77.5º) for the single patch, however, is too wide. In order to reduce the beamwidth in the E-plane, a linear array of two or more elements is needed along the vertical axis (z-axis). The pattern of a two-element linear array is first calculated to determine if only 2 array elements would meet the desired antenna performance. Two isotropic point sources spaced one-half wavelength apart and with identical amplitude and phase currents are assumed. The array factor, AF, is obtained using Equation (2-13) [8]:

$$AF(\theta) = \frac{sin\left(n\frac{\psi(\theta)}{2}\right)}{n\,sin\left(\frac{\psi(\theta)}{2}\right)} \tag{2-13}$$

where $\psi(\theta) = \beta d cos(\theta) + \alpha$, d is the element spacing $\left(\frac{\lambda_0}{2}\right)$, β is the wave number $\left(\frac{2\pi}{\lambda_0}\right)$, α is the phase shift between elements, n is the number of elements in the array and $0 < \theta < \pi$.

Figure 2-18(a) and Figure 2-18(b) show the element pattern and the array factor for a two-element array, respectively. Figure 2-19 is the resulting pattern for a two-element array with elements spaced one-half wavelength apart. Only the elevation cuts (E-plane) are shown.

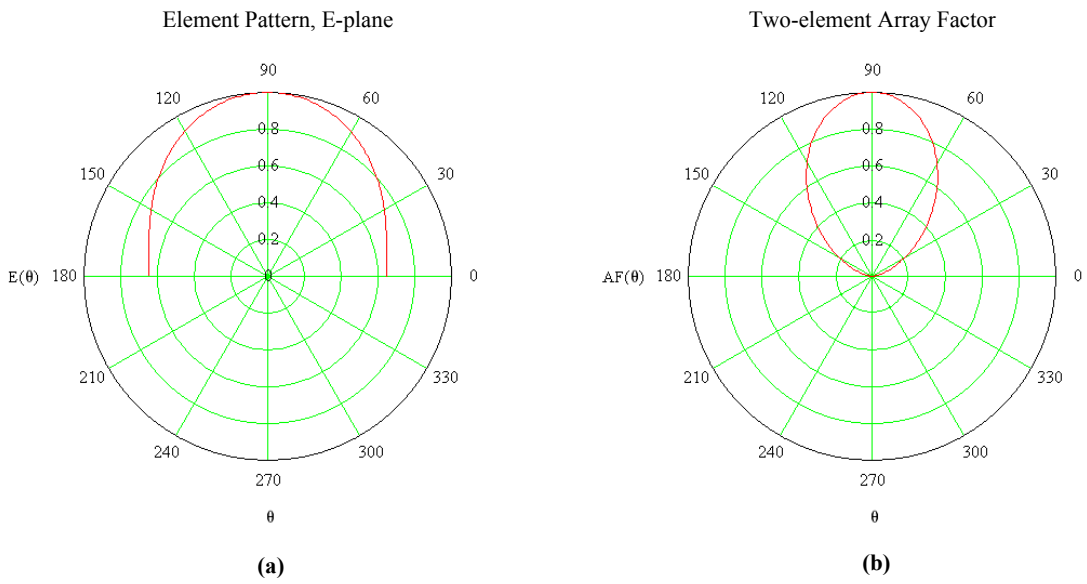

Figure 2-18. (a) Normalized Element Pattern (E-plane) and (b) Array Factor of a Two-element Array Consisting of Isotropic Sources of Equal Amplitude and Phase Currents Spaced Half a Wavelength Apart

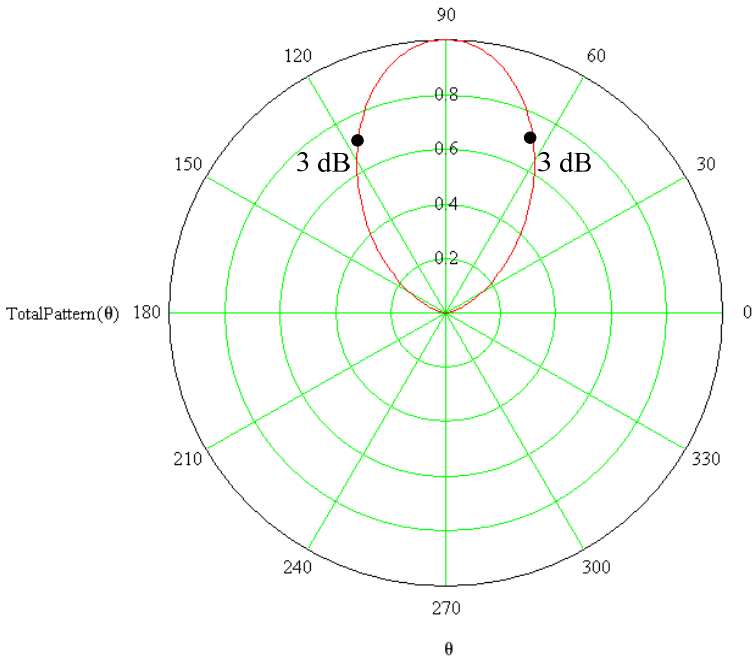

Figure 2-19. Normalized E-plane Pattern (Element Pattern x Array Factor) for a Two-element Array of Microstrip Patches

The 3 dB points occur at angles ±27º from broadside. This is within the desired half power beamwidth ($\pm 15^{\circ} \leq \theta_{3dB} \leq \pm 30^{\circ}$); therefore, a two-element linear array meets the radiation pattern desired performance of the low gain antenna shown in Table 2-1.

The same equations used for calculating the directivity of a single patch (Equations (2-9) and (2-10)) are used to approximate the directivity of the two-element array. The pattern factor, $Pattern(\theta, \phi)$, must be replaced by the Total Pattern, which is the pattern factor for a single element obtained from Equation (2-6) multiplied by the linear array factor given by Equation (2-13). The theoretical directivity is calculated to be 10.47 or 10.20 dBi.

For the two-element array, the length and width of the patches are kept the same as that of the single patch model (0.089 inch and 0.160 inch, respectively). The center-to-center spacing of the patches is designed to be half the free space wavelength. The half-wavelength is approximately 0.169 inch at the center frequency of 34.965 GHz, hence a spacing of 0.169 inch is chosen.

2.2.5.1 Initial Designs – Corporate Feed Network

A corporate feed network is used to feed the structure. The design consists of a 50 Ω feed line centered on the board to later accommodate a connector, but then it is routed left of the array where a microstrip T-junction is used to feed the two patches with equal length transmission lines, as illustrated in Figure 2-20.

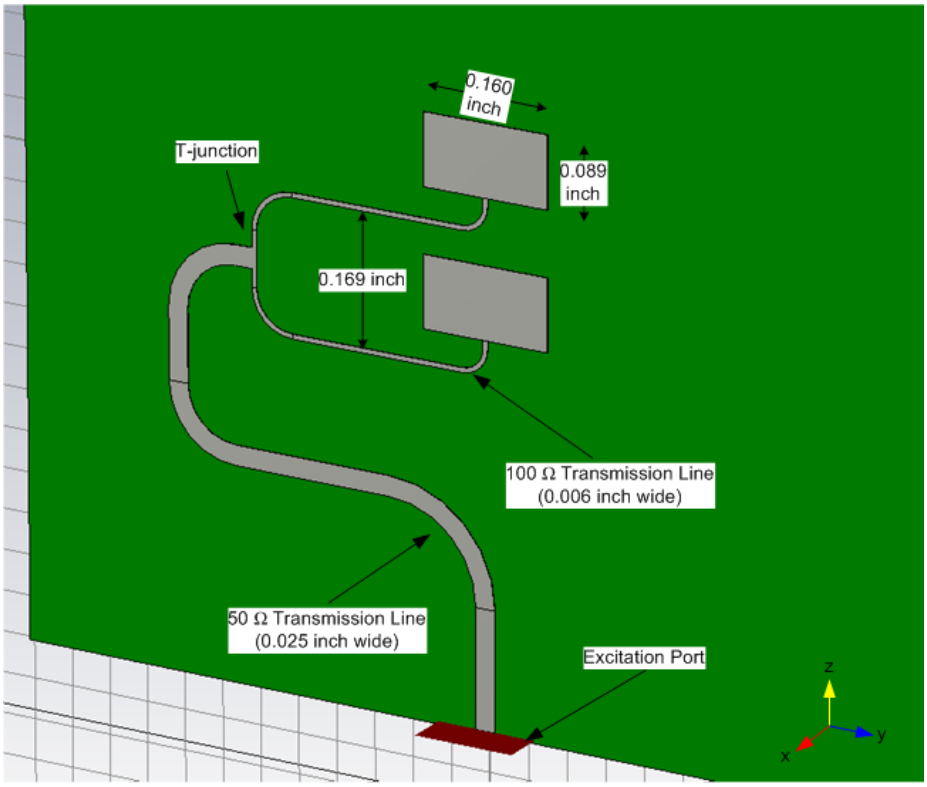

Figure 2-20. Two-element Array with a T-junction Corporate Feed and 0.169 inch Patch-to-Patch Spacing

Because of equal line lengths to each element in the patch, the corporate feed allows for good amplitude and phase tracking with frequency [7]. A simple power splitter provides equal amplitude and phase to both patches regardless of frequency.

The array depicted in Figure 2-20 is modeled in CST Microwave Studio and a far-field radiation pattern is obtained (Figure 2-21). The number of mesh cells automatically generated by the software is about 443,000. The vertically polarized pattern results show distortion and unexpected side lobes that do not achieve the desired performance of the antenna. Although the peak directivity, 9.76 dBi, is to within 0.5 dBi of the expected directivity (10.20 dBi), the side lobe level (SLL) is not at an acceptable value as a large side lobe is present 90º from broadside along the vertical (+z) axis.

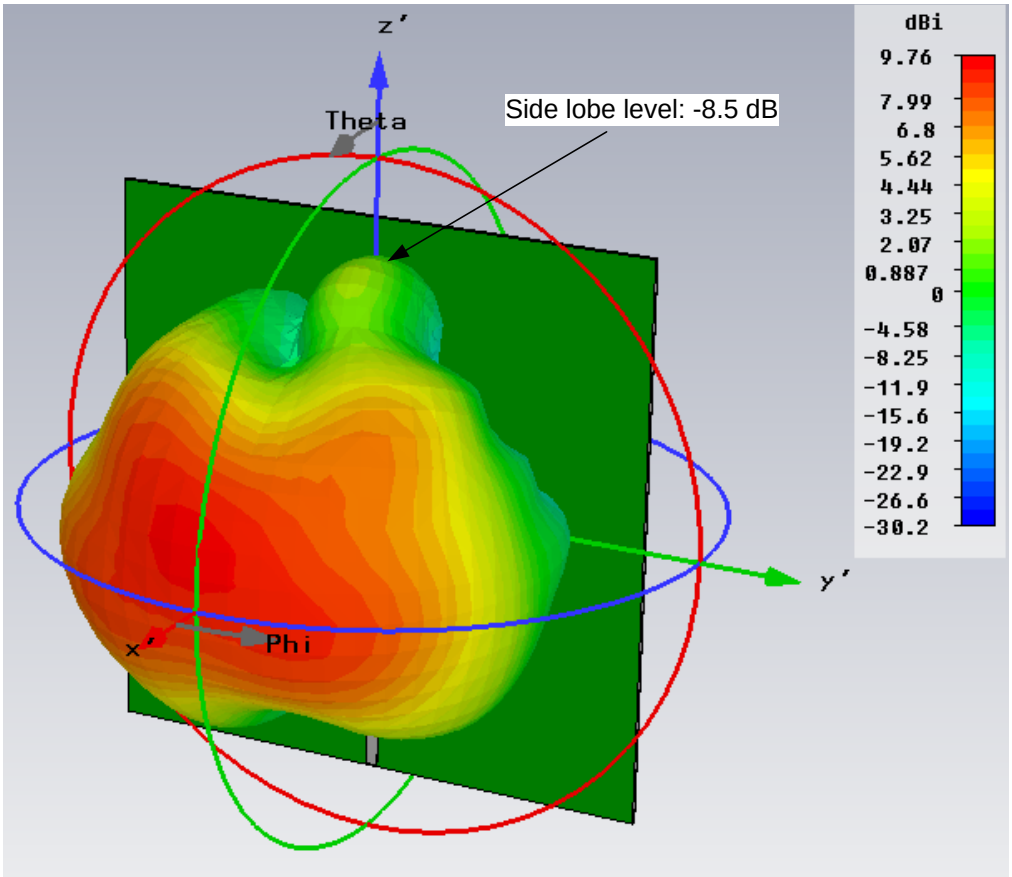

Figure 2-21. Radiation Pattern for a Two-element Array with a T-junction Corporate Feed and 0.169 inch Patch-to-Patch Spacing

The side lobe level desired performance is -20 dB, hence the first iteration is not acceptable. The next step is to determine the cause of this unwanted side lobe in order to eliminate it. Array theory shows that for an array of N elements, there will be N-2 side lobes [8]. Therefore, the two-element array should have zero side lobes and because it doesn't, there is a disagreement between the theoretical far-field pattern and the simulated pattern. The theoretical radiation pattern does not account for any radiation resulting from the feed network; hence changes to the model are made in order to determine what the feed line effects are on the radiation pattern. The effects of element spacing variations, 50 Ω line length variations, adjustments to the proximity of the T-

junction to the elements, and replacement of the T-junction with a Y-junction are all investigated.

2.2.5.1.1 Element Spacing Variations

One of the major disadvantages of feeding patch arrays with microstrip lines is that the feed lines themselves radiate [9]. Hence, the cause of the pattern distortion was originally thought to be radiation and interference due to the 100 Ω feed lines with the 90º bends feeding the patches. A first attempt at reducing the side lobe is to vary the spacing between the two patches.

The element spacing of the array is reduced in order to have a better understanding of the effect of the 100 Ω line bends on the radiation pattern, thereby decreasing the bend radius of the 90º bends feeding the patches. A reduction in spacing should also decrease the level of minor lobes in the array factor [5]. The spacing is reduced to 0.160 inch (Figure 2-22), and Figure 2-23 shows the corresponding radiation pattern. The results show an increase in SLL and distortion; hence reducing the spacing does not improve performance.

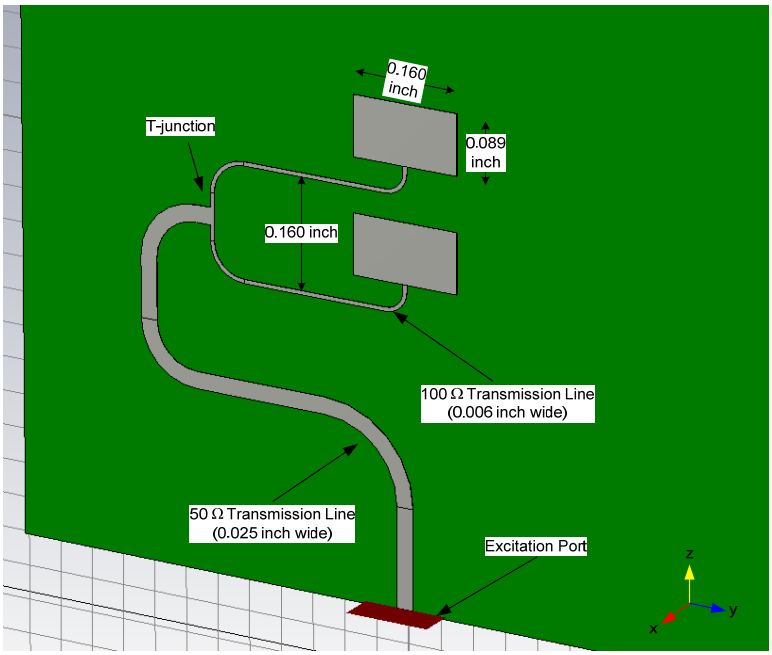

Figure 2-22. Two-element Array with a T-junction Corporate Feed and 0.160 inch Patch-to-Patch Spacing

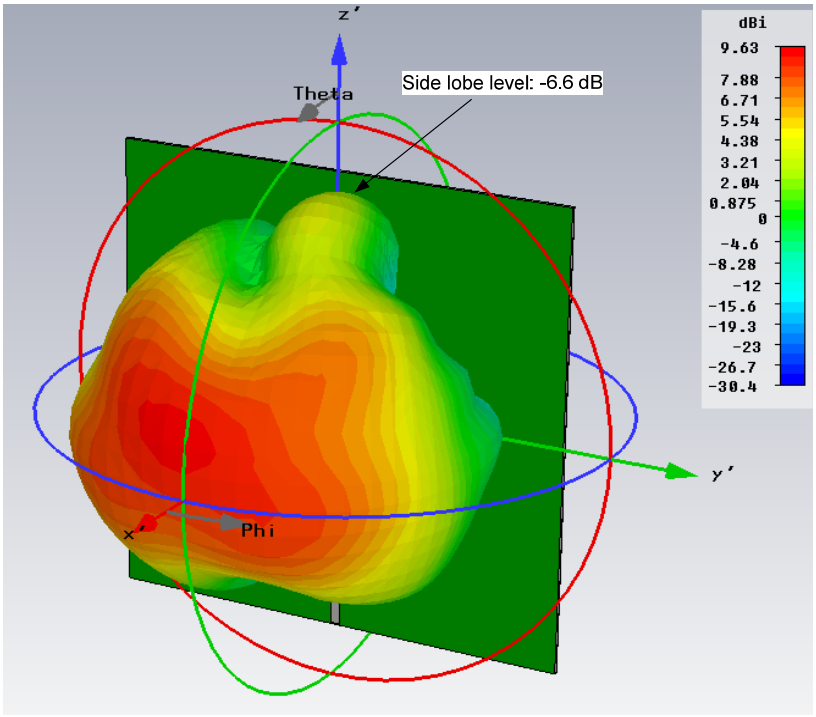

Figure 2-23. Radiation Pattern for a Two-element Array with a T-junction Corporate Feed and 0.160 inch Patch-to-Patch Spacing

The next option explored is to increase the spacing to see what the effects are on the pattern. The spacing is increased to 0.181 inch, thereby, *increasing* the bend radius and reducing radiation from the microstrip line. This is modeled (Figure 2-24) and a vertical polarization radiation pattern is obtained (Figure 2-25).

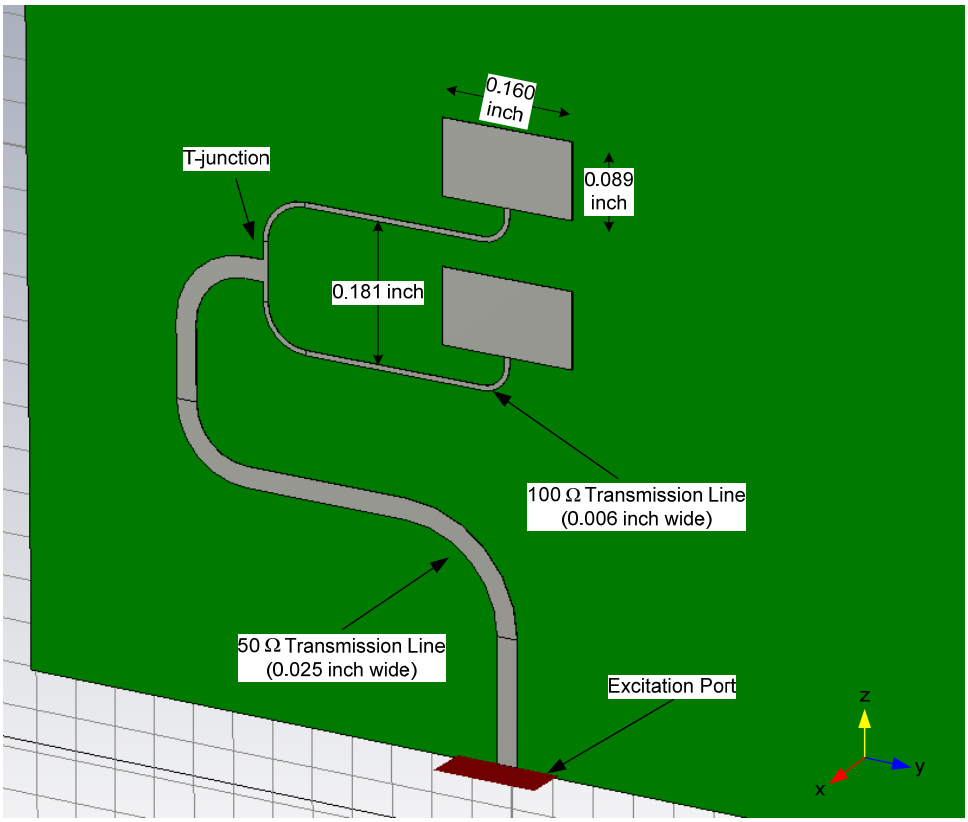

Figure 2-24. Two-element Array with a T-junction Corporate Feed and 0.181 inch Patch-to-Patch Spacing

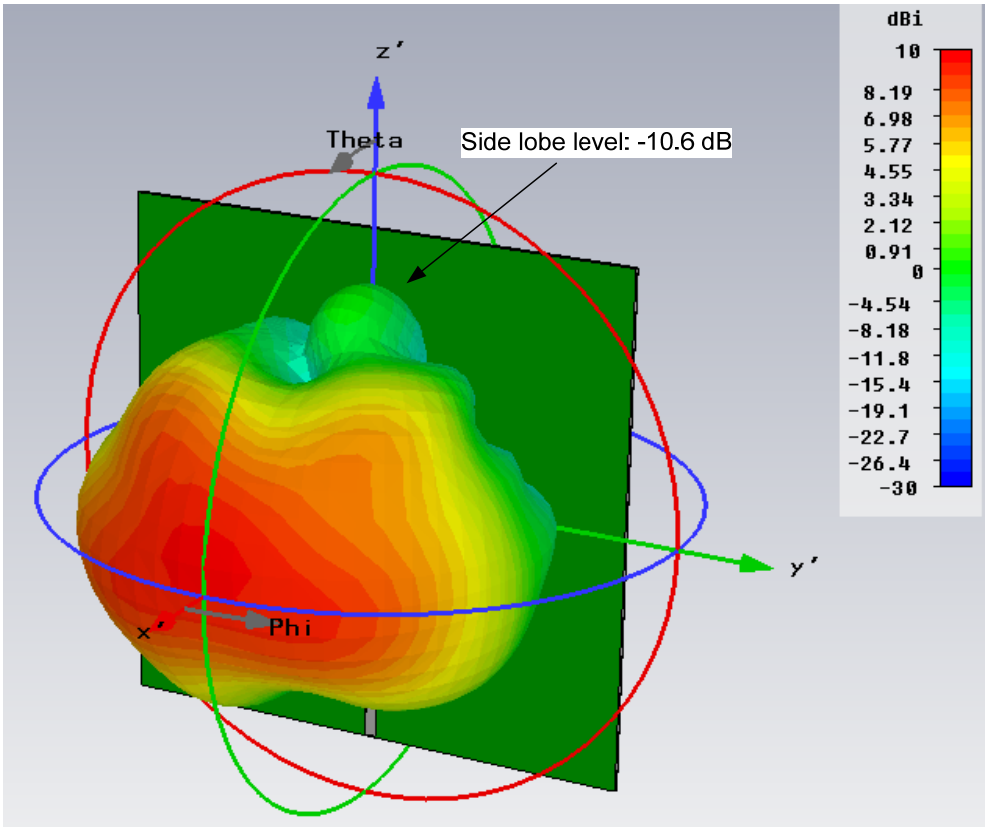

Figure 2-25. Radiation Pattern for a Two-element Array with a T-junction Corporate Feed and 0.181 inch Patch-to-Patch Spacing

The SLL is reduced by increasing the element spacing of the array; however, in order to bring the SLL down enough to achieve the desired performance, the spacing approaches values on the order of one wavelength. This results in grating lobes [5]. Also, despite the improvement of one side lobe, other areas of the pattern continue to appear distorted. Adjustment of the element spacing alone does not achieve the desired SLL, therefore other modifications are considered in the design.

2.2.5.1.2 Moving the 50 Ω line further away from the array

The next possible cause of radiation from the feed network is the center-fed 50 Ω line, and its first bend away from the array elements. A new model is created which

increases the vertical dimension of the board along the z-axis (Figure 2-26). All other parameters of the array are held constant (e.g. element spacing remained 0.169 inch) except the 50 Ω bend is moved 0.250 inch further away from the array. The pattern for this design is shown in Figure 2-27.

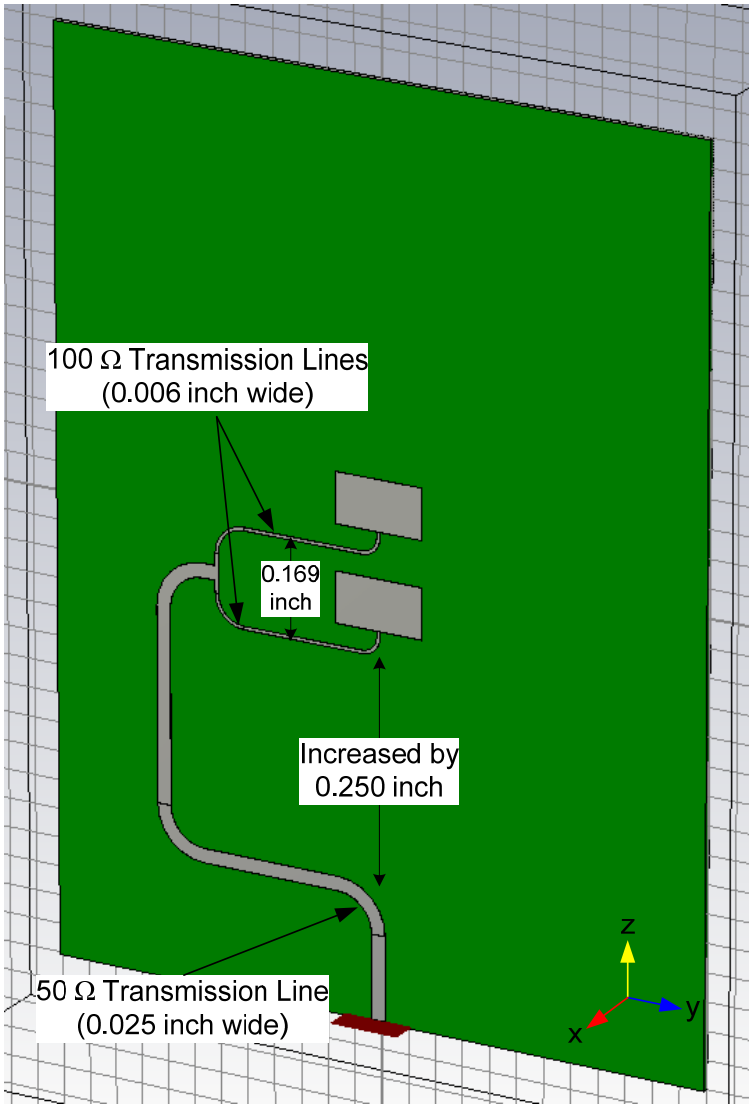

Figure 2-26. Two-element Array with a T-junction Corporate Feed and 50 Ω Bend Moved Further Away from the Array

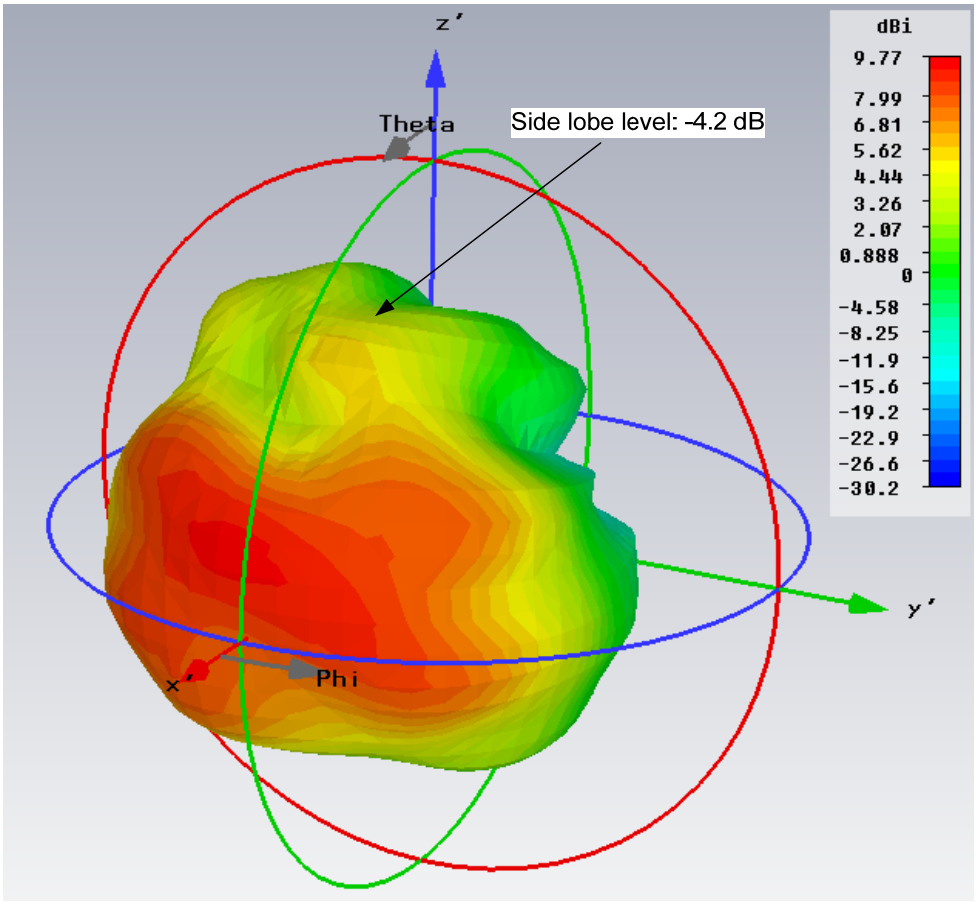

Figure 2-27. Radiation Pattern for a Two-element Array with a T-junction Corporate Feed and 50 Ω Bend Moved Further Away from the Array

When comparing Figure 2-27 to Figure 2-21, moving the microstrip feed transmission line away from the array causes more distortion of the pattern and a worse SLL.

2.2.5.1.3 Proximity of the T-junction

Applying the information obtained from the antenna in Figure 2-26, where moving the microstrip lines further away from the array elements makes performance worse, it is thought that moving the T-junction *closer* would perhaps improve radiation pattern distortion. The distance from the patches to the T-junction (less bends) is 0.220 inch. The same model file shown in Figure 2-20 is modified so that the 100 Ω feed lines

are reduced in length by 0.050 inch giving a spacing of 0.170 inch as shown in Figure 2-28.

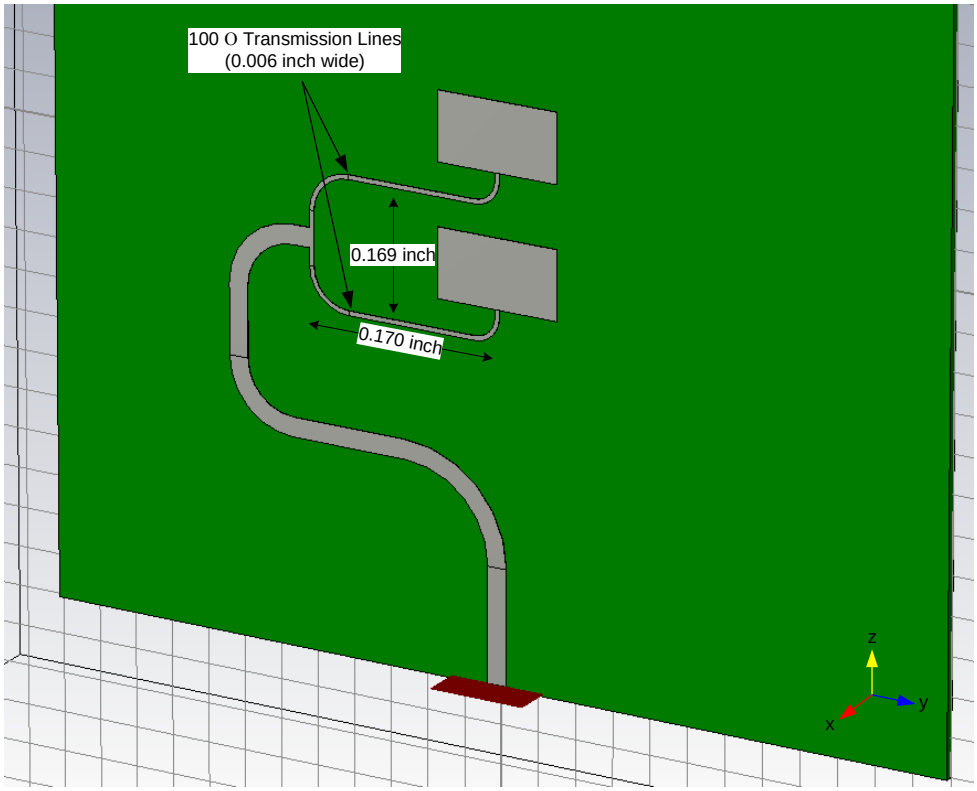

Figure 2-28. Two-element Array with the T-junction Moved Closer to Array Elements by 0.050 inch (0.170 inch Spacing to Patches)

The corresponding simulated radiation pattern is shown in Figure 2-29. There is a 5.8 dB improvement in SLL and the pattern appears to have less distortion compared to the results of the original configuration (Figure 2-27); though, the SLL does not yet achieve the desired SLL.

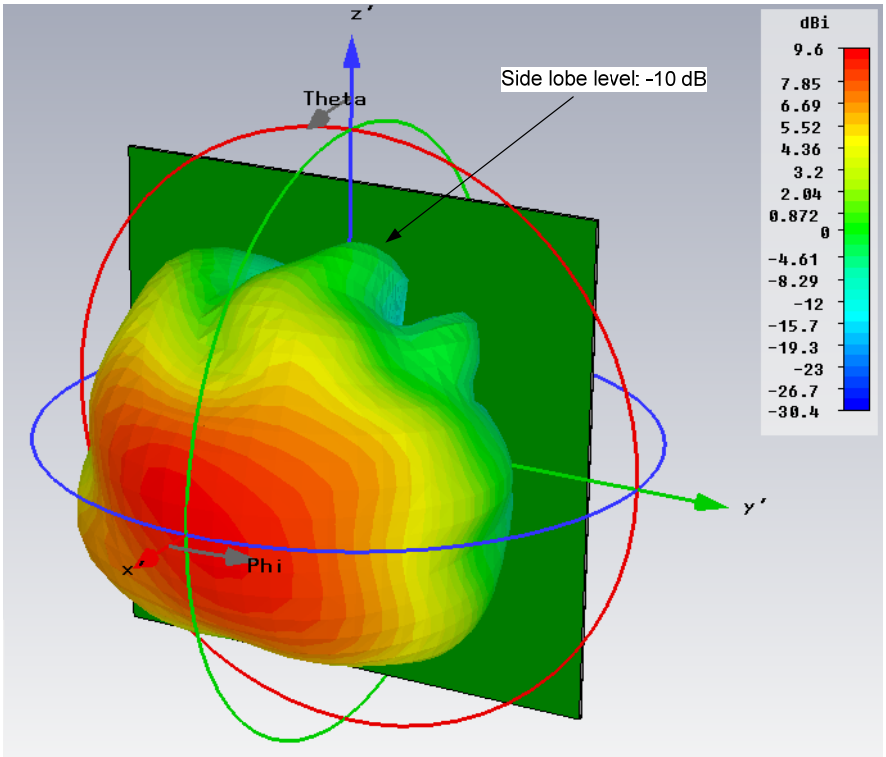

Figure 2-29. Radiation Pattern for a Two-element Array with the T-junction Moved Closer to Array Elements by 0.050 inch (0.170 inch Spacing to Patches)

It is anticipated that moving the T-junction even closer will lead to better results. The 100 Ω line length is successively reduced by 0.075 inch and 0.100 inch, respectively, and the corresponding radiation patterns are shown in Figure 2-30 and Figure 2-31, respectively.

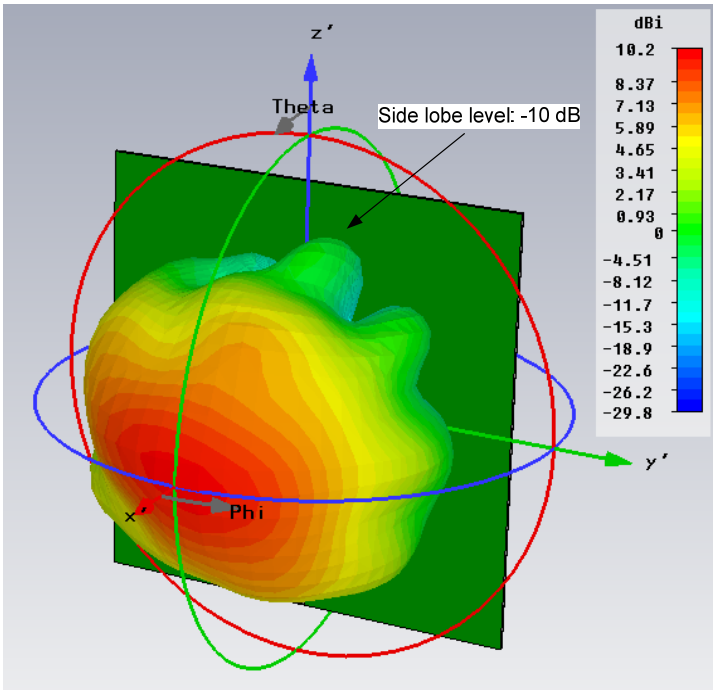

Figure 2-30. Radiation Pattern for a Two-element Array with the T-junction Moved Closer to Array Elements by 0.075 inch (0.145 inch Spacing to Patches)

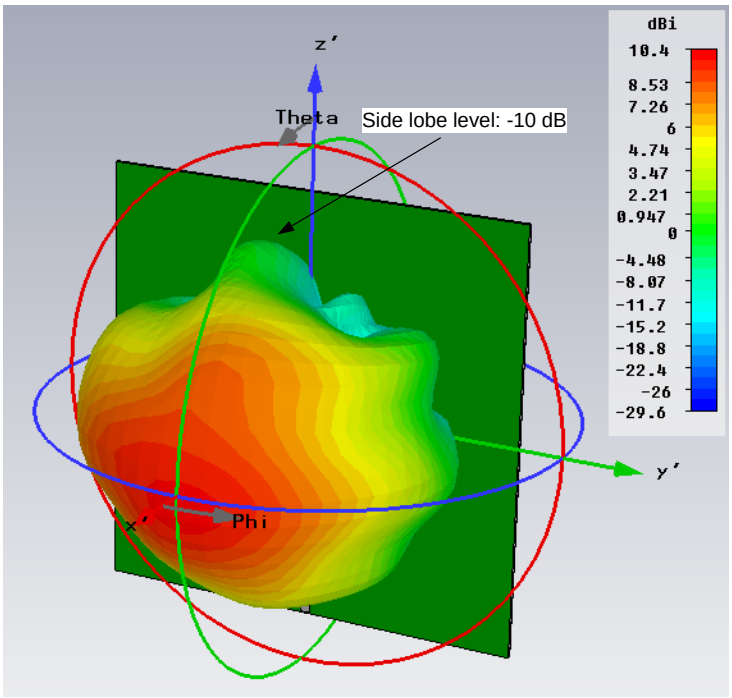

Figure 2-31. Radiation Pattern for a Two-element Array with the T-junction Moved Closer to Array Elements by 0.100 inch (0.120 inch Spacing to Patches)

It is noted that the SLL in both figures remains at -10 dB; however, the location of the side lobe moves from the right of the +z axis to the left of the +z axis with a 0.025 inch difference in T-junction proximity to the patches. Despite an improved pattern compared to the pattern of the original corporate feed design (directivity increased from 9.76 dBi to 10.4 dBi and SLL reduced from -8.5 dB to -10 dB), radiation greater than -15 dB from the peak directivity is still present 90º from broadside in the vertical axis.

2.2.5.1.4 Replacing the T-junction with a Y-junction

Another design consideration to achieve an improved radiation is to replace the T-junction splitter with a Y-junction splitter that has been shown to radiate less than the T-junction [10]. The resulting geometry is shown in Figure 2-32. Using the previous results obtained from the positioning of the T-junction with respect to the array elements, only models with distances of 0.145 and 0.120 inch from the Y-junction to the patches are simulated, as short microstrip lines have lower radiation pattern distortion.

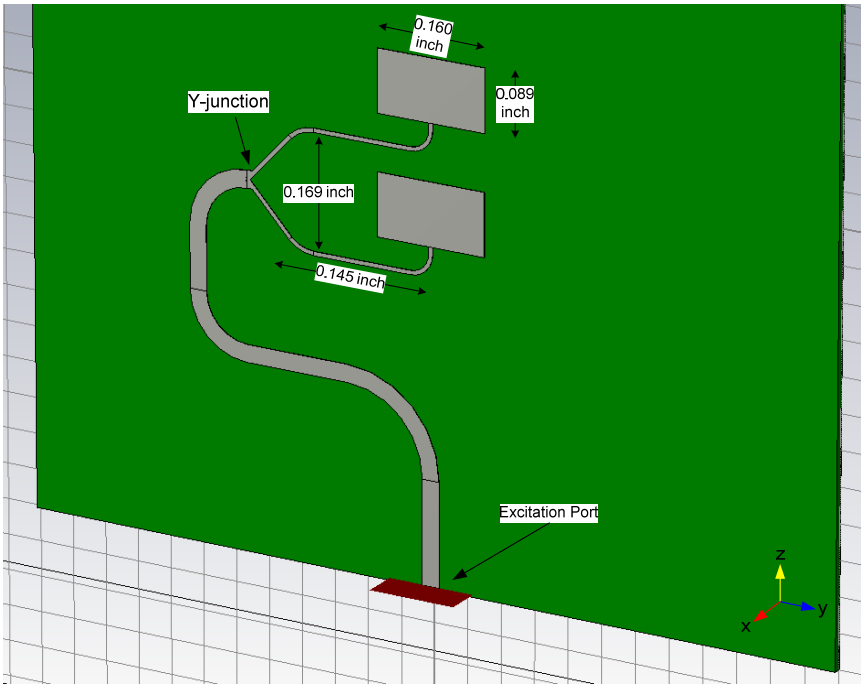

Figure 2-32. Two-element Array with the Y-junction Located 0.145 inch Away from the Array Elements

The corresponding radiation patterns are shown in Figure 2-33 and Figure 2-34, respectively.

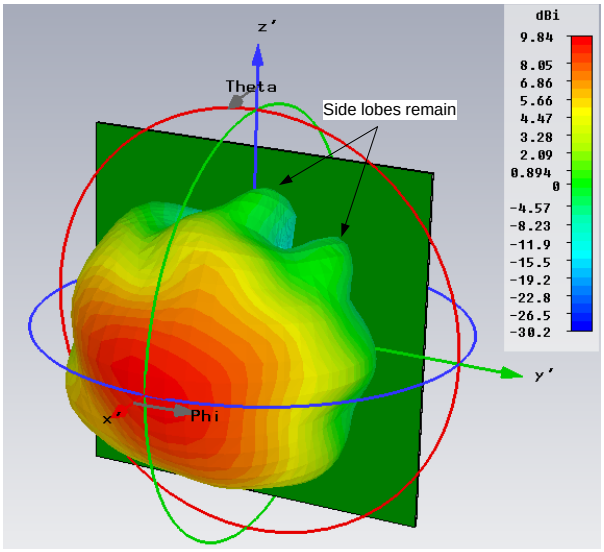

Figure 2-33. Radiation Pattern for a Two-element Array with the Y-junction Located 0.145 inch Away from the Array Elements

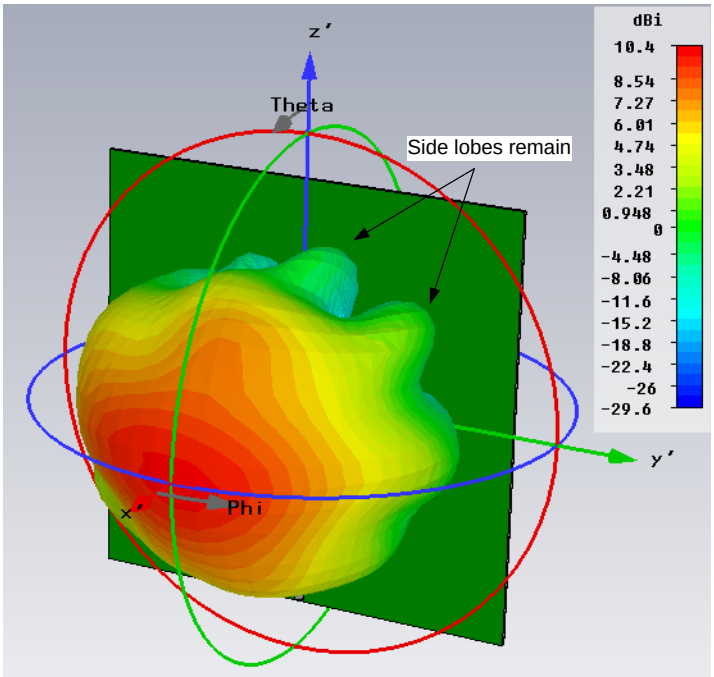

Figure 2-34. Radiation Pattern for a Two-element Array with the Y-junction Located 0.120 inch Away from the Array Elements

Both figures show no signs of improvement of the pattern as the SLLs remain at about -10 dB. Although it was known early in the design that corporate feed networks radiate and can affect the radiation pattern, the aforementioned modeling results are evidence of the severity of the distortion. Hence, it is decided to abandon the corporate feed and use another approach to achieve the desired performance of the antenna.

2.2.5.2 Design Change to a Series-Fed Array

Series-fed arrays are typically not used when the number of elements in the array is too large, as the elements furthest from the feed line do not receive the same power as the elements nearer the feed line due to losses in the transmission line connecting the elements. Series-fed arrays are simpler and require less space on the board when compared to corporate fed arrays [7].

A very basic series-fed array is modeled to determine if there is less pattern distortion than in the case of the corporate fed array. A direct-coupled feed is used. The transmission line connecting the two patches is designed with a width as thin as practical to minimize the disturbance of the fields in the slots [11]. A 0.006 inch width is used; smaller widths begin to approach the limits of fabrication. The line is curved or meandered to reach a line length of half a wavelength in the dielectric in order to achieve the same phase excitation for both patches in the array. A line length of 0.0926 inch is achieved. The array is matched to 50 Ω using a quarter wave transformer similar to the case of the single patch modeled in Section 2.2.4. The length of each patch is 0.092 inch. The geometry modeled in CST Microwave Studio is shown in Figure 2-35.

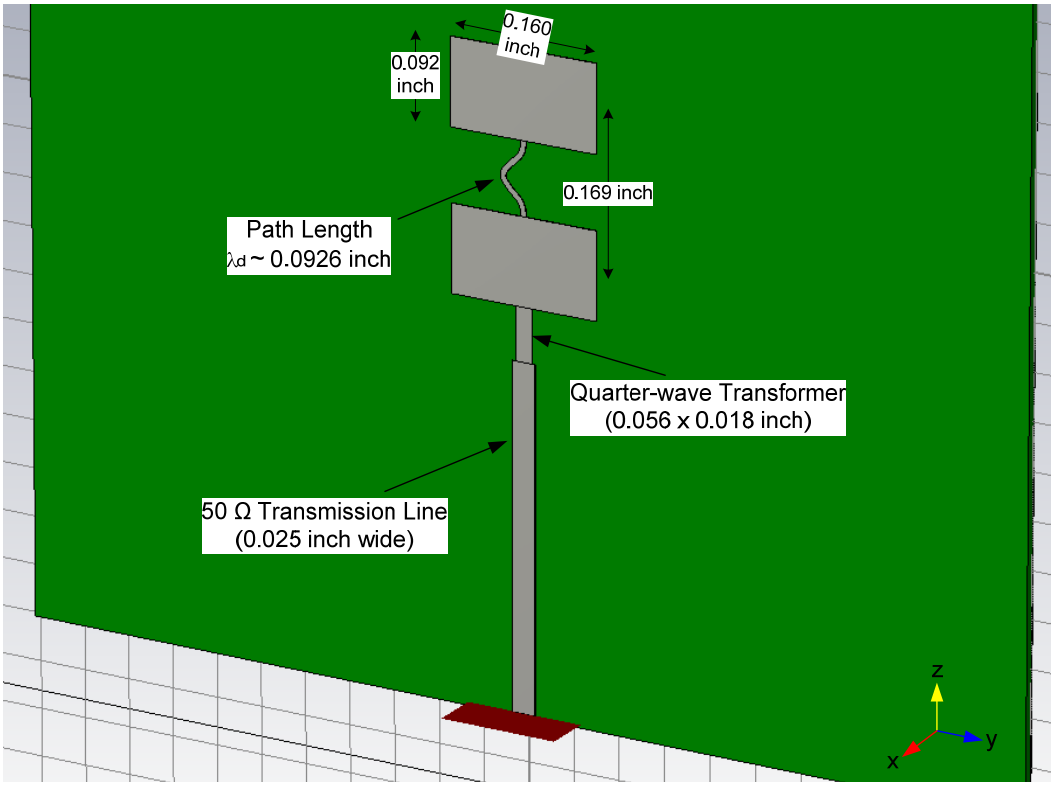

Figure 2-35. Two-element Array with a Series Feed

The return loss is shown in Figure 2-36 for multiple passes using the adaptive mesh refinement feature in CST Microwave Studio, and the pattern results for the series-fed model are shown in Figure 2-37. The pattern distortion is no longer present in the series-fed array. The SLL of the indicated lobe is -19.4 dB. A peak directivity of 10.6 dBi shows improvement of about 1 dB from the various corporate-fed simulated results.

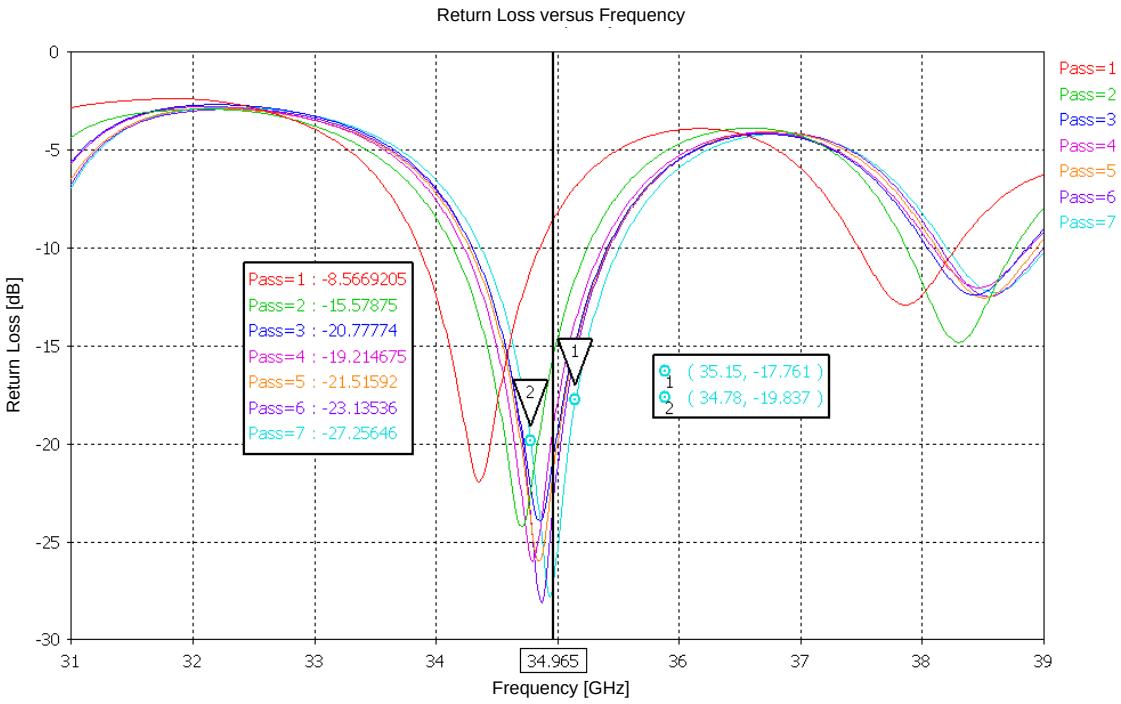

Figure 2-36. Return Loss for the Two-element Array with a Series Feed

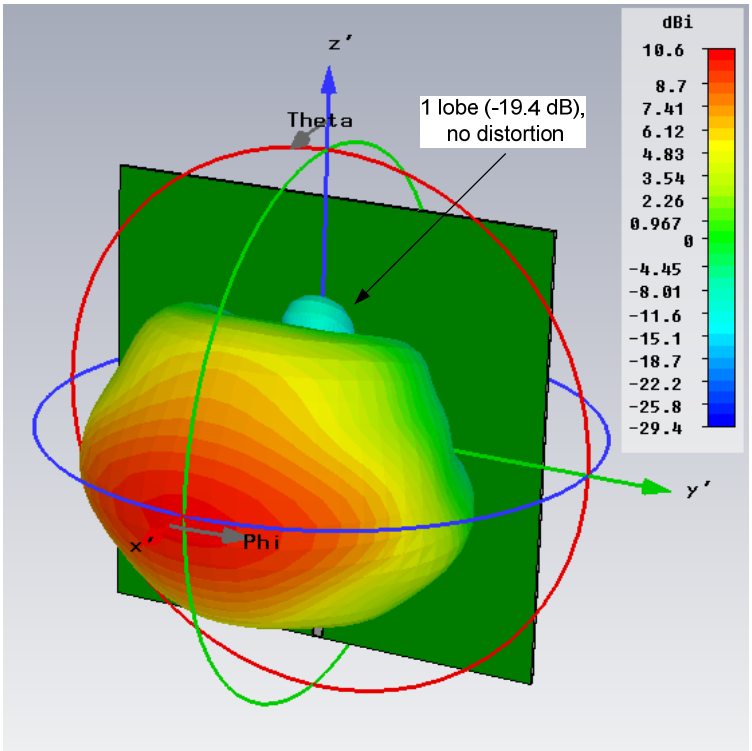

Figure 2-37. Radiation Pattern for the Two-element Array with a Series Feed

The results of the simulation indicate that the series-fed configuration provides the best approach to feeding the two-element array.

2.2.5.2.1 Choosing a connector and the effects on the radiation pattern

With the series feed model exhibiting good results, the next step in the design process is to select a 2.40 mm connector, and model the effects of the connector on the performance of the antenna. The End Launch connector family from Southwest Microwave [12] is the connector of choice, specifically model number 1492-03-5. This connector has a unique clamping mechanism that accommodates a wide range of board thicknesses and provides a continuous ground connection between the end launch and the circuit board. An exploded view of the connector assembly is shown in Figure 2-38.

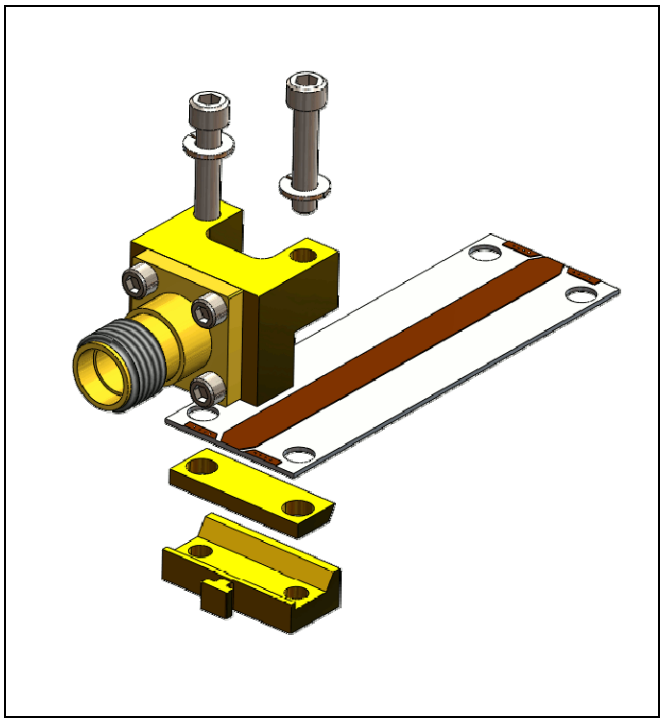

Figure 2-38. End Launch Connector, Model # 1492-03-5 [12]

A 50 Ω coaxial cable will be connected to the jack on the 2.40 mm connector when the antenna is built and tested. The launch pin of the connector makes contact with the 50 Ω feed line as intended by the connector manufacturer. However for modeling purposes, a simplified version of the connector is used in order to reduce simulation times. The modeled connector does not have the 2.40 mm jack and the launch pin to make contact with the trace. Therefore the reference plane of the excitation source remains similar to that of previous models; the launch begins at the edge of the board and is not passed through the connector. The reason for this is that the coaxial cable (and 2.40 mm connector) transition to microstrip cannot be modeled without the design details of the connector, which is proprietary information. Figure 2-39 shows the connector geometry added to the model in CST Microwave Studio, and the corresponding radiation pattern results are shown in Figure 2-40.

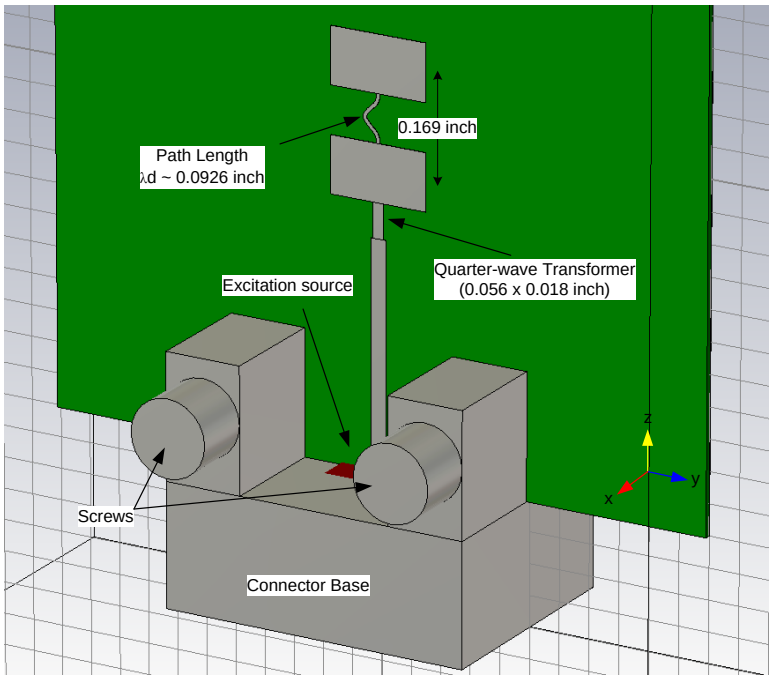

Figure 2-39. Two-element Array with a Series Feed and the 1492-03-5 Connector

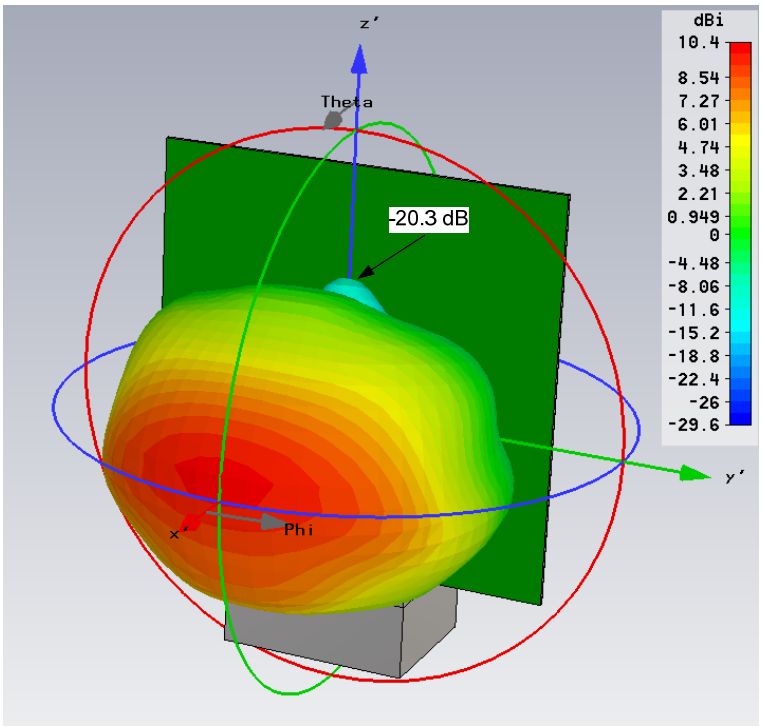

Figure 2-40. Radiation Pattern for the Two-element Array with a Series Feed and the 1492-03-5 Connector

The effects of the connector on the identified side lobe actually improve the SLL by almost 1 dB, perhaps because the connector is interfering with radiation from the feed line, which has been the source of side lobes in previous simulated results. However, a new lobe is present near the connector in the lower half of the elevation pattern. This undesirable result is seen when viewing the E-plane principal plane pattern (Figure 2-41) where $\phi = 0°$ and $0° < \theta < 180°$.

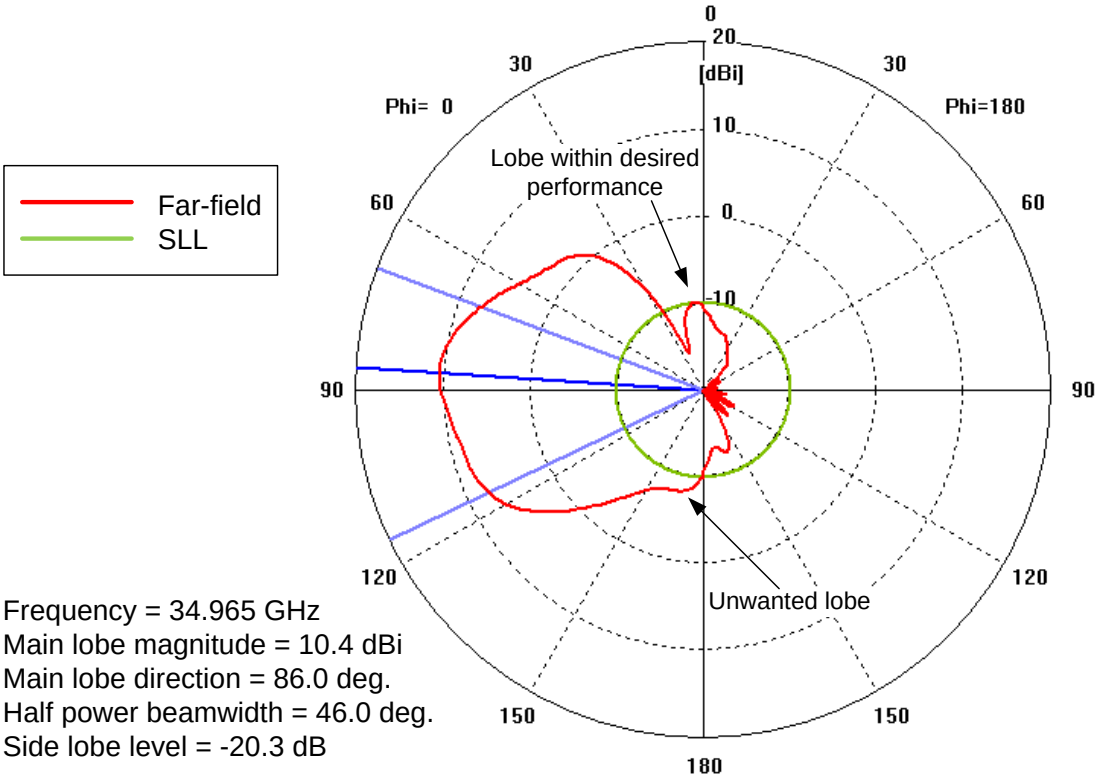

Figure 2-41. E-plane Pattern for the Two-element Array with a Series Feed and the 1492-03-5 Connector

ϕ=0°, 0° <θ < 180°

The connector has reduced the peak directivity of the antenna by 0.2 dBi, which is most likely due to the alteration in radiation pattern and the development of a bottom lobe.

Because the magnitude of the unwanted lobe (-18 dB) does not achieve the desired SLL, other design options are explored. The screws are the tallest part of the connector. Eliminating the screws, or using a non-conductive material for the screws such as nylon, might minimize the lobe because it is the addition of the connector that created the lobe in the first place. From communications with the connector manufacturer (Southwest Microwave) to verify the possible use of nylon screws, another connector model was found. The new connector is a low profile version of the 1492-03-5, produced only for special orders and is not available in their inventory.

The low profile connector (part number 1492-03-6) is a variant of the 1492-03-5 connector, except the screws no longer extend above the height of the connector base, but rather the tops of the screws are level with the base height (Figure 2-42).

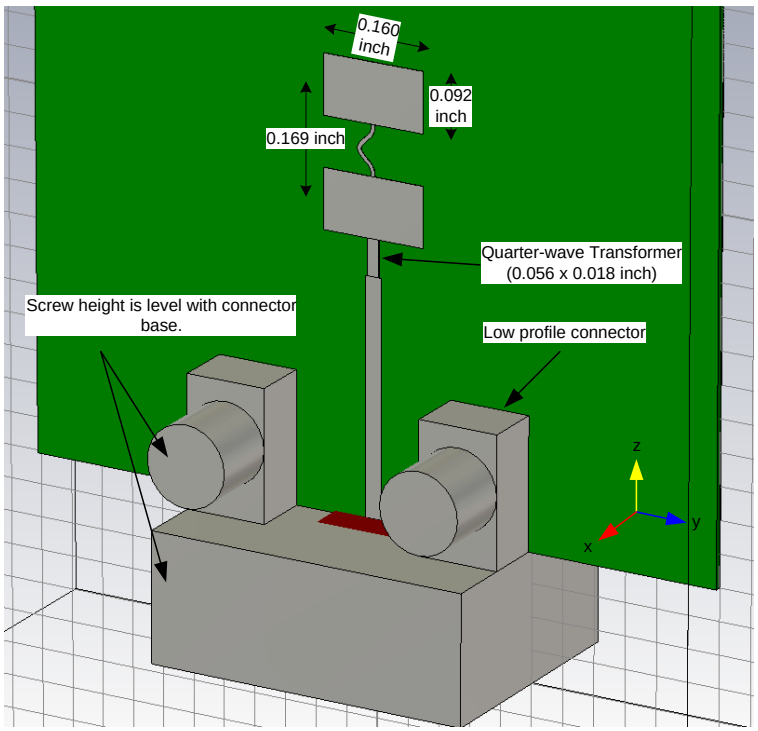

Figure 2-42. Two-element Array with a Series Feed and Low Profile Connector

The 1492-03-5 connector is replaced by the low profile connector in the CST model. The corresponding radiation pattern results are shown in Figure 2-43. The E-plane Principal Pattern in Figure 2-44 shows the bottom side lobe is no longer present and that the low profile connector is definitely an improvement from the originally selected connector. The peak directivity value is increased to 11.0 dBi after the bottom side lobe is removed.

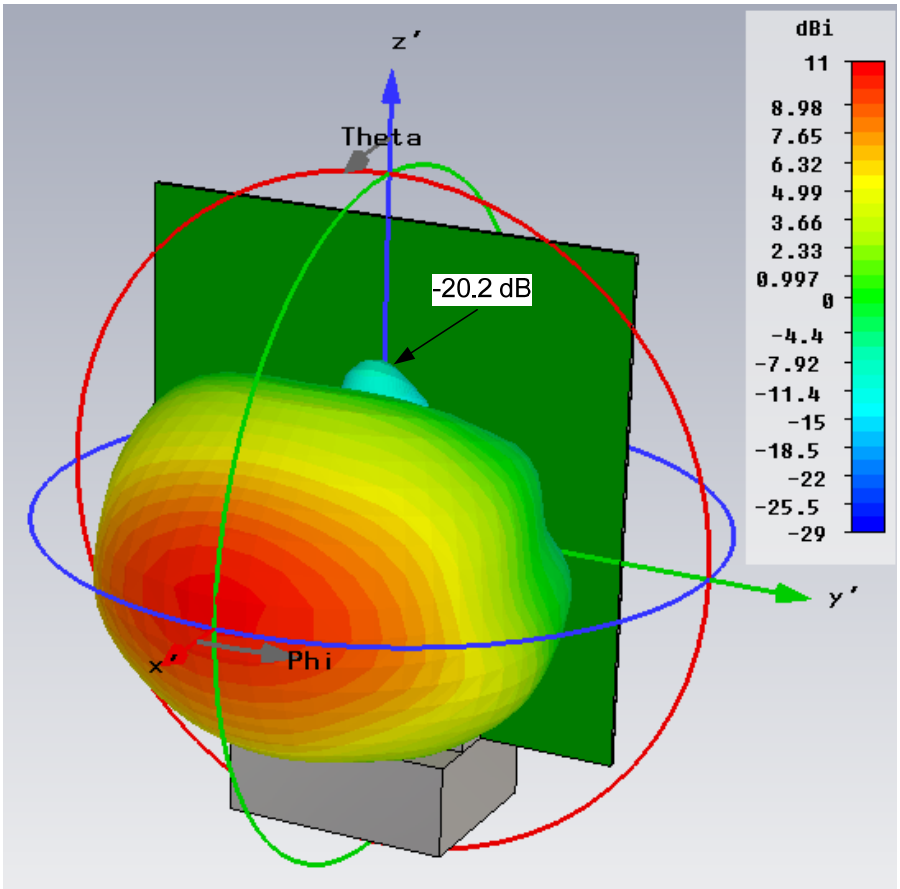

Figure 2-43. Radiation Pattern for the Two-element Array with a Series Feed and Low Profile Connector

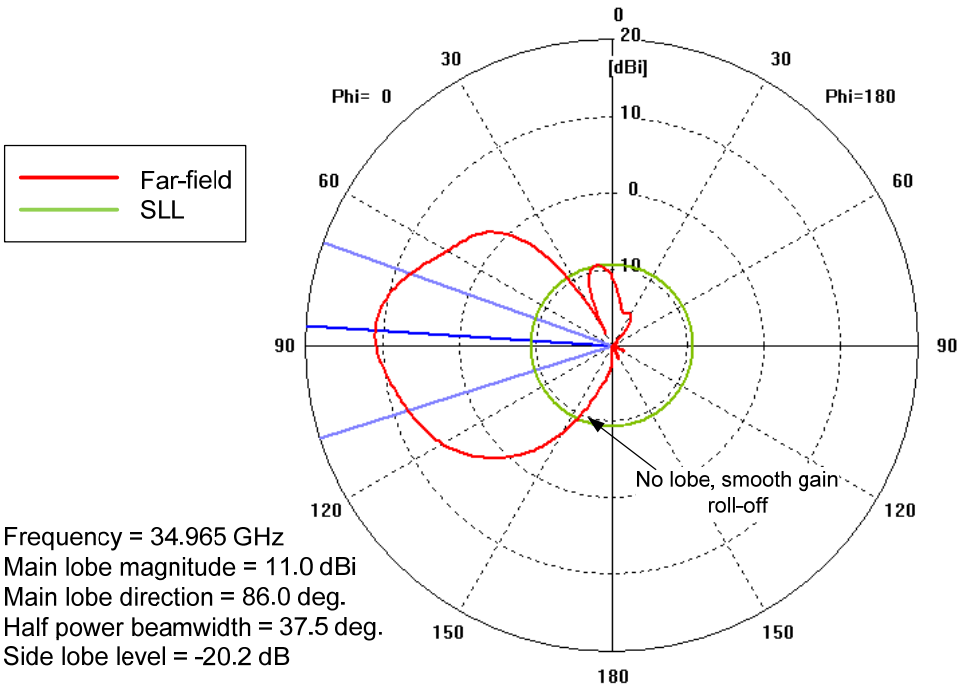

Figure 2-44. E-plane Pattern for the Two-element Array with a Series Feed and Low Profile Connector

$\phi=0°, 0° < \theta < 180°$

As a final step, the manufacturer's recommended board launch design is added to the model, and the antenna is optimized for matching. The design layout consists of 3 grounding vias on each side of the launch with a tapered section of transmission line in the center. The tapered section of line is how the impedance transitions from that of the coaxial connector to a 50 Ω impedance microstrip line. This transition cannot be modeled completely as the design of the connector is the intellectual property of the manufacturer. Hence the source excitation is translated in the positive z-direction by 0.040 inch in order to match at the true 50 Ω reference plane. When the antenna is fabricated and assembled, the center conductor of the coaxial connector will be soldered at the beginning of the tapered section as recommended by the manufacturer. The layout incorporated into the CST Microwave Studio model is shown in Figure 2-45.

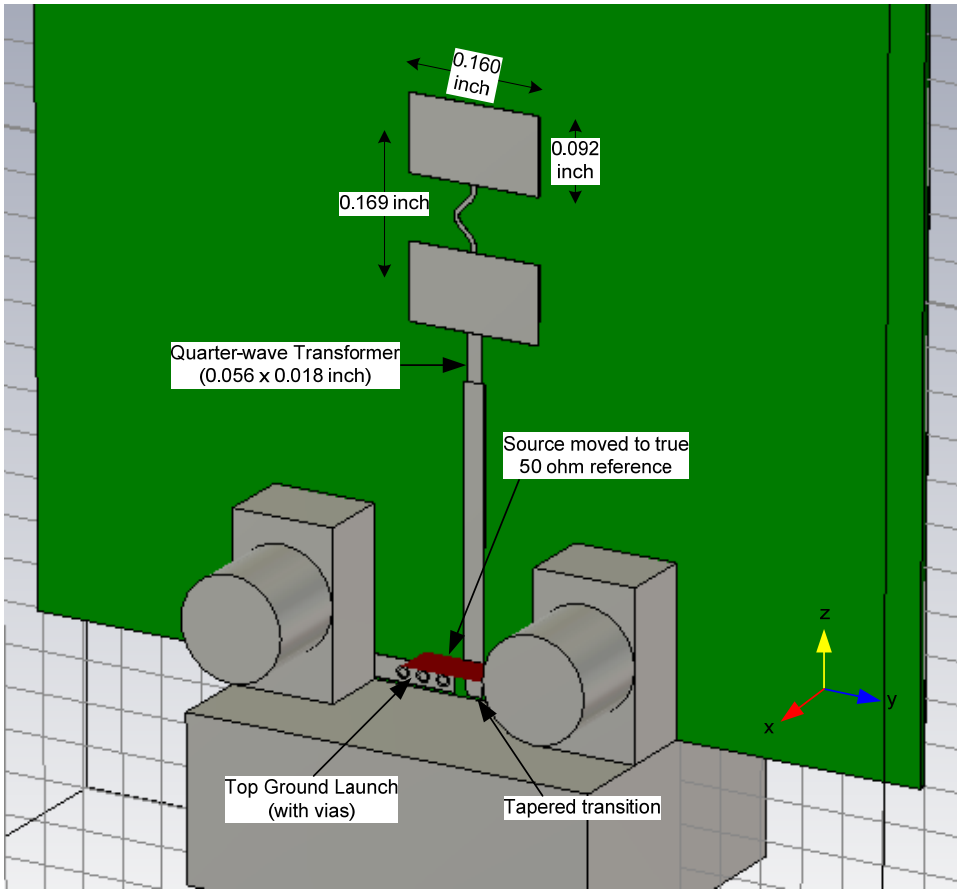

Figure 2-45. Final Geometry of the Two-element Array with a Series Feed, Low Profile Connector, and Board Launch Design

Figures 2-46 through 2-49 illustrate the results for the final design of the array. The radiation pattern (Figure 2-46) is smooth with no side lobes and yields a peak directivity of 10.7 dBi. The E-plane Principal Pattern (Figure 2-47) shows clearly that no side lobes are present, and that the half power beamwidth of 41.9º is within the desired performance of greater than 30º and less than 60º. The H-plane Principal Pattern (Figure 2-48) also shows the half power beamwidth is 60.5º; hence the desired performance of 60º is attained. Table 2-4 summarizes the comparisons between the theoretical and simulated array characteristics.

Table 2-4. Comparison of the Two-element Array Calculated versus Simulated Characteristics

	Calculated	Simulated	% Difference
Peak directivity (dBi)	10.2	10.7	11.5%
E-plane half power beamwidth	54º	41.9º	25%
H-plane half power beamwidth	73.1º	60.5º	19%

Finally, the return loss is shown for multiple passes using the adaptive mesh refinement feature in CST. The result from Pass 4 has the greatest number of mesh cells, about 8,350,000, and shows values of the return loss to be -22.88 dB at the low end of the frequency band and -17.22 dB at the high end of the frequency band. These values of return loss correspond to a VSWR of 1.155 and 1.32, respectively.

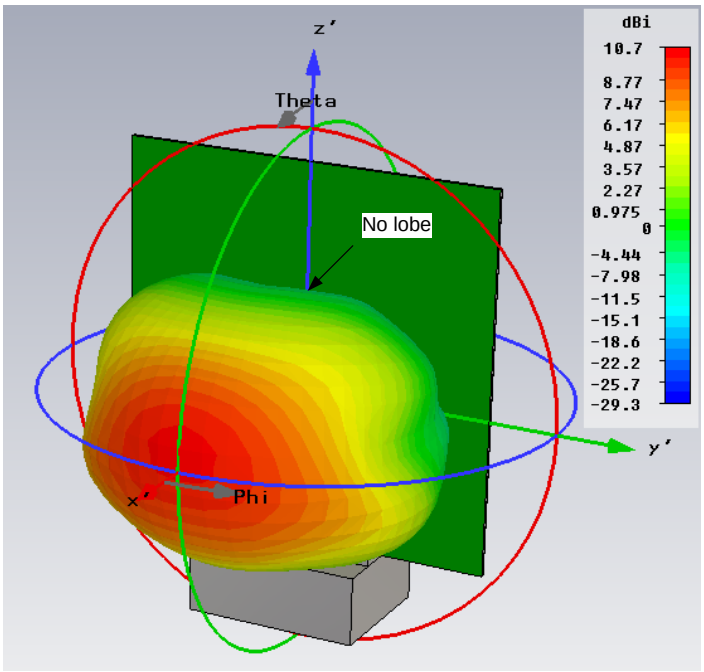

Figure 2-46. Radiation Pattern for the Final Geometry of the Two-element Array with a Series Feed, Low Profile Connector, and Board Launch Design

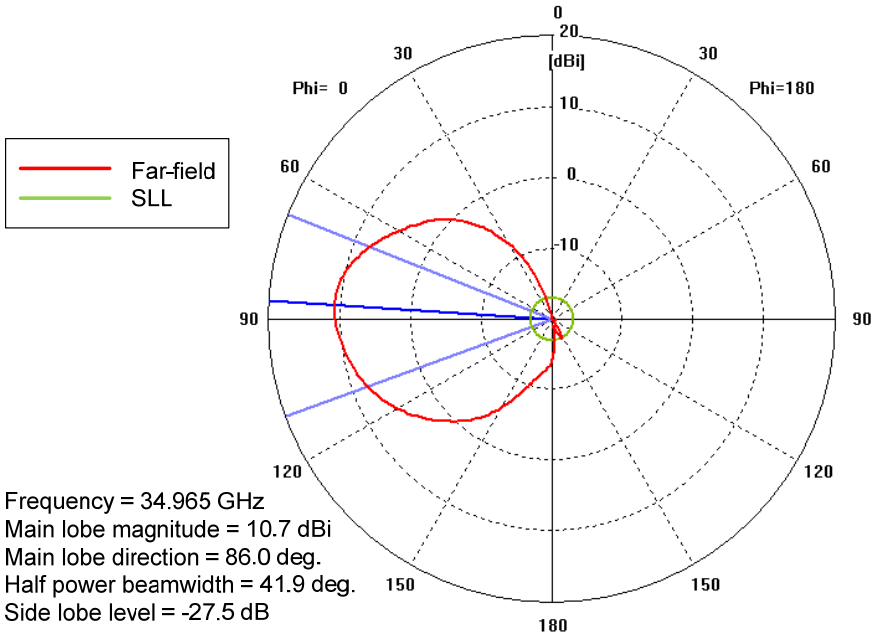

Figure 2-47. E-plane Pattern for the Final Geometry of the Two-element Array with a Series Feed, Low Profile Connector, and Board Launch Design

$\phi=0°, 0° < \theta < 180°$

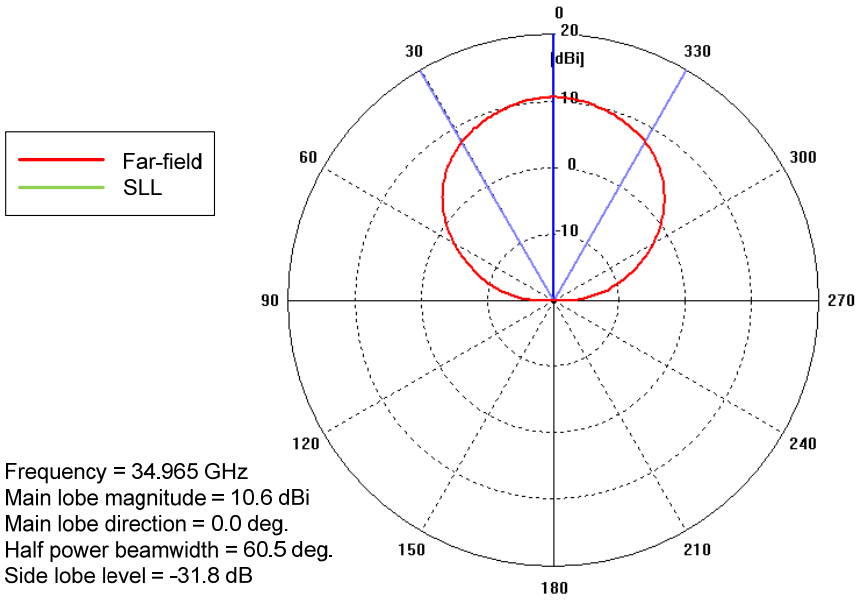

Figure 2-48. H-plane Pattern for the Final Geometry of the Two-element Array with a Series Feed, Low Profile Connector, and Board Launch Design

$0° < \phi < 360°, \theta = 90°$

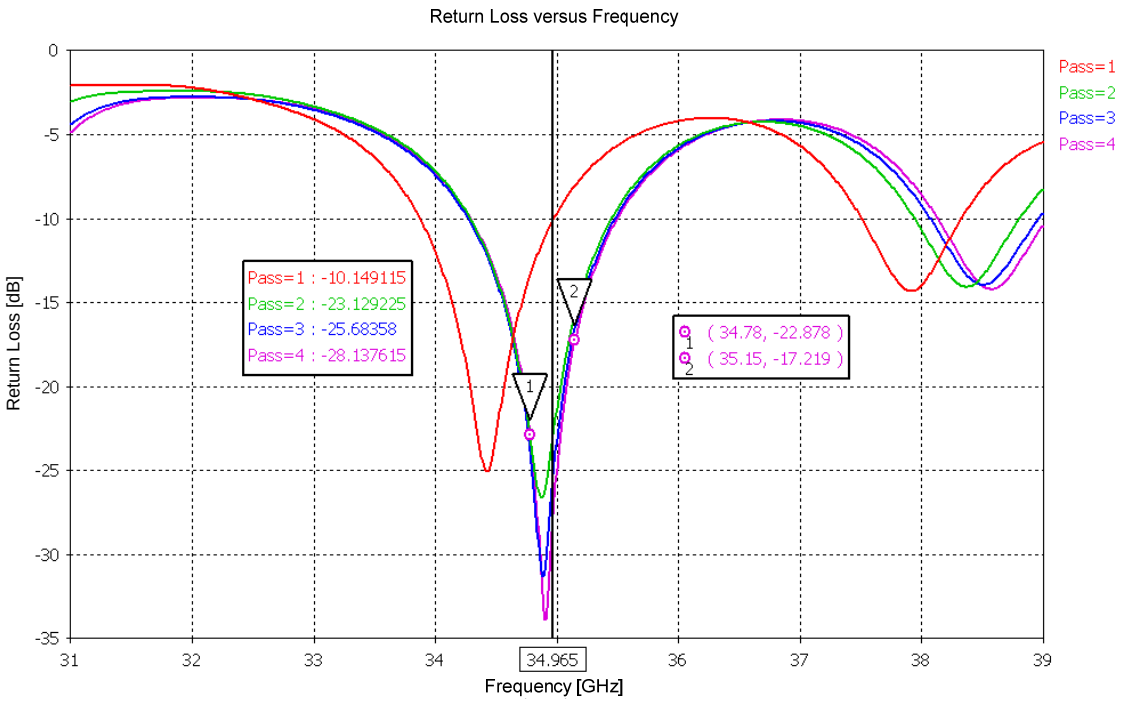

Figure 2-49. Return Loss for the Final Geometry of the Two-element Array with a Series Feed, Low Profile Connector, and Board Launch Design

2.3 Conclusion

Modeling using CST Microwave Studio indicates that all design specifications for the low gain antenna are met, and the desired performance of the antenna is accomplished by using a two-element series-fed array with a low profile connector. The corporate feed structure proves to have unacceptable effects on the radiation pattern of the array, and hence a series feed is used. The antenna structure is matched to 50 Ω using a quarter-wave transformer. The radiation pattern is also affected by the originally selected 2.40 mm connector due to its high profile. A low profile version of the connector is found and used in the final design model. The simulated radiation patterns obtained in Chapter 2 can be directly compared to the measured vertically polarized radiation patterns in Chapter 4.

2.4 References

[1] J.R. James, and P.S. Hall. *Handbook of Microstrip Antennas*, Vols. 1 and 2, Peter Peregrinus, London, UK, 1989, pp. 1-7.

[2] Roger's Corporation. "RT/duroid®6002 High Frequency Laminates." http://www.rogerscorp.com/acm/products/12/RT-duroid-6002-6202-6006-6010-PTFE-Ceramic-Laminates.aspx.

[3] David R. Jackson. "Microstrip Antennas" in *Antenna Engineering Handbook,* Fourth Edition, John L. Volakis, The McGraw-Hill Companies, New York, 2007, pp.2-5.

[4] K.R. Carver and J. W. Mink. "Microstrip Antenna Technology." *IEEE Trans. Antennas & Propagation*, Vol. AP-29, pp. 2-24, Jan. 1981.

[5] Constantine A. Balanis, *Antenna Theory: Analysis and Design*, 2nd Ed., New York, John Wiley & Sons, Inc., 1997, pp 257-264, 722-752.

[6] Bahl, I. J. and Bhartia, P., "Rectangular Microstrip Antennas" in *Microstrip Antennas*, Artech House, Dedham Mass, 1980, pp. 31-84.

[7] D.M. Pozar & D.H. Schaubert, "Review of Microstrip Antenna Array Techniques", in *Microstrip Antennas, The Analysis and Design of Microstrip Antennas and Arrays*, IEEE Press New York, 1995, pp. 269-273.

[8] W.L. Stutzman and G.A. Thiele, *Antenna Theory & Design*, 2nd Ed. John Wiley & Sons, Inc., 1998, pp 37-43, 87-103, 210-218.

[9] D.M. Pozar & D.H. Schaubert, "A Review of Bandwidth Enhancement Techniques for Microstrip Antennas", in *Microstrip Antennas, The Analysis and Design of Microstrip Antennas and Arrays*, IEEE Press New York, 1995, pp. 157-166.

[10] Leonard Lewin, "Spurious Radiation from a Microstrip Y-junction," *IEEE Transactions on Microwave Theory and Techniques*, Vol. MTT-26, No. 11, November 1978.

[11] Anders G. Derneryd, "Linearly Polarized Microstrip Antennas," *IEEE Transactions on Antennas and Propagation*, Vol. 24, pp. 846-851, Nov. 1976.

[12] Southwest Microwave. "End Launch Connector Series." http://www.southwestmicrowave.com/mpd/catalog/index.php?pdf=end_launch.pdf.

3 DESIGN AND MODELING OF AN EIGHT-ELEMENT MICROSTRIP PATCH ARRAY

3.1 Introduction

Typical high gain antennas in use for radar-based autonomous landing systems are pyramidal horn structures with a half power azimuth beamwidth of about 45° and a half power elevation beamwidth of about 20°. The reason for developing a microstrip patch array to be used as a high gain antenna is to minimize cost. The patch antenna is designed and modeled to have a radiation pattern similar to that of typical horn antennas. The return loss, when matched to 50 Ω, is less than -20 dB at the center frequency. The radiation pattern meets the design objectives. The simulated peak directivity is greater than 14.5 dBi. The design procedure is described along with modeling results.

3.2 Methodology

3.2.1 Antenna Desired Performance

The desired performance of the high gain antenna is provided in Table 3-1.

Table 3-1. High Gain Array Desired Performance

Center Frequency, f_r:	34.965 GHz
Bandwidth:	±185 MHz
Polarization:	linear, vertical
RF feed characteristic impedance:	50 Ω
RF feed VSWR:	1.5:1 maximum
Gain at 0° azimuth, 0° elevation:	greater than 14.0 dBi
H-plane half power beamwidth (azimuth cut):	$40^o \leq \phi \leq 50^o$ $(\pm 20^o \leq \phi \leq \pm 25^o)$
E-plane half power beamwidth (elevation cut):	$20^o \leq \theta \leq 40^o$ $(\pm 10^o \leq \theta \leq \pm 20^o)$
Side lobe level (SLL):	less than -13 dB

3.2.2 Substrate Selection

The substrate used in the design of the low gain antenna in Chapter 2, RT/duroid® 6002 High Frequency Laminate, is also used for the high gain array.

3.2.3 Coordinate System

The coordinate system used in Chapter 3 and in the entire thesis is the same as the coordinate system shown in Figure 2-4.

3.2.4 Determining the Number of Array Elements

Given the desired performance characteristics in Table 3-1, the element pattern and array factor are used to determine the number of elements in the array. The pattern equations used for a single patch are defined in Equations (3-1) and (3-2) [1].

$$E(\theta) = \frac{sin\left[\frac{\beta h}{2} cos\,(\theta)\right]}{\frac{\beta h}{2} cos\,(\theta)} cos\left[\frac{\beta Length}{2} cos(\theta)\right], \phi = 0° \tag{3-1}$$

$$H(\phi) = sin\left(\phi + \frac{\pi}{2}\right) \frac{sin\left[\frac{\beta Width}{2} cos\left(\phi + \frac{\pi}{2}\right)\right]}{\frac{\beta Width}{2} cos\left(\phi + \frac{\pi}{2}\right)}, \theta = 90° \tag{3-2}$$

where $0 < \theta < \pi$, $-\frac{\pi}{2} < \phi < \frac{\pi}{2}$, β is the wave number, $\frac{2\pi}{\lambda_0}$, and h is the substrate thickness.

Figure 3-1(a) and Figure 3-1(b) are graphical representations of the E- and H-plane patterns, respectively, over the defined intervals for θ and ϕ for the single-element patch designed in Chapter 2.

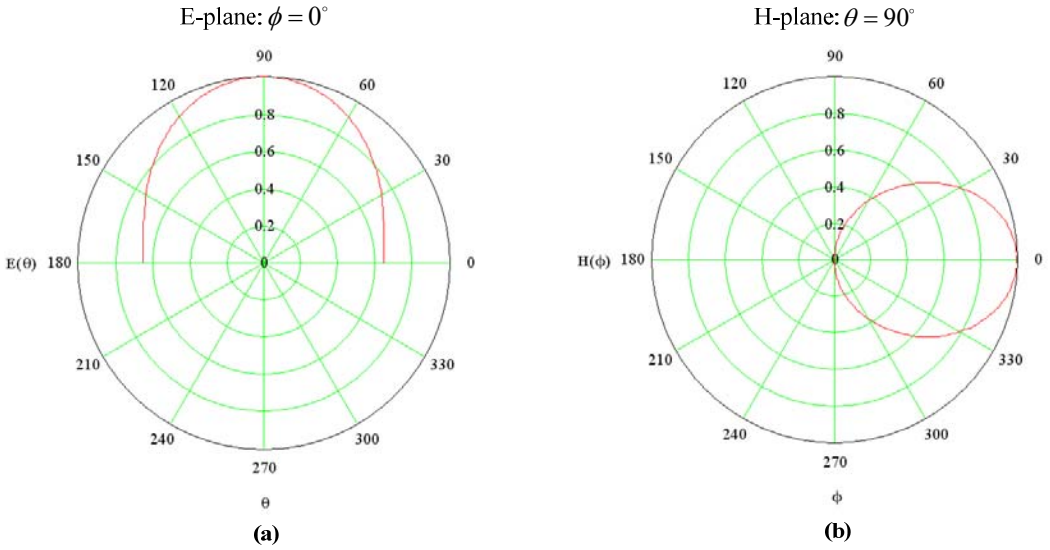

Figure 3-1. Calculated E- and H-plane Radiation Patterns for a Single-element Patch obtained from Equations (3-1) and (3-2), respectively

The broad beam pattern of the single patch in the H-plane (3 dB points at ±36º) does not achieve the azimuth half power beamwidth desired performance (±20º ≤ ϕ_{3dB} ≤ ±25º). In order to narrow the half power beamwidth to within the desired performance, additional elements are required in the H-plane (along the y-axis) because the greater the number of elements in an array the smaller the half power beamwidth becomes. Likewise, the E-plane pattern from the two-element array with 3 dB points at ±27º of Chapter 2 does not achieve the elevation half power beamwidth desired performance; hence the number of elements in the E-plane (along the z-axis) must also be increased. The results in Chapter 2 for an array consisting of one element along the y-axis and two elements along the z-axis are used as a baseline for realizing the number of elements required, hence increasing the number of elements to two and three along the y-axis and z-axis, respectively is evaluated. The analysis of the two-element array is simple because the array is a linear array consisting of a single column of elements, whereas a two-element by three-element array is considered a two-dimensional planar array and consists of two columns and three rows of elements (Figure 3-2).

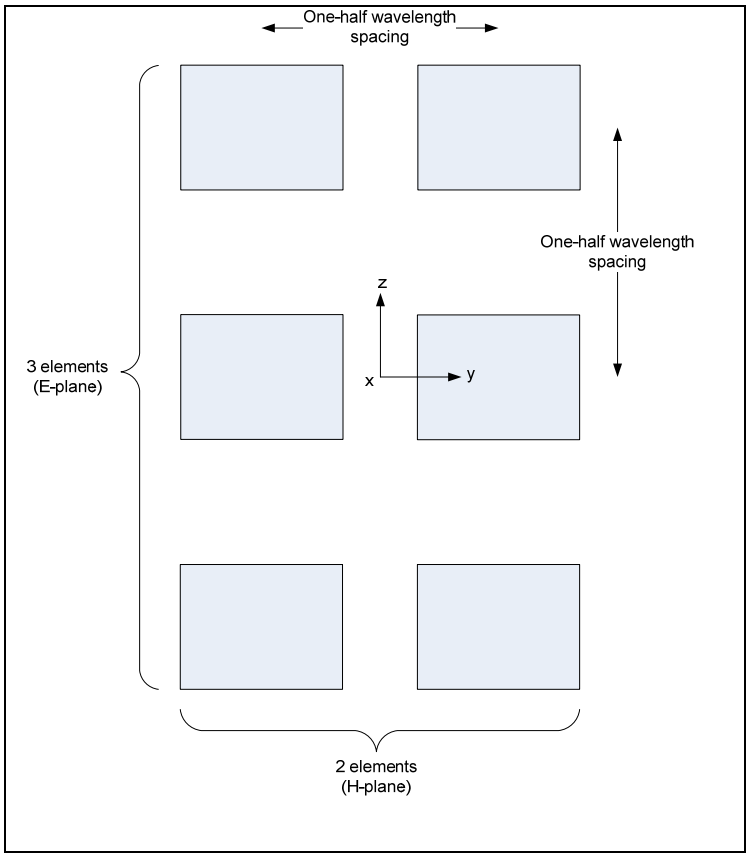

Figure 3-2. Two-dimensional Array with Three Elements in the E-plane and Two Elements in the H-Plane

The two-dimensional array factor is the product of the two linear array factors associated with the row and column current distributions [2]. For the patterns in the principal planes of a two-dimensional array, a linear array for a single row or column is applied; hence the E- and H-plane patterns are calculated independently.

For the H-plane, two isotropic point sources with identical amplitudes and phase currents are assumed. The two sources are spaced one-half wavelength apart with zero phase shift between them. Equation (3-3) represents the array factor, AF, for an m-element array [2]:

$$AF(\phi) = \frac{sin\left[m\frac{\psi\left(\phi+\frac{\pi}{2}\right)}{2}\right]}{m\,sin\left[\frac{\psi\left(\phi+\frac{\pi}{2}\right)}{2}\right]} \tag{3-3}$$

where $\psi(\phi) = \beta d cos(\phi) + \alpha, d$ is the element spacing $\left(\frac{\lambda_0}{2}\right)$, β is the wave number $\left(\frac{2\pi}{\lambda_0}\right)$, α is the phase shift between elements, m is the number of elements in the array and $-\frac{\pi}{2} < \phi < \frac{\pi}{2}$.

Figure 3-3(a) and Figure 3-3(b) show the element pattern and the array factor for a two-element array, respectively. Figure 3-4 is the resulting pattern for a two-element array of patch antennas with elements spaced one-half wavelength apart.

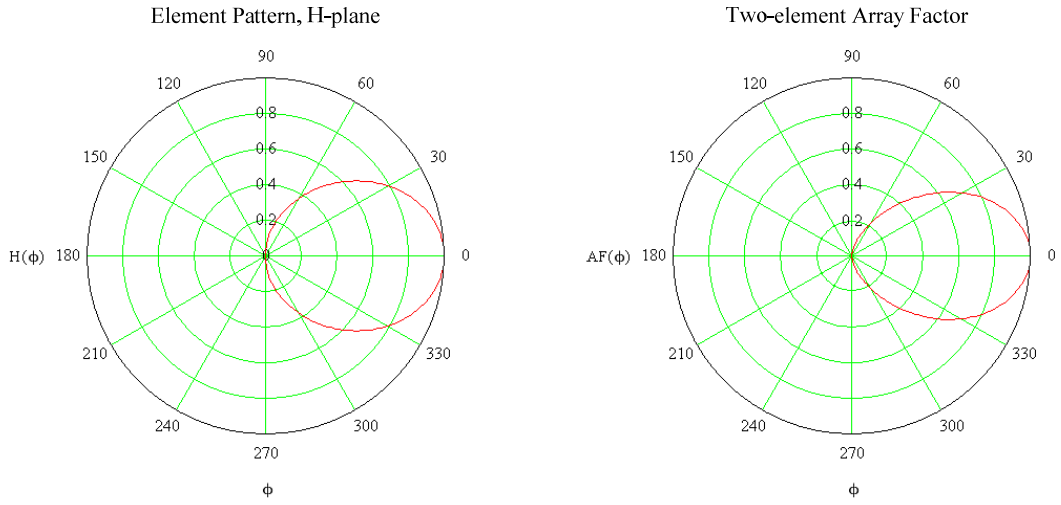

Figure 3-3. (a) Normalized Element Pattern (H-plane) and (b) Array Factor of a Two-element Array Consisting of Isotropic Sources of Equal Amplitude and Phase Currents Spaced Half a Wavelength Apart

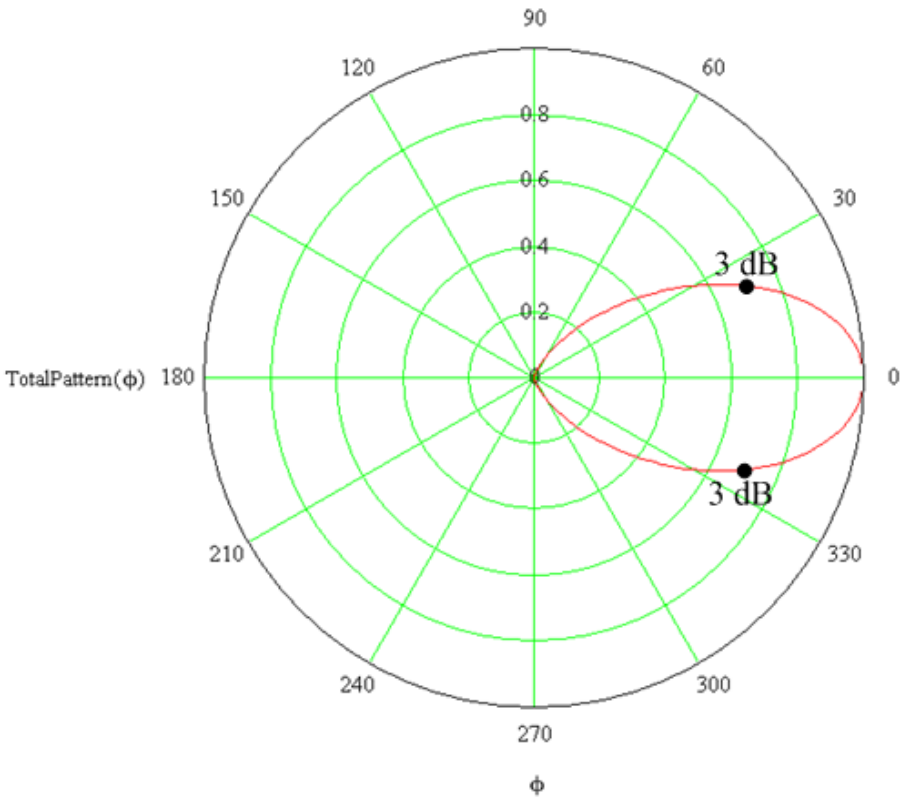

Figure 3-4. Normalized H-plane Pattern (Element Pattern x Array Factor) for a Two-element Array of Microstrip Patches

The 3 dB points occur at angles ±23º. This is within the desired beamwidth performance, (±20º ≤ ϕ ≤ ±25º) and therefore two elements along the y-axis are sufficient.

Based on the results from Chapter 2 where θ_{3dB}= ±27º, placing two elements along the z-axis does not reduce the half power beamwidth as much as dictated by the specifications for the high gain antenna. Therefore three elements along the z-axis are considered for obtaining the required half power beamwidths in the E-plane (±10º ≤ θ_{3dB} ≤ ±20º). Three isotropic point sources spaced half a wavelength apart, with identical

amplitudes and phase currents are assumed. Equation (3-4) gives an expression for the array factor for an array of three elements:

$$AF(\theta) = \frac{sin\left(n\frac{\psi(\theta)}{2}\right)}{n\,sin\left(\frac{\psi(\theta)}{2}\right)} \tag{3-4}$$

where $\psi(\theta) = \beta d cos(\theta) + \alpha$, d is the element spacing $\left(\frac{\lambda_0}{2}\right)$, β is the wave number $\left(\frac{2\pi}{\lambda_0}\right)$, α is the phase shift between elements, n is the number of elements in the array and $0 < \theta < \pi$.

Figure 3-5(a) and Figure 3-5(b) show the element pattern and the array factor for a three-element array, respectively. Figure 3-6 is the resulting pattern for a three-element array with elements spaced one-half wavelength apart.

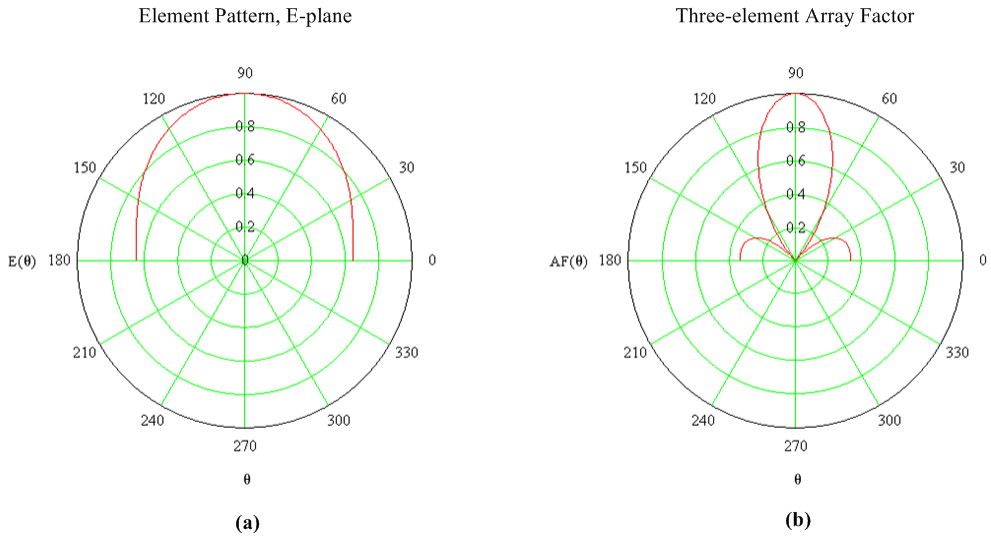

Figure 3-5. (a) Normalized Element Pattern (E-plane) and (b) Array Factor for a Three-element Array Consisting of Isotropic Sources of Equal Amplitude and Phase Currents Spaced Half a Wavelength Apart

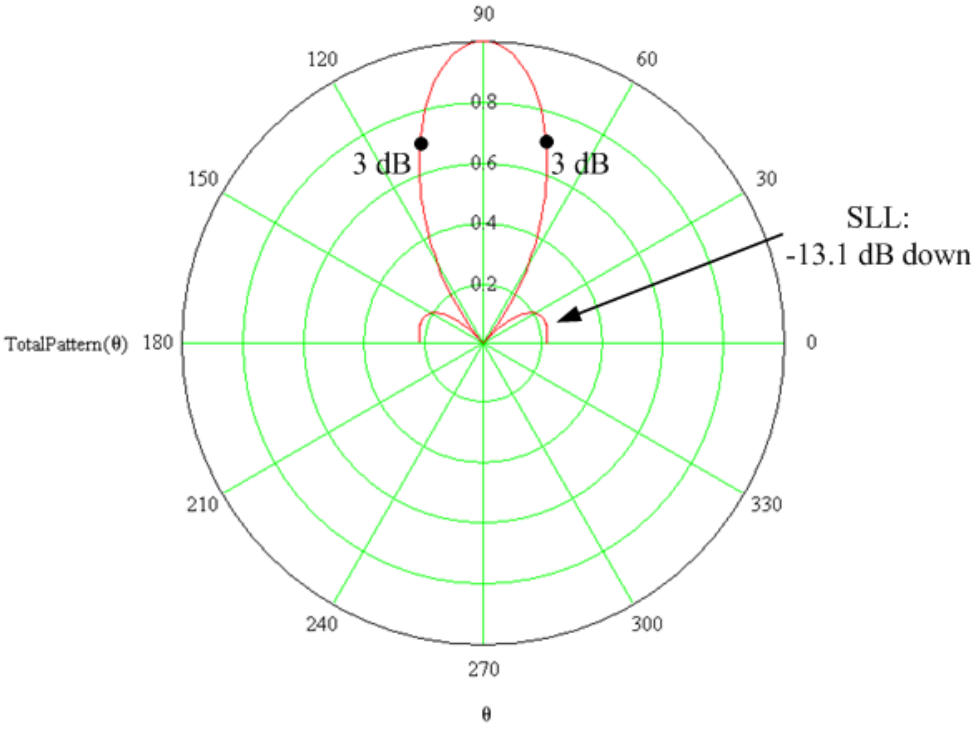

Figure 3-6. Normalized E-plane Pattern (Element Pattern x Array Factor) for a Three-element Array of Microstrip Patches

The 3 dB points occur at angles ±17º from broadside. The side lobe level is 0.221 or -13.1 dB. This is within the beamwidth desired performance, and therefore an array of three elements along the z-axis is sufficient.

The above analysis concludes that a six-element array having two-elements along the y-axis and three-elements along the z-axis will achieve the antenna radiation pattern desired performance characteristics.

3.2.4.1 Six-element Array Directivity Verification

The calculations for a planar two- by three-element microstrip patch array provide the necessary beamwidths for replacement of the directional horn antenna. However, the antenna must also have at least 14.0 dBi of gain. Neglecting copper losses, the gain is

approximately equal to the directivity. The directivity for a single microstrip patch has been calculated in Chapter 2 using Equations (2-9) and (2-10). The same equations are used to approximate the directivity of the six-element two-dimensional array. The pattern factor in Equation (2-10) however, must be replaced by the Total Pattern, which is the pattern factor for a single microstrip patch element multiplied by the array factor. The two-dimensional array factor, $AF2D$, is given by:

$$AF2D(\theta,\phi) = \frac{sin\left(n\frac{\psi(\theta)}{2}\right)}{n\,sin\left(\frac{\psi(\theta)}{2}\right)} \frac{sin\left[m\frac{\psi\left(\phi+\frac{\pi}{2}\right)}{2}\right]}{m\,sin\left[\frac{\psi\left(\phi+\frac{\pi}{2}\right)}{2}\right]} \tag{3-5}$$

where n is the number of elements in the E-plane, m is the number of elements in the H-plane, $0 < \theta < \pi$, and $-\frac{\pi}{2} < \phi < \frac{\pi}{2}$. The theoretical directivity for a six-element array is calculated to be 23.57 or 13.72 dBi. This directivity does not achieve the desired performance given in Table 3-1; therefore an array with a higher directivity must be synthesized.

3.2.4.2 Eight-element Array

A two- by four-element array (Figure 3-7) is considered next in order to increase the directivity knowing it would also further reduce the half power beamwidth in the E-plane without changing the half power beamwidth in the H-plane.

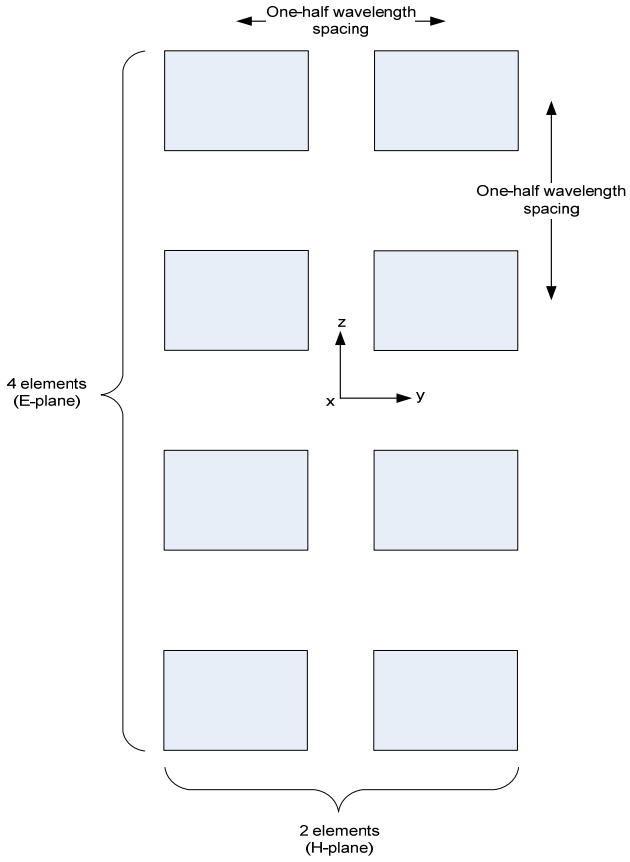

Figure 3-7 . Two-dimensional Array with Four Elements in the E-plane and Two Elements in the H-Plane

Because the number of elements in the H-plane remains the same, the H-plane patterns previously obtained (Figure 3-3 and Figure 3-4) are still relevant to the eight-element array.

Because a linear array for a single column of a two-dimensional array gives the pattern of the principal plane, a four-element array factor is used to obtain the E-plane principal plane pattern. Figure 3-8(a) and Figure 3-8(b) show the element pattern and the array factor for a four-element array, respectively. Figure 3-9 is the resulting radiation pattern for a four-element array with elements spaced one-half wavelength apart.

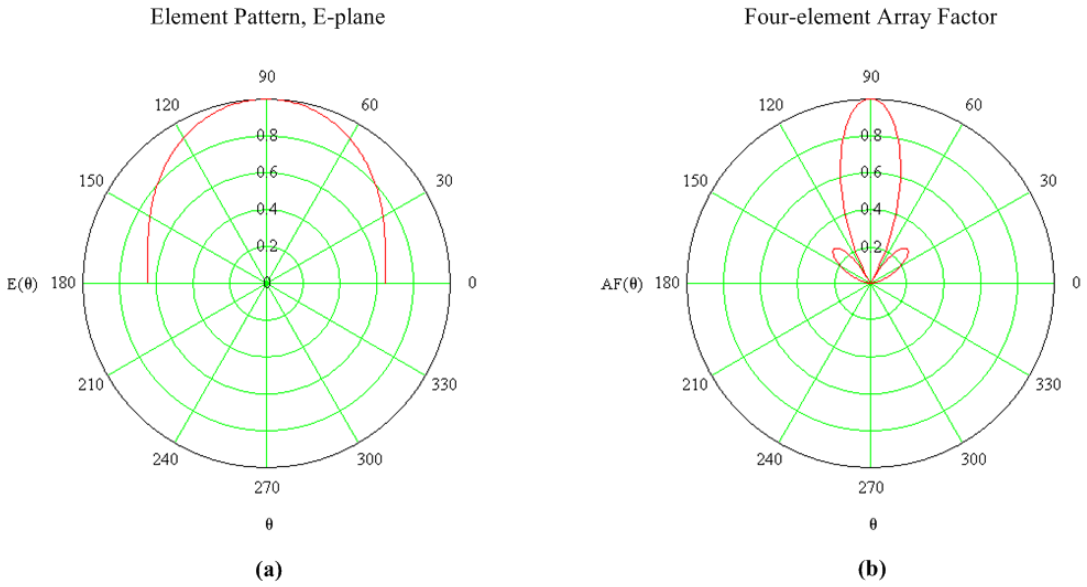

Figure 3-8. (a) Normalized Element Pattern (E-plane) and (b) Array Factor for a Four-element Array Consisting of Isotropic Sources of Equal Amplitude and Phase Currents Spaced Half a Wavelength Apart

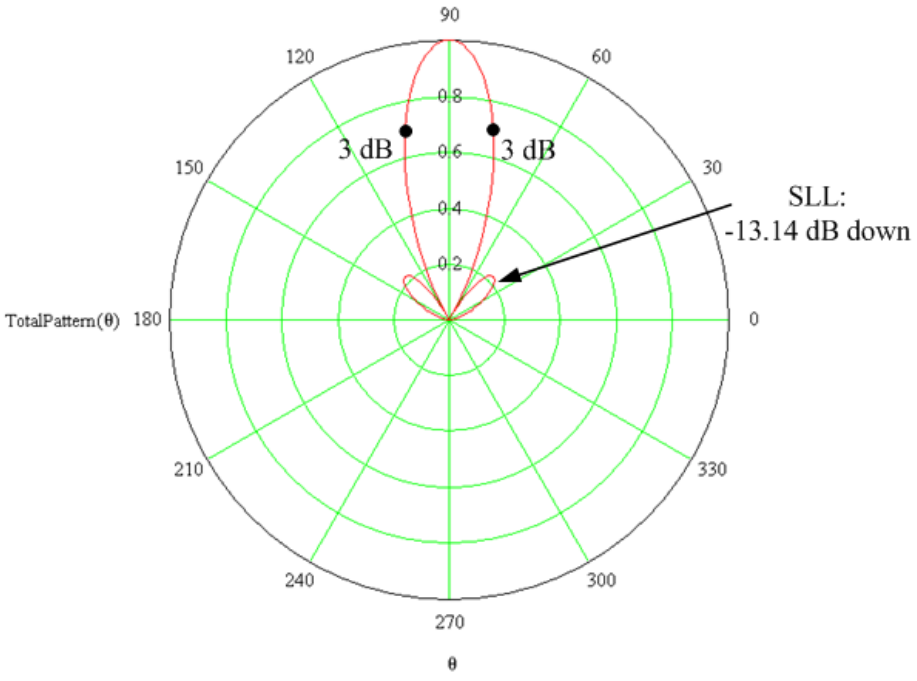

Figure 3-9. Normalized E-plane Pattern (Element Pattern x Array Factor) for a Four-element Array of Microstrip Patches

The 3 dB points occur at angles ±13º from broadside, which still achieves the desired half power beamwidth performance of $\pm 10^{\circ} \leq \theta_{3dB} \leq \pm 20^{\circ}$. The SLL, 0.22 or -13.14 dB, is very close to the calculated SLL obtained for a three-element array (0.221 or -13.1 dB).

The theoretical analysis concludes that an eight-element microstrip patch array having two elements along the y-axis and four elements along the z-axis achieves the desired antenna beam pattern performance characteristics.

3.2.4.2.1 Directivity Verification

The calculated directivity from Equation (2-9) for the eight-element array is 30.84 or 14.89 dBi; therefore an eight-element array also meets the design characteristic of a directivity greater than 14.0 dBi.

3.2.5 Feed Methods

Based on the conclusions made in Chapter 2, a series feed is used for the eight-element array. However, because the array is no longer linear, a two-way splitter is implemented at the end of the 50 Ω feed line, similar to the antenna in [3], which is shown in Figure 3-10.

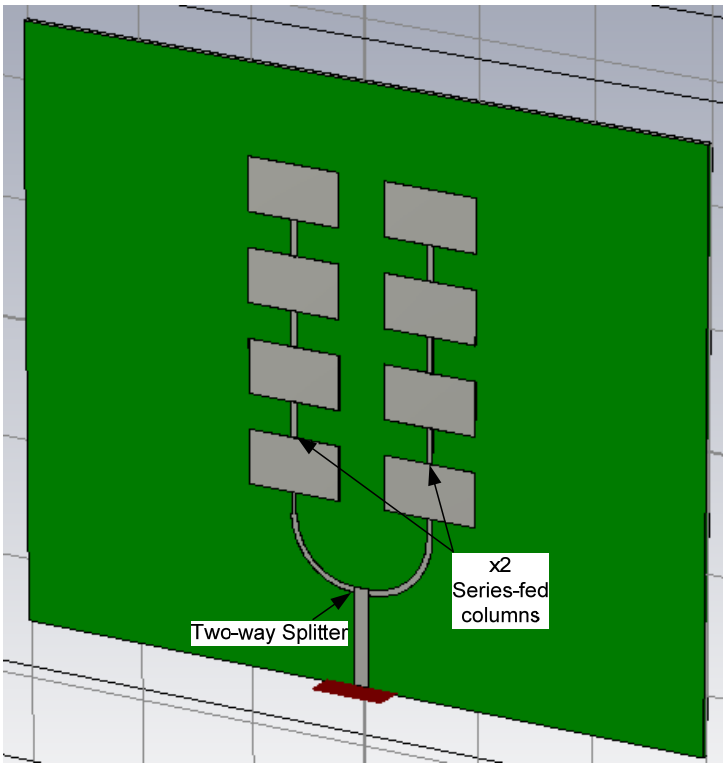

Figure 3-10 . Antenna from [3] Showing a Two-way Splitter and Two Series-fed Columns

3.2.6 Modeling of the Eight-element Array

3.2.6.1 Simulation Parameters

Similar to the two-element array, a copper thickness of 0.0007 inch is used for the ground plane and top layer conductor. However, the material definition used in CST Microwave Studio is "Perfect Electric Conductor" and does not take into account copper losses. Using a non-lossy material definition reduces simulation time. For the substrate, Roger's 6002 material [4] is used from the CST Microwave Studio predefined material library package.

The method of excitation used is a waveguide port and the boundary conditions chosen are "open (add space)." A time domain solver is used for the high gain array simulations.

3.2.6.2 Model Iterations

An eight-element array of microstrip patches has been modeled in CST Microwave Studio (Figure 3-11). The dimensions of the board are 1.16 inches (width) by 1.16 inches (height). The initial model uses a microstrip Y-junction to split a single 50 Ω input line into two 100 Ω lines to feed each column of patches. Two quarter-wave transformers are used to match each column of patches to 100 Ω. The spacing between patches in both the y-direction and z-direction is half-wavelength or 0.169 inch. A very thin meandered line is used to connect the patches in each column. The length of this series line is 0.093 inch, which is equal to the length of the patches (slightly less than one-half wavelength in the dielectric).

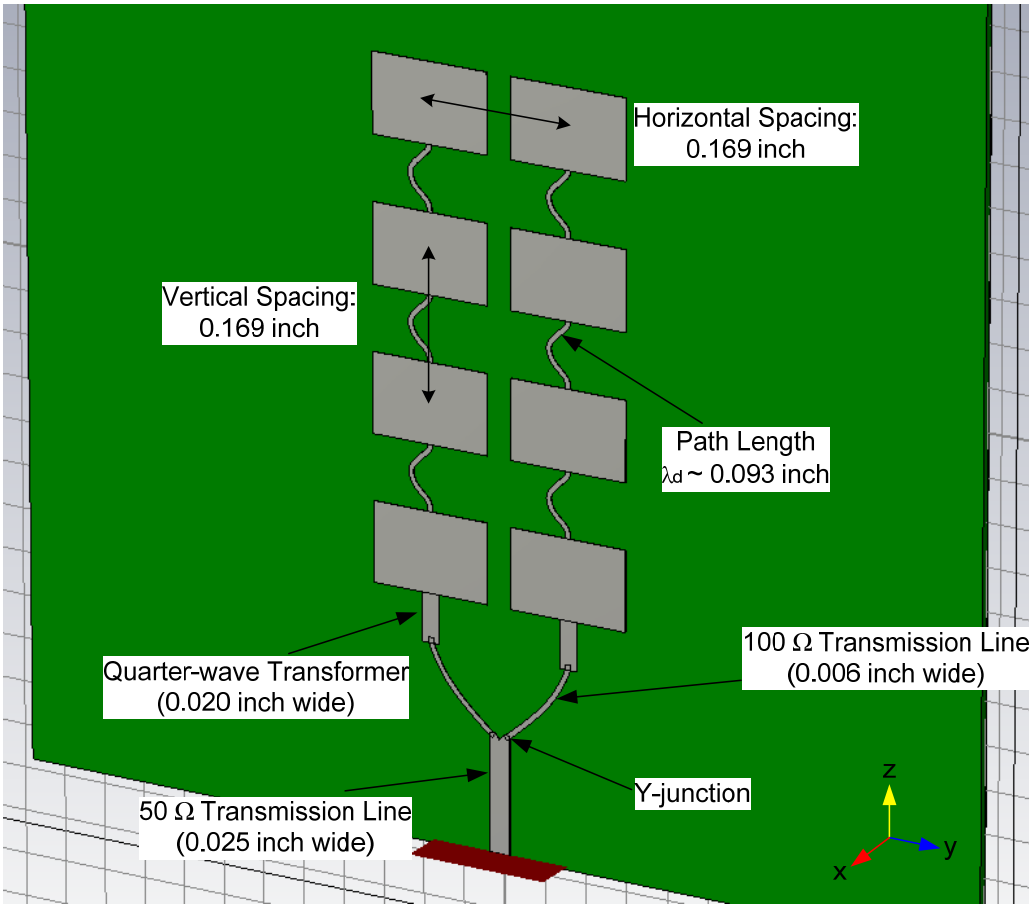

Figure 3-11. Eight-element Array of Microstrip Patches with a Horizontal and Vertical Patch-to-Patch Spacing of 0.169 inch

The patch length and width are 0.093 inch and 0.140 inch, respectively. The width of the patches for the high gain array is reduced from that of the low gain array to allow for greater edge-to-edge spacing between the elements in the H-plane. Because the horizontal spacing of patch centers is 0.169 inch, the 0.160 inch width of the low gain patches only allows a 0.009 inch gap between the elements in the H-plane. To reduce the variation of array performance caused by mutual coupling effects, the separation between elements must typically be greater than $0.10\lambda_0$ or 0.034 inch [5].

The simulated three-dimensional far-field pattern of the array in Figure 3-11 is presented in Figure 3-12. A major side lobe in the +z direction is present. A SLL of -11.1 dB is obtained in the principal E-plane pattern (Figure 3-13). Figure 3-15 shows no side lobes in the H-plane pattern and a half power beamwidth of 46.9º, which is only 0.9º greater than the theoretical H-plane half power beamwidth, 46º. Because of the desirable H-plane pattern results, the following iterations focus on the reduction of SLL in the E-plane pattern.

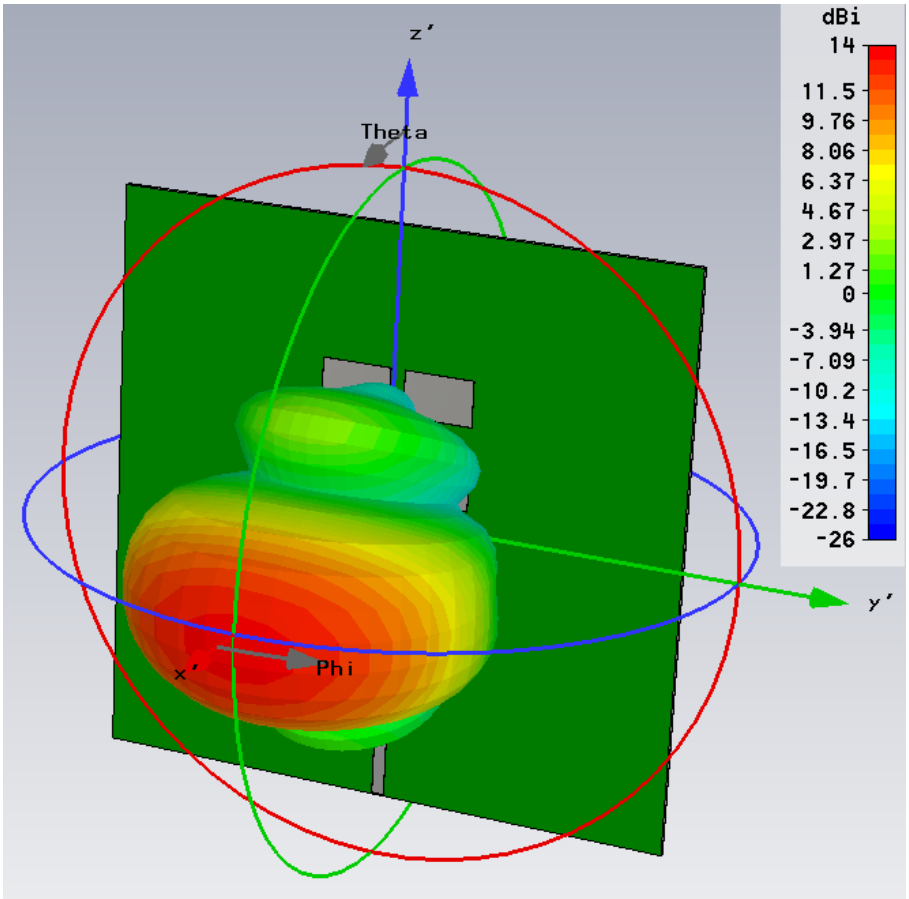

Figure 3-12. Radiation Pattern for an Eight-element Array of Microstrip Patches with a Horizontal and Vertical Patch-to-Patch Spacing of 0.169 inch

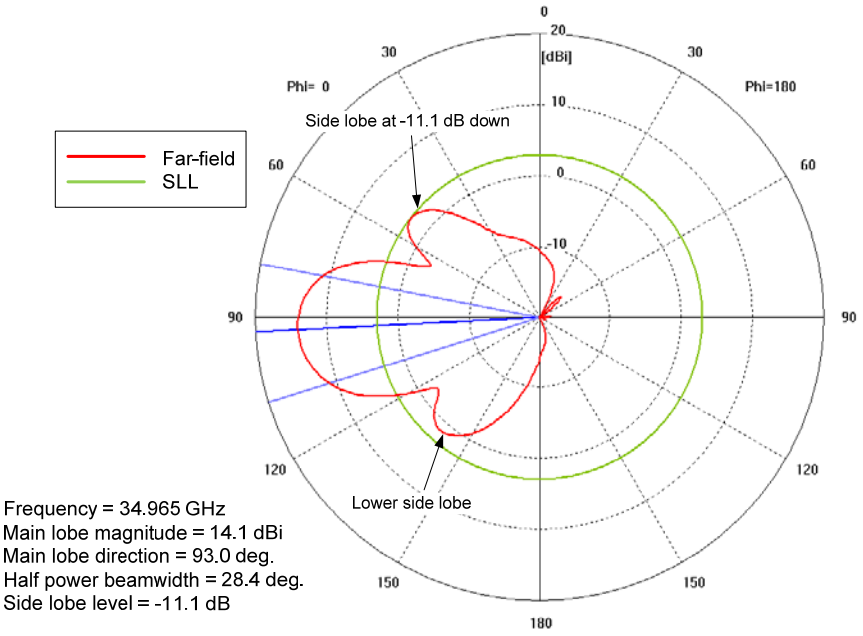

Figure 3-13. E-plane Pattern for an Eight-element Array of Microstrip Patches with a Horizontal and Vertical Patch-to-Patch Spacing of 0.169 inch

$\phi=0°, 0° < \theta < 180°$

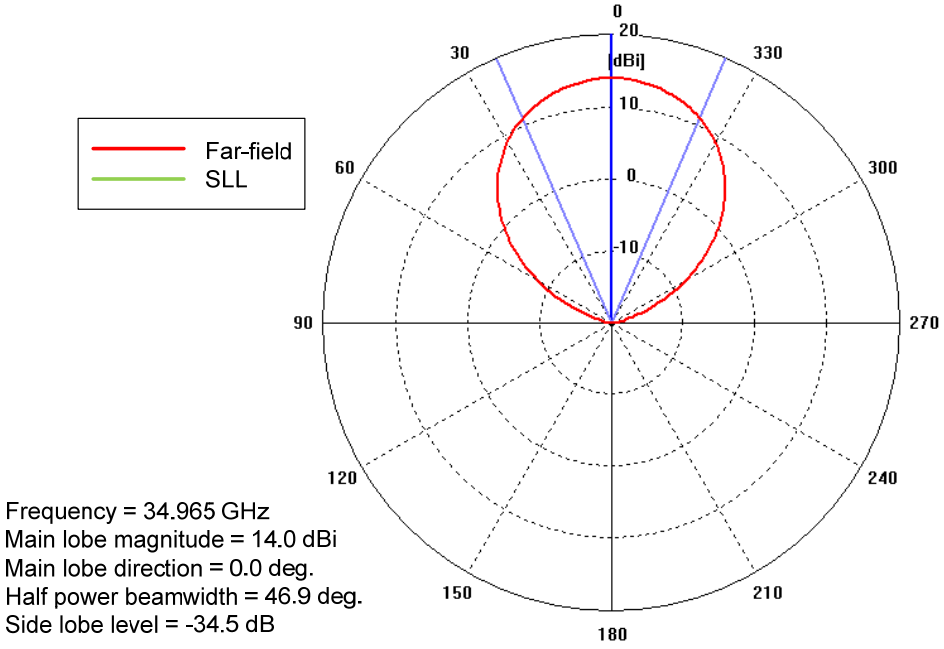

Figure 3-14. H-plane Pattern for an Eight-element Array of Microstrip Patches with a Horizontal and Vertical Patch-to-Patch Spacing of 0.169 inch

$0° < \phi < 360°, \theta = 90°$

The array model achieves the performance for directivity (14 dBi), however the desired SLL is not attained and is 2 dB higher than the calculated value of -13.1 dB. As established in earlier results, decreasing the element spacing reduces the SLL, and can therefore be applied to the E-plane. In order to reduce the SLL in the next iteration, the patch spacing in the vertical direction is reduced to slightly less than half-wavelength (Figure 3-15). The path length of the series line is held constant along with all other parameters.

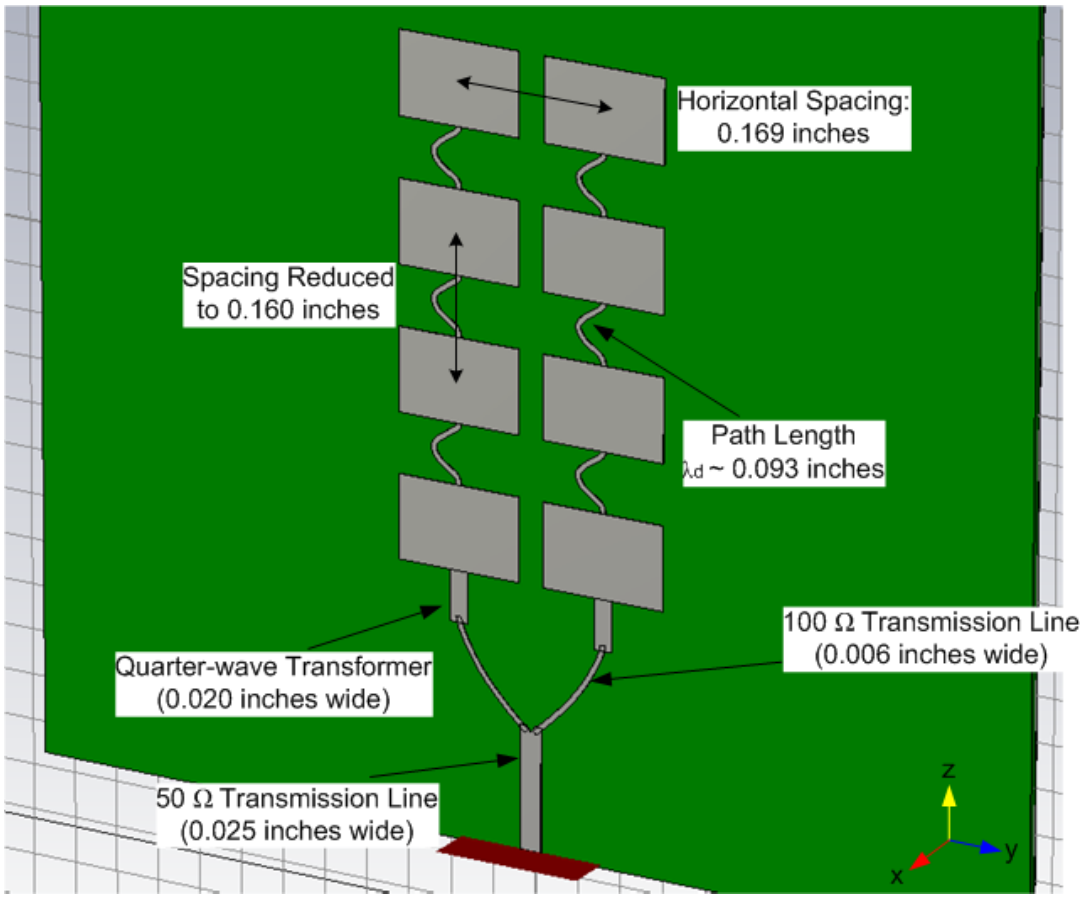

Figure 3-15. Eight-element Array of Microstrip Patches with a Horizontal and Vertical Patch-to-Patch Spacing of 0.169 inch and 0.160 inch, respectively

Figure 3-16 is a polar plot of the E-plane pattern that confirms a reduction in SLL as the element spacing is decreased. The SLL has decreased by 0.7 dB as a result of reducing the spacing between the patches, however the peak directivity also decreased (by 0.2 dB).

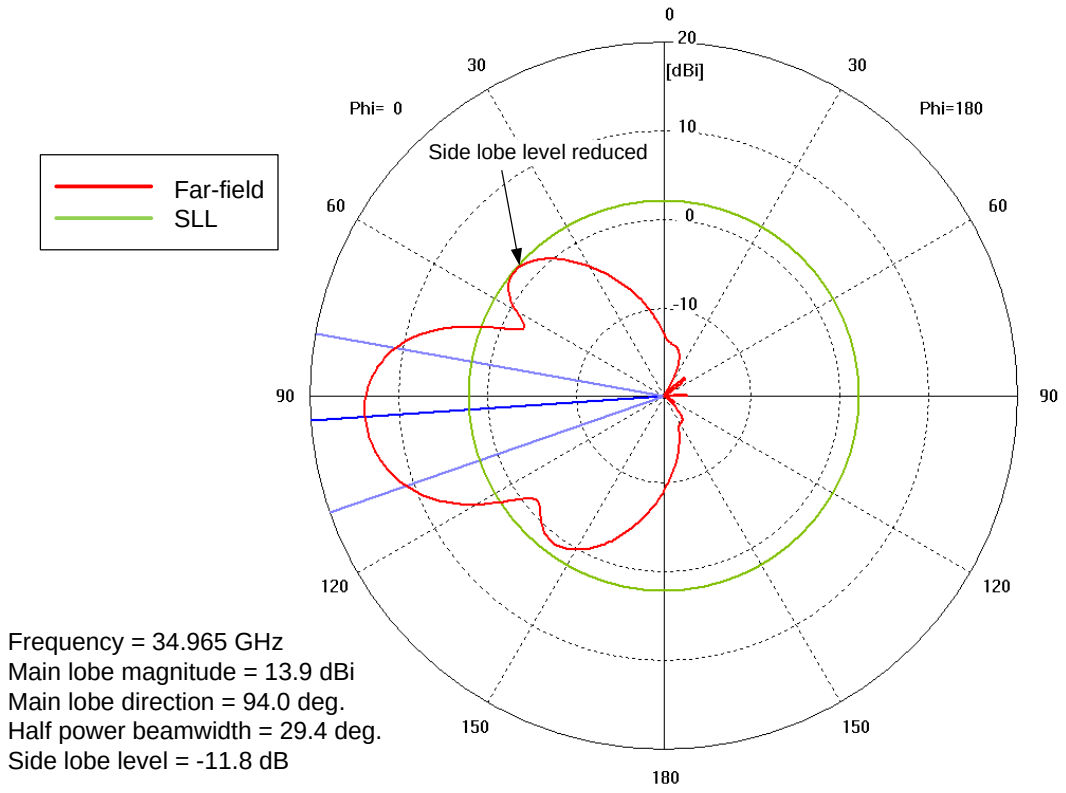

Figure 3-16. E-plane Pattern for an Eight-element Array with a Horizontal and Vertical Patch-to-Patch Spacing of 0.169 inch and 0.160 inch, respectively

$\phi=0°, 0° < \theta < 180°$

Due to the favorable results of lower SLL, the reduced vertical spacing of 0.160 inch is used in all subsequent iterations of the model.

Next, the same connector described in Chapter 2 is added to the model to observe the effects on the radiation pattern and SLL. A new model with the connector is shown in Figure 3-17.

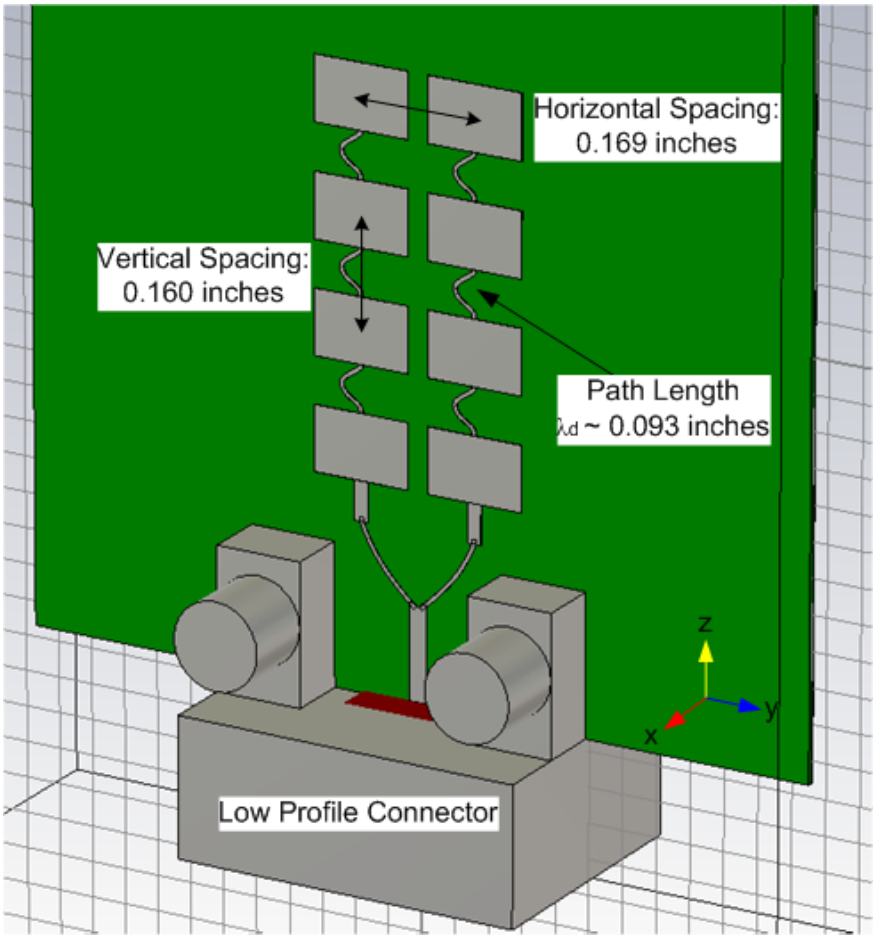

Figure 3-17. Eight-element Array Geometry from Figure 3-15 with a Low Profile Connector

The computed three-dimensional radiation and E-plane patterns are shown in Figure 3-18 and Figure 3-19, respectively.

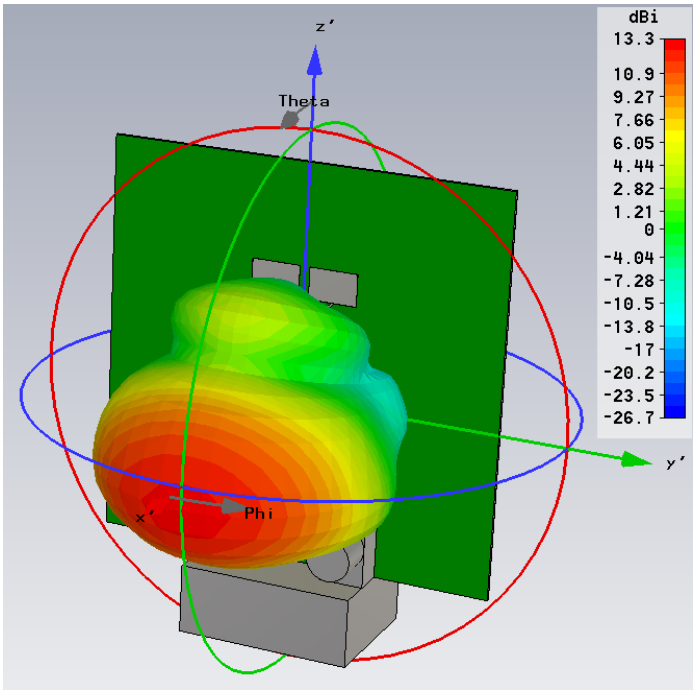

Figure 3-18. Radiation Pattern for the Eight-element Array of Figure 3-17

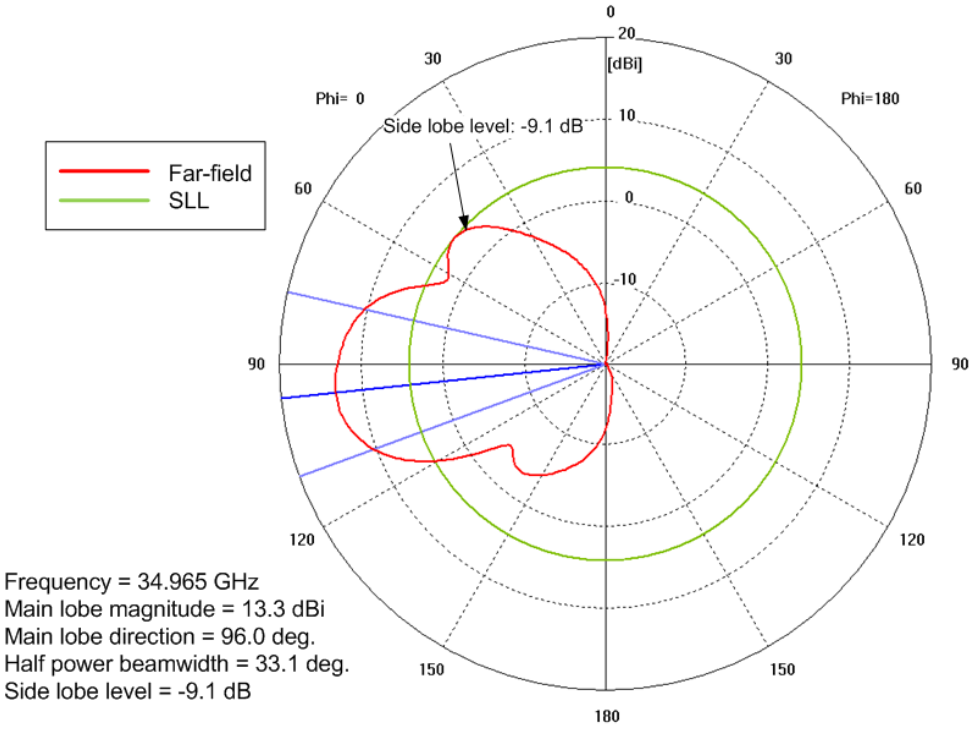

Figure 3-19. E-plane Pattern for the Eight-element Array of Figure 3-17

ϕ=0°, 0° <θ < 180°

It is evident that the connector has adverse effects on both the directivity and SLL as the directivity is reduced by 0.6 dB and the SLL is increased by 2.7 dB as compared to when the connector is absent. The low profile connector already shows to have the least effect on pattern of the available arrays; hence other methods for attaining the design specification must be considered.

Although the vertical spacing between the elements is fixed at 0.160 inch, the path length of the series lines connecting each element can be varied while still maintaining the vertical spacing. The path length is varied from 0.093 inch to 0.100 inch to determine if there was an optimum value for an improved SLL. The reason for the increase in length is because the path length of the series line is what controls the phase at which the patches are fed. A trial and error approach is used for various path lengths until an optimum length yielding the lowest SLL is found. The model having the most favorable SLL results is one with series line path length of 0.097 inch; this geometry and its corresponding radiation pattern are shown in Figure 3-20 and Figure 3-21, respectively.

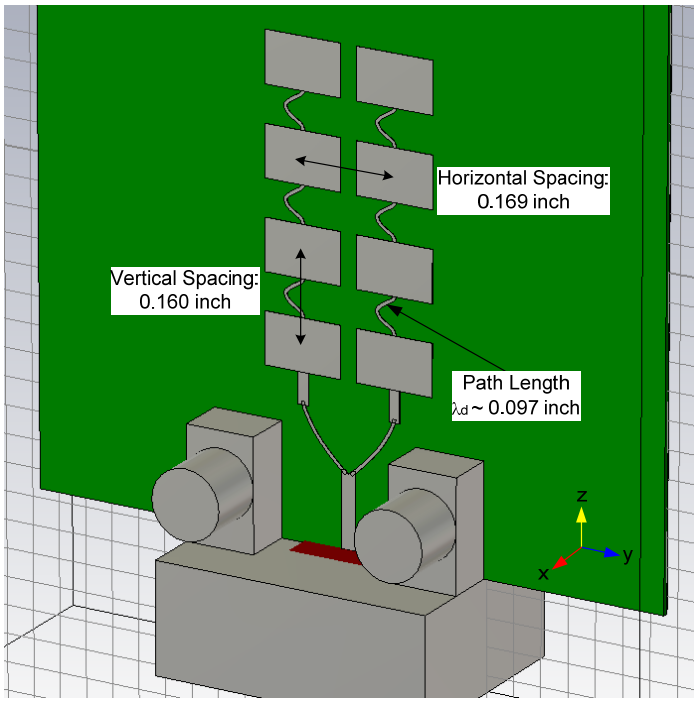

Figure 3-20. Eight-element Two-dimensional Microstrip Patch Array with Series Line Path Lengths of 0.097 inch

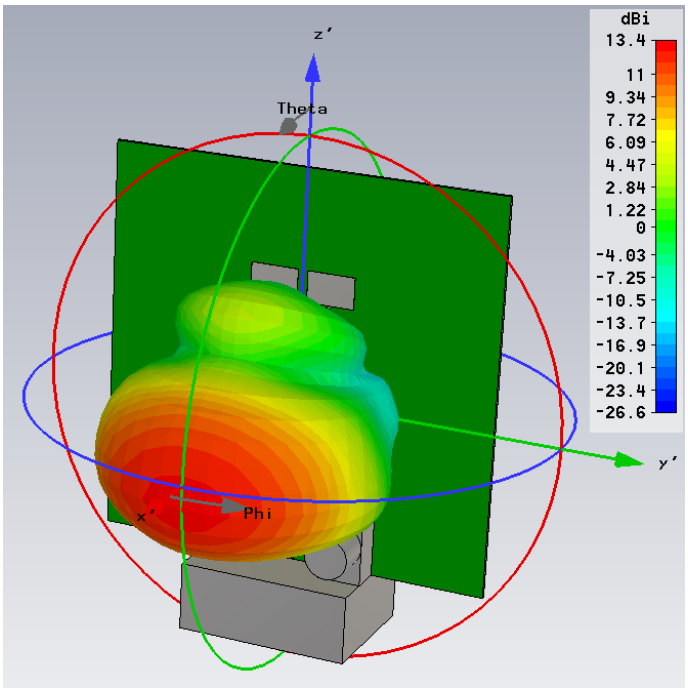

Figure 3-21. Radiation Pattern for the Eight-element Array shown in Figure 3-20 with Series Line Path Lengths of 0.097 inch

Though still not within the desired performance of -13 dB, the SLL did improve by 0.3 dB as a result of "tuning" the series line path length (Figure 3-22).

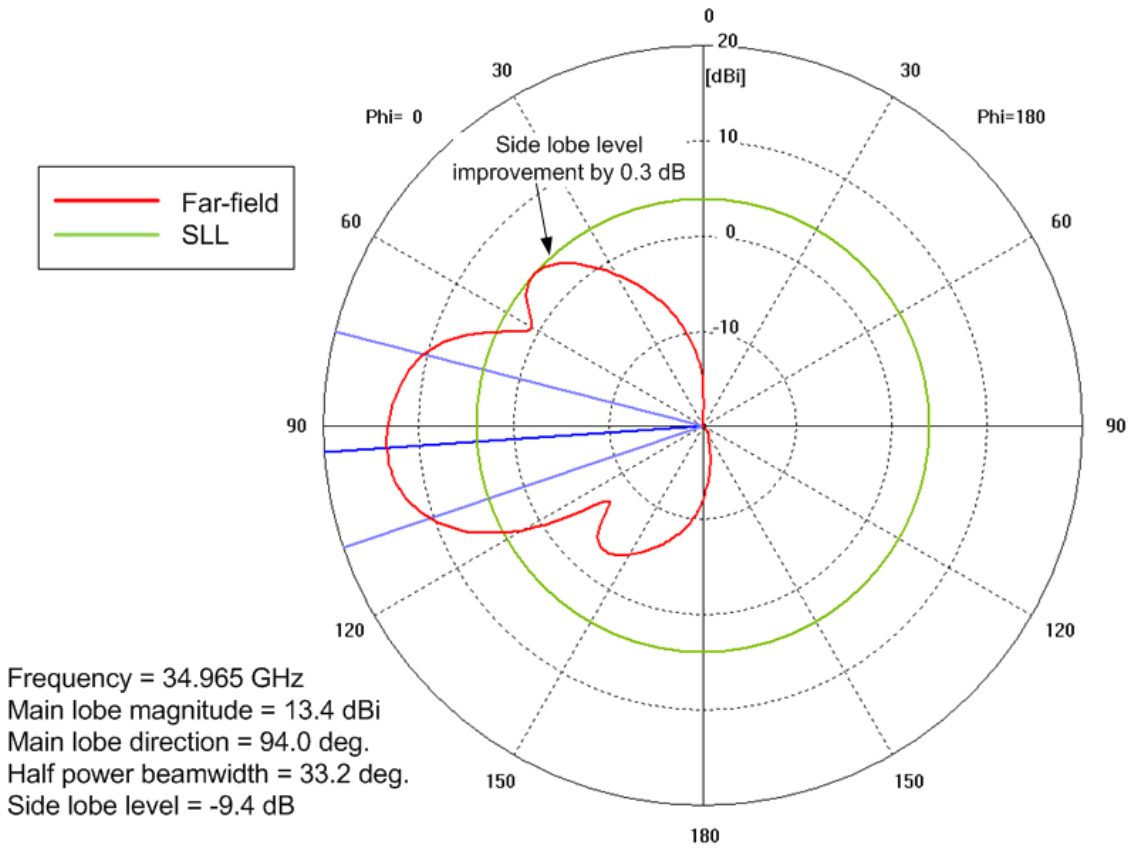

Figure 3-22. E-plane Pattern for the Eight-element Array with Series Line Path Lengths of 0.097 inch

ϕ=0°, 0° <θ < 180°

Another SLL reduction strategy was to shorten the length, *l*, of the microstrip line segments which enter the patches (Figure 3-23) [6].

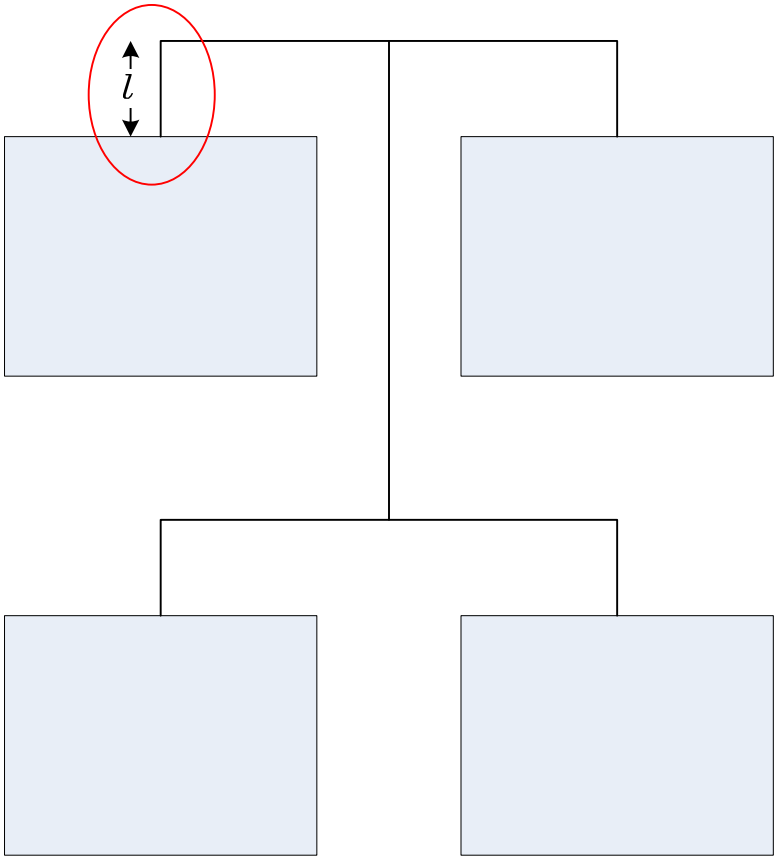

Figure 3-23. Four-element Array Used in [6] to Reduce SLL by Decreasing *l*

This idea was applied not to the series feed lines but to the quarter wave transformers. A meandering curved line of width 0.020 inch and path length 0.056 inch (the same dimensions as that of the previously implemented quarter-wave transformer) was modeled to replace the standard quarter wave transformer. Replacing the straight quarter-wave transformers with curved lines also required modification of the Y-junction. The angle at which the 100 Ω lines split was reduced. The geometry of the new model is shown in Figure 3-24.

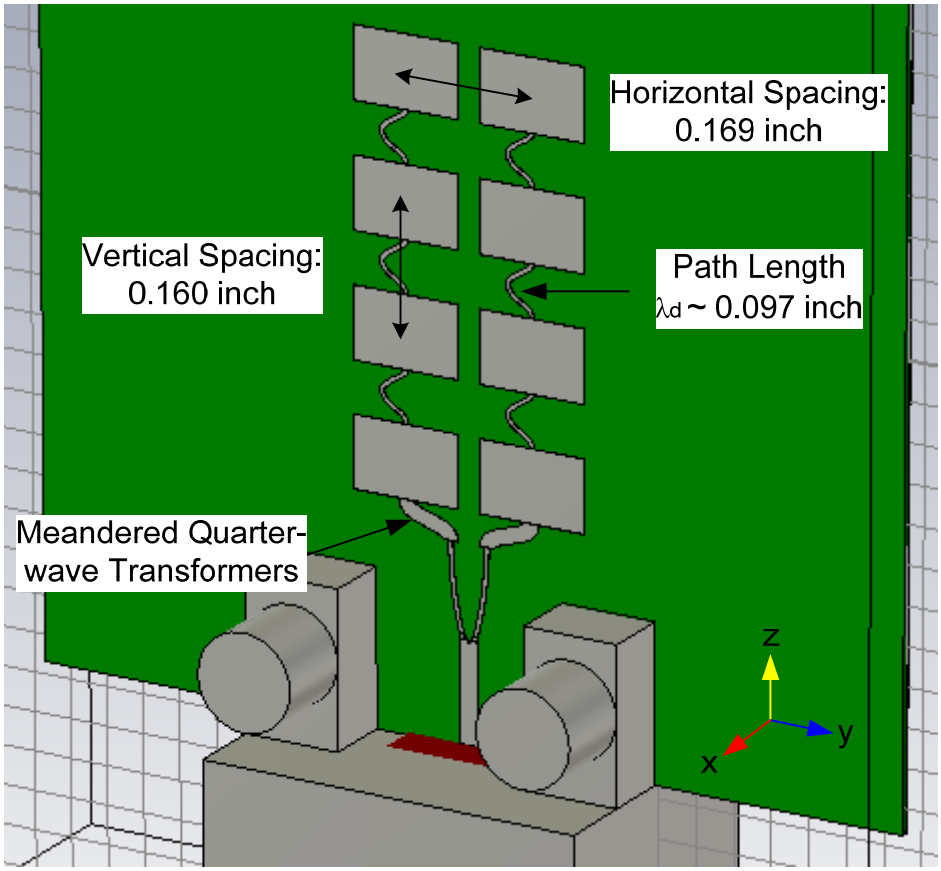

Figure 3-24. Eight-element Two-dimensional Array of Microstrip Patches with Meandered Quarter-wave Transformers

Figure 3-25 and Figure 3-26 show the radiation pattern and E- and H-plane patterns, respectively. As a result of meandering the quarter-wave transformers, the peak directivity is increased from 13.4 dBi to 14.3 dBi and the SLL is improved by more than 4 dB. Because the meander effectively reduced the length of the line segment entering the patch, the SLL level was reduced to -13.5 dB, which is 0.5 dB better than the required maximum specification.

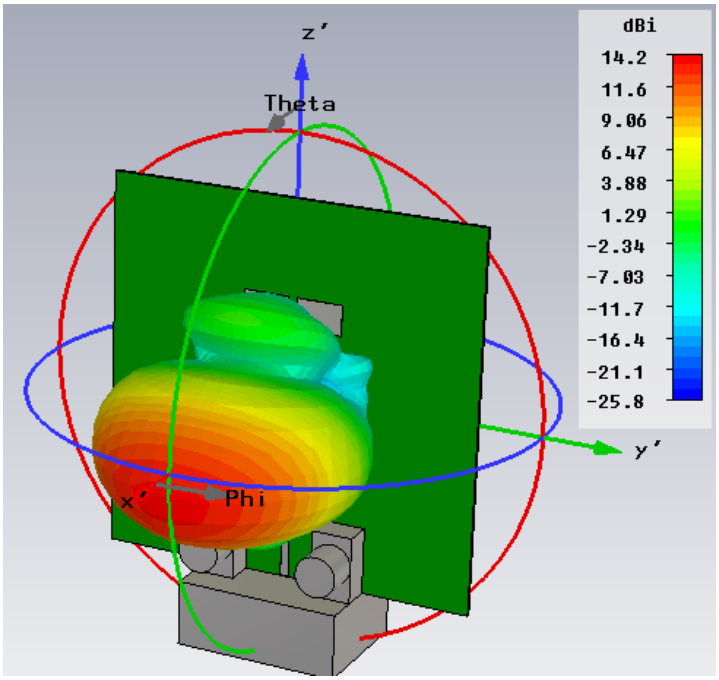

Figure 3-25. Radiation Pattern for the Eight-element Array of Microstrip Patches with Meandered Quarter-wave Transformers shown in Figure 3-24

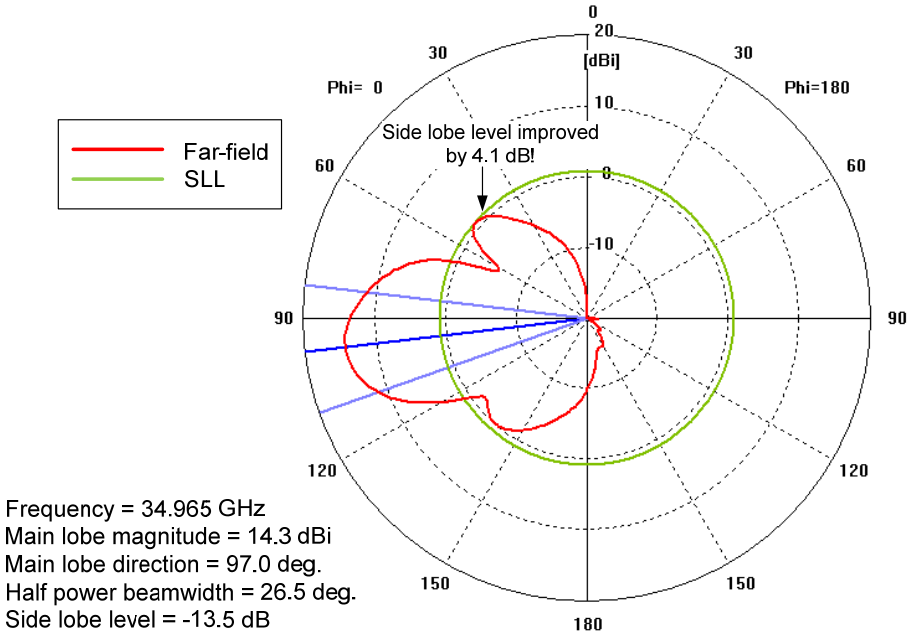

Figure 3-26. E-plane Pattern for the Eight-element Array of Microstrip Patches with Meandered Quarter-wave Transformers shown in Figure 3-24

ϕ=0°, 0° <θ < 180°

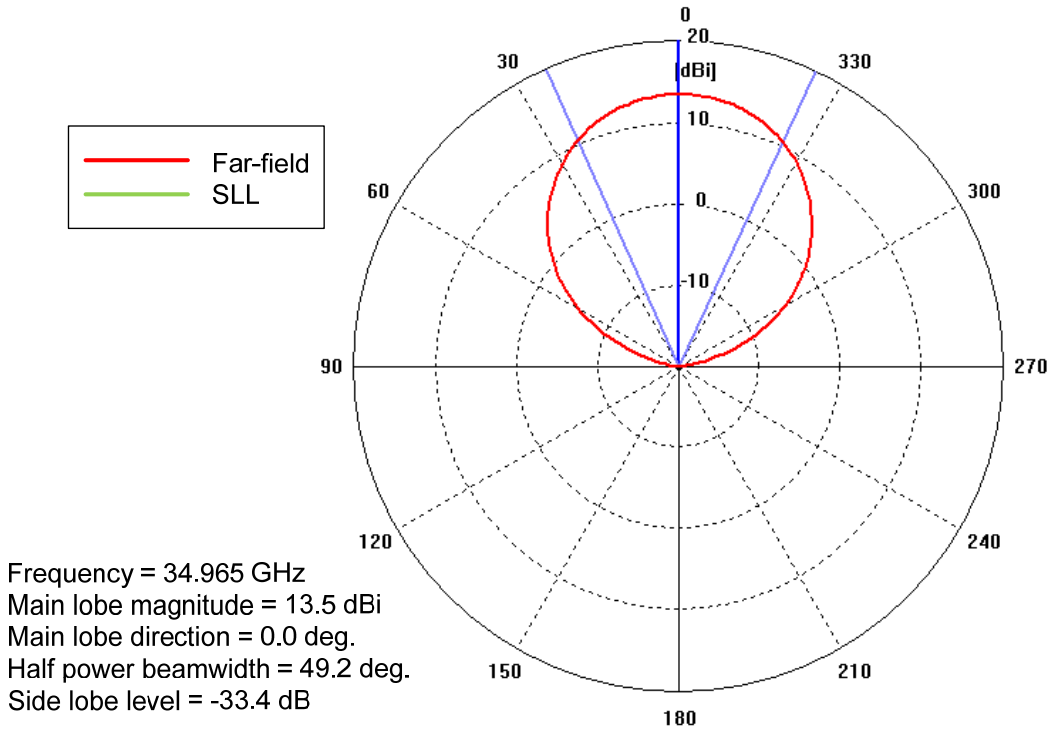

Figure 3-27. H-plane Pattern for the Eight-element Array of Microstrip Patches with Meandered Quarter-wave Transformers shown in Figure 3-24

$\phi=0°, 0° < \theta < 180°$

The results for the antenna model in Figure 3-24 compare well with the theoretical calculations made for the eight-element array (Section 3.2.4.2). Table 3-2 summarizes the comparisons between the theoretical and simulated array characteristics.

Table 3-2. Comparison of the Theoretical versus Simulated Characteristics for the Eight-element Array shown in Figure 3-24

	Calculated	Simulated	% Difference
Peak directivity (dBi)	14.89	14.3	13.6%
E-plane half power beamwidth	26º	26.5º	1.9%
H-plane half power beamwidth	46º	49.2º	6.7%
E-plane SLL (dB)	-13.14	-13.5	4%

A probable reason for the numerically computed directivity being about 0.6 dBi lower than the theoretical value is the reduction of patch spacing in the vertical direction. The same reason may also account for a lower SLL. The half power beamwidths for the E- and H-plane show good agreement and are to within 2% and 7% of the theoretical values, respectively.

3.2.6.3 Increasing the Directivity

The SLL in the E-plane has been the main concern up to this point in the design because no model iterations achieve the desired performance until the geometry with the meandered quarter-wave transformer was implemented. The H-plane pattern however exhibits very low side lobes. At the risk of increased SLL in the H-plane, the spacing between the patches in the horizontal direction was increased in order to obtain higher directivity out of the array.

Given that the directivity increases as the element spacing increases, up to a spacing of λ for a broadside array [2], the horizontal spacing was increased to 0.184 inch (Figure 3-28).

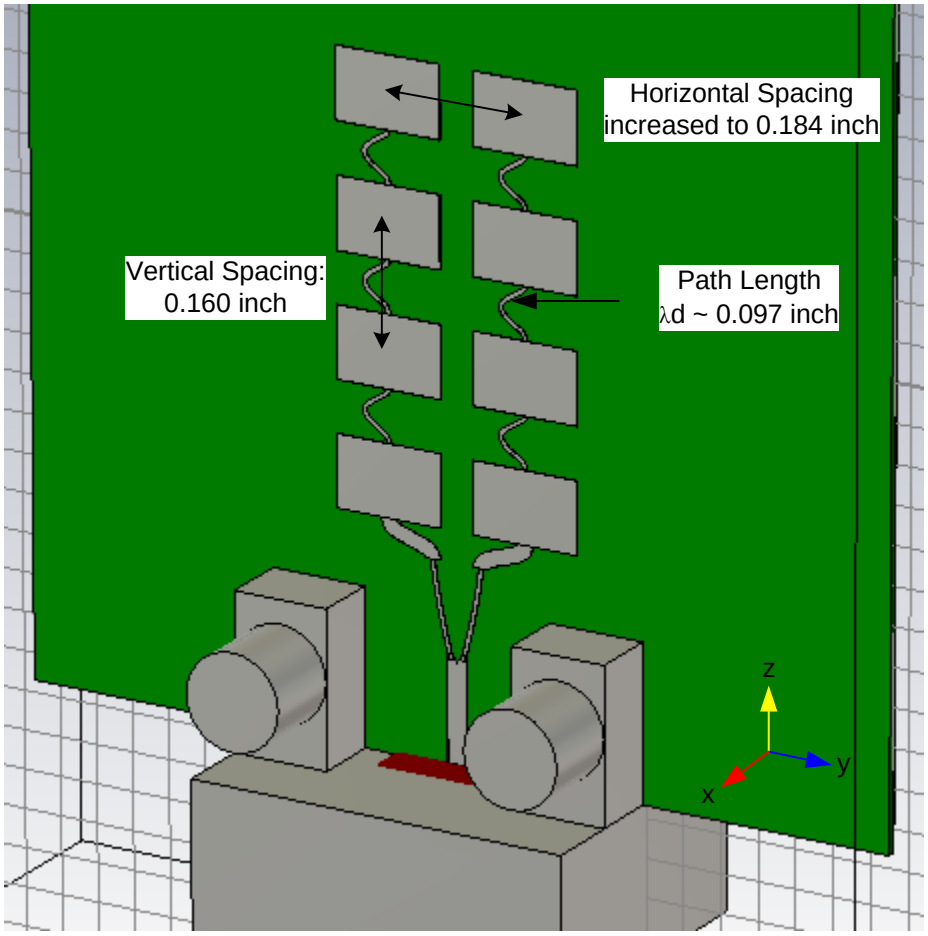

Figure 3-28. Eight-element Array of Microstrip Patches with Horizontal Spacing Increased to 0.184 inch

Increasing the horizontal spacing to 0.184 inch was successful as the peak directivity increased to 14.6 dBi. As expected, a very small side lobe begins to form in the H-plane, however this SLL is still lower than -30 dB. The E- and H-plane patterns are shown in Figure 3-29 and Figure 3-30, respectively.

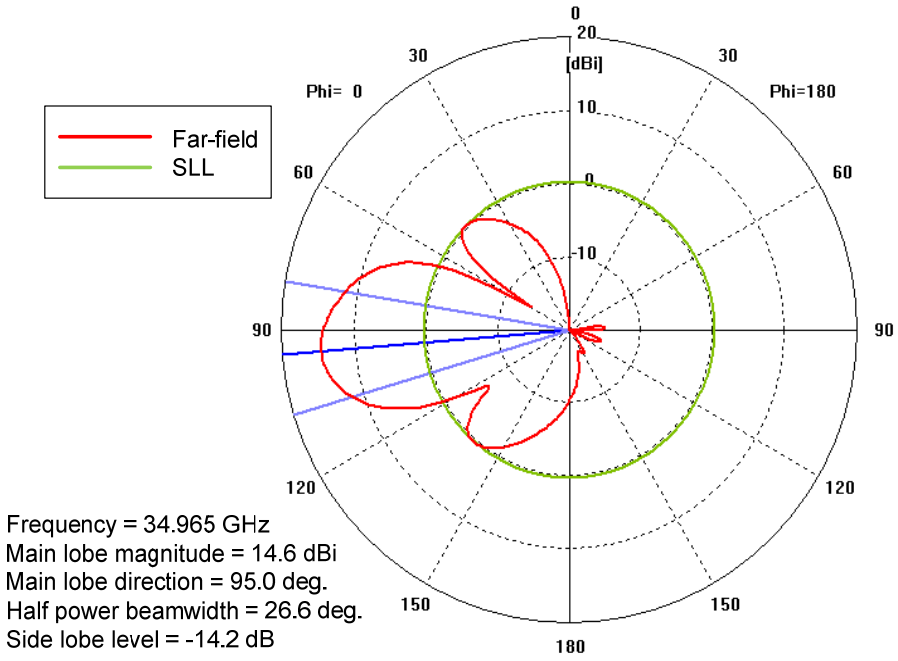

Figure 3-29. E-plane Pattern for an Eight-element Array of Microstrip Patches with Horizontal Spacing Increased to 0.184 inch

ϕ=0°, 0° <θ < 180°

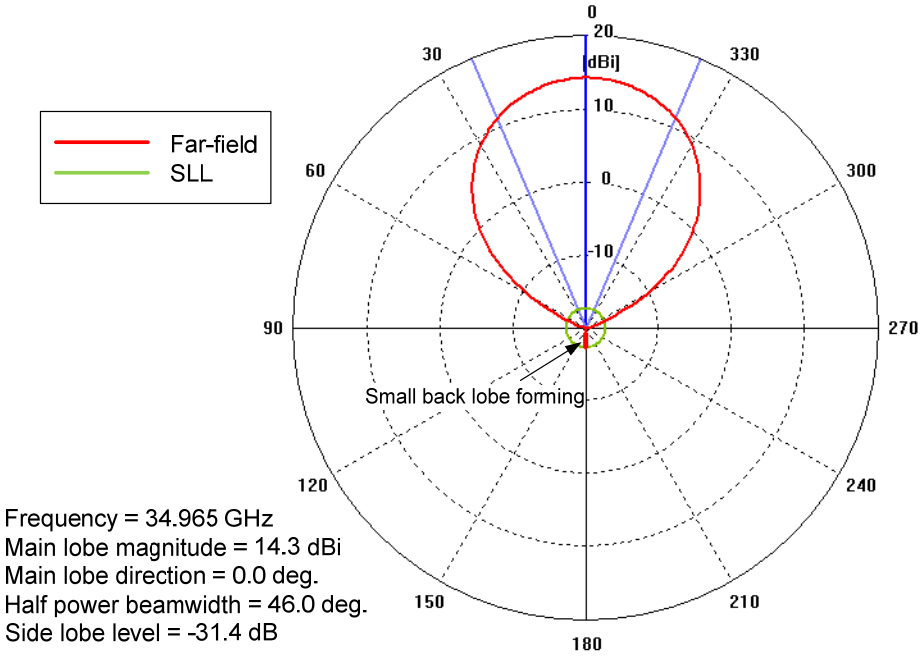

Figure 3-30. H-plane Pattern for an Eight-element Array of Microstrip Patches with Horizontal Spacing Increased to 0.184 inch

0° <ϕ < 360°, θ = 90°

Because the back lobe forming in the H-plane is still very small, another increase in the element spacing is evaluated. A horizontal spacing of 0.200 inch is modeled. All other parameters of the geometry are held constant (Figure 3-31).

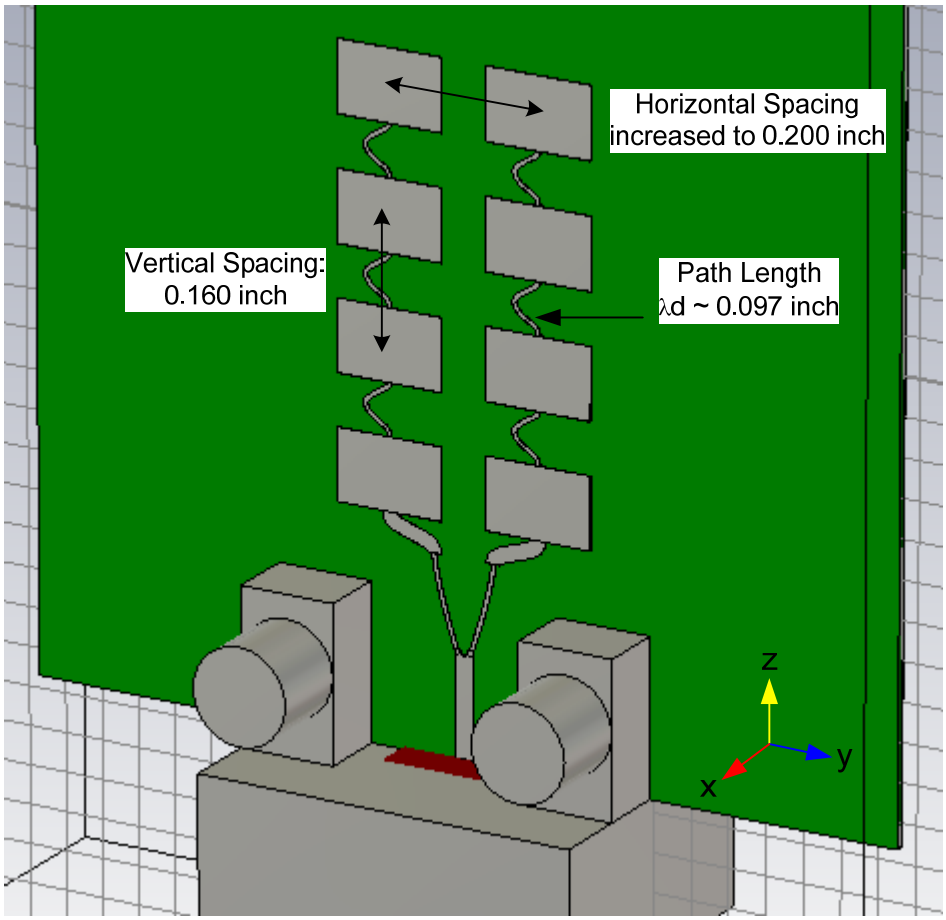

Figure 3-31. Eight-element Array of Microstrip Patches with Horizontal Spacing Increased to 0.200 inch

The corresponding E- and H-plane patterns are shown in Figure 3-32 and Figure 3-33. The peak directivity is increased to 15.0 dBi. The H-plane SLL increases to -29.1 dB. Because now enough margin in directivity (1 dB greater than required) has been achieved, it was decided to maintain the horizontal spacing at 0.200 inch.

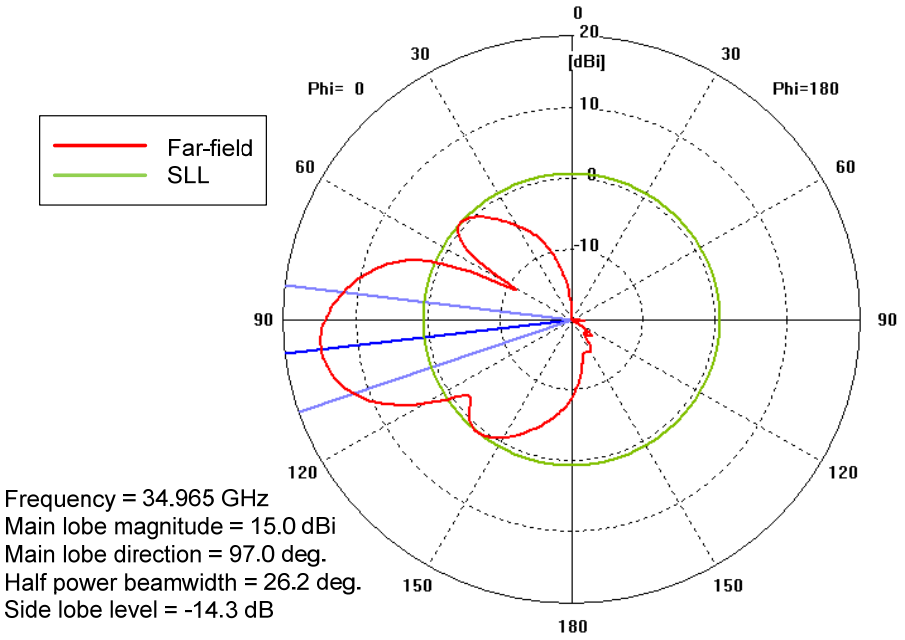

Figure 3-32. E-plane Pattern for an Eight-element Array of Microstrip Patches with Horizontal Spacing Increased to 0.200 inch

$\phi=0°, 0° < \theta < 180°$

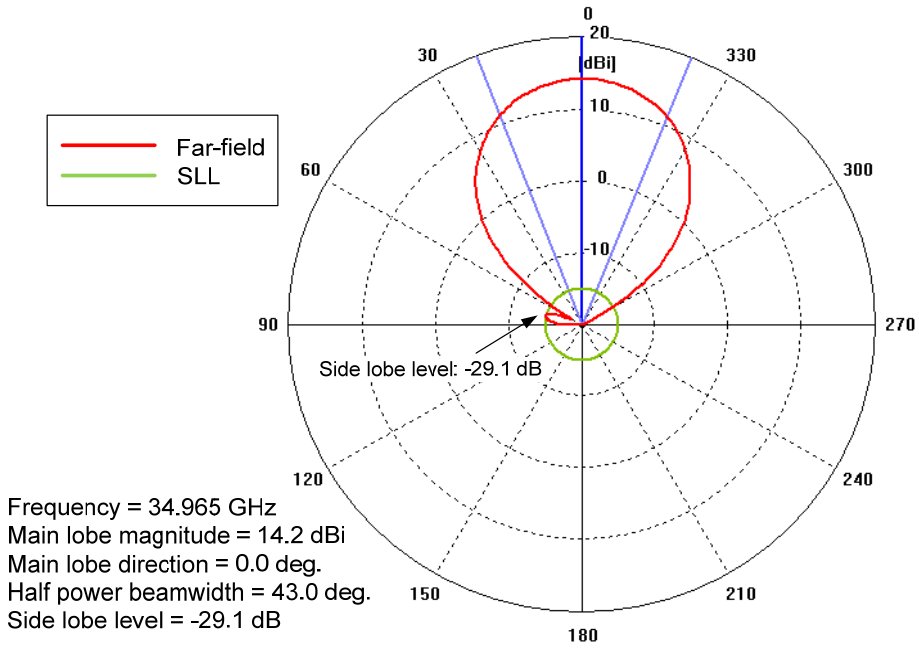

Figure 3-33. H-plane Pattern for an Eight-element Array of Microstrip Patches with Horizontal Spacing Increased to 0.200 inch

$0° < \phi < 360°, \theta = 90°$

As a final modification to the geometry of the planar eight-element array, the recommended board launch design is added to the model. The same launch design used for the low gain antenna is used for the high gain antenna. The design layout consists of 3 grounding vias on each side of the launch with a tapered section of transmission line in the center (Figure 3-34).

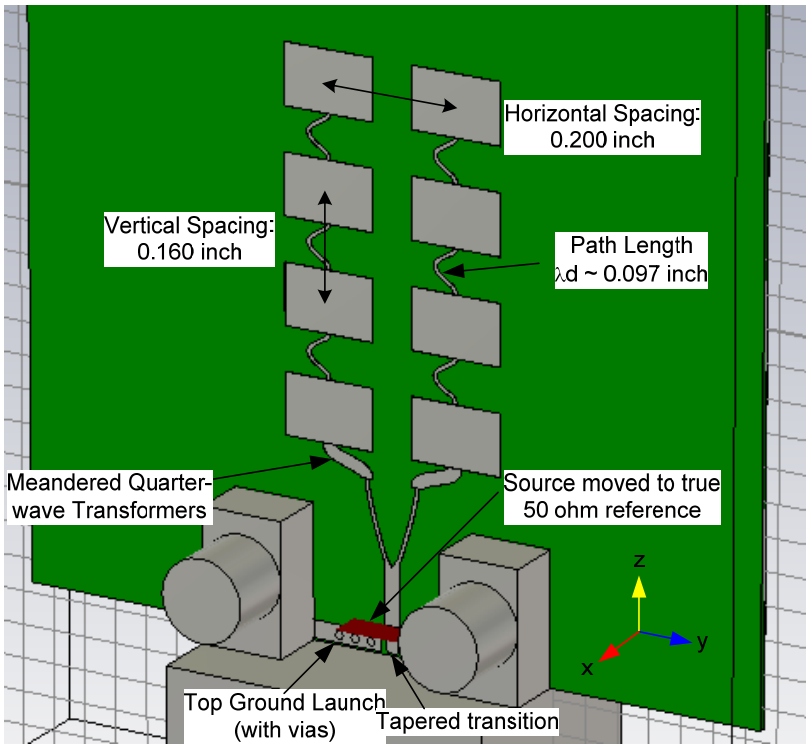

Figure 3-34. Final Geometry of the Eight-element Array of Microstrip Patches with 0.200 inch Horizontal Spacing, Low Profile Connector, and Board Launch Design

The three-dimensional radiation pattern, the E- and H-plane principal patterns, and the return loss results for the final geometry of the eight-element array are shown in Figures 3-35 through 3-38. The peak directivity is 14.7 dBi, and the E- and H-plane half power beamwidths are 26.7º and 45.3º, respectively.

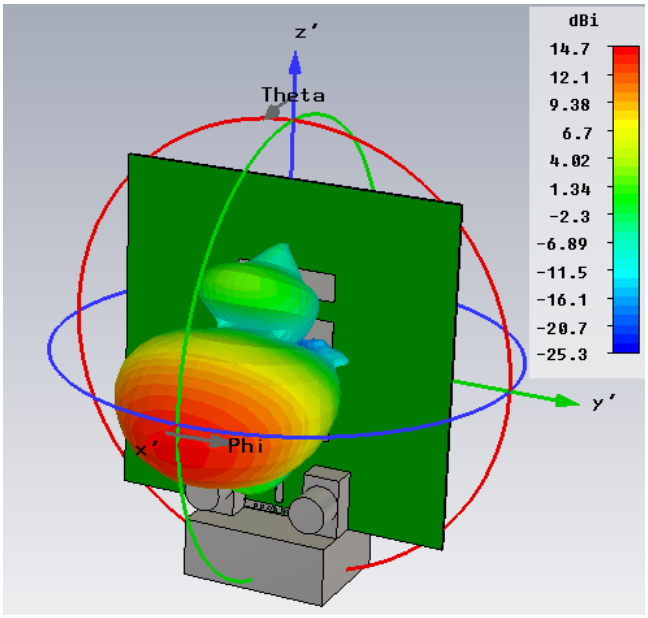

Figure 3-35. Radiation Pattern for the Final Geometry of the Eight-element Planar Microstrip Array with 0.200 inch Horizontal Spacing, Low Profile Connector, and Board Launch Design

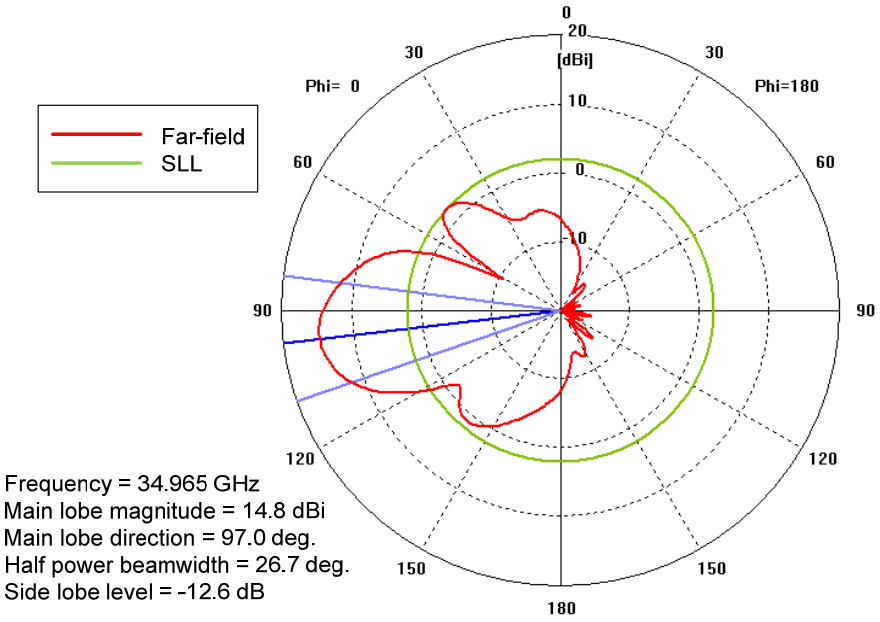

Figure 3-36. E-plane Pattern for the Final Geometry of the Eight-element Planar Microstrip Array with 0.200 inch Horizontal Spacing, Low Profile Connector, and Board Launch Design

$\phi=0°, 0° < \theta < 180°$

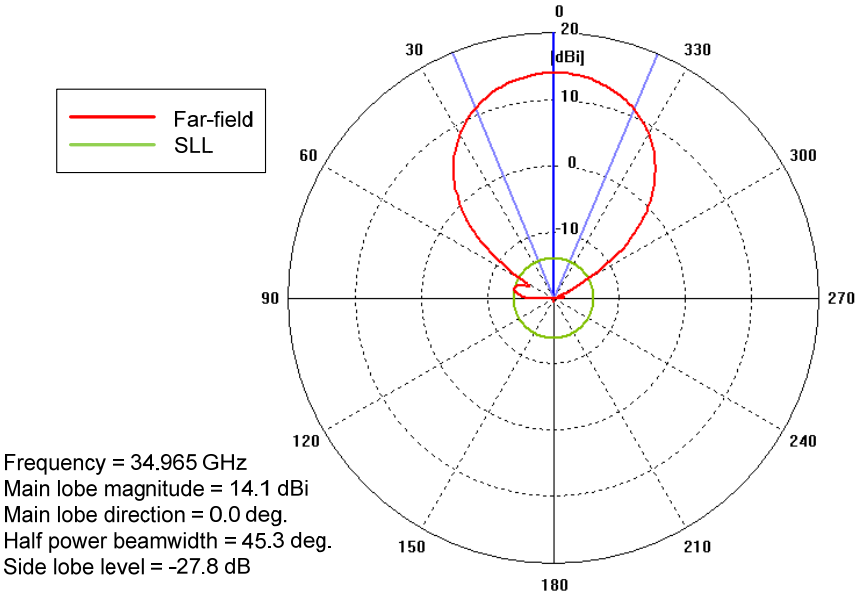

Figure 3-37. H-plane Pattern for the Final Geometry of the Eight-element Planar Microstrip Array with 0.200 inch Horizontal Spacing, Low Profile Connector, and Board Launch Design

$0° < \phi < 360°, \theta = 90°$

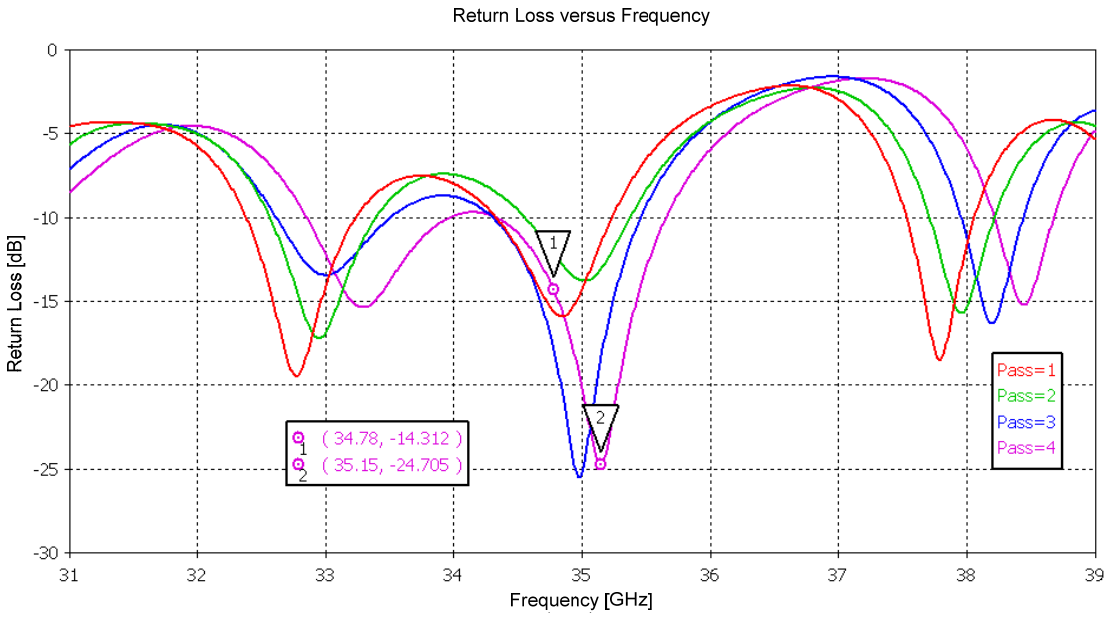

Figure 3-38. Return Loss for the Final Geometry of the Eight-element Planar Microstrip Array with 0.200 inch Horizontal Spacing, Low Profile Connector, and Board Launch Design

3.3 Conclusion

Modeling of the high gain antenna using CST Microwave Studio has yielded results indicating that the desired performance characteristics are achieved and are accomplished using an eight-element planar microstrip array with a low profile connector. A Y-junction splitter is used to feed 2 columns of patches, each column having 4 patches, which are fed by a series feed line. The antenna structure is matched to 50 Ω. The radiation pattern did show adverse effects because of the connector; however, improvements were made by meandering the quarter-wave transformers and adjusting the spacing between patch elements in order to achieve the desired performance. The simulated radiation patterns obtained in Chapter 3 are directly compared to the measured vertically polarized radiation patterns in Chapter 4.

3.4 References

[1] Bahl, I. J. and Bhartia, P., "Rectangular Microstrip Antennas" in *Microstrip Antennas*, Artech House, Dedham Mass, 1980, pp. 31-84.

[2] W.L. Stutzman and G.A. Thiele, *Antenna Theory & Design*, 2nd Ed. John Wiley & Sons, Inc., 1998, pp 87-103, 112-116.

[3] Wu, K-L., Spenuk, M., Litva, J., and Fang, D.-G., "Theoretical and experimental study of feed network effects on the radiation pattern of series-fed microstrip antenna arrays," *IEE Proc. H, Microwaves, Antennas & Propagation*, 1991, 138, pp. 238-242.

[4] Roger's Corporation. "RT/duroid®6002 High Frequency Laminates." http://www.rogerscorp.com/acm/products/12/RT-duroid-6002-6202-6006-6010-PTFE-Ceramic-Laminates.aspx.

[5] Constantine A. Balanis, *Antenna Theory: Analysis and Design*, 2nd Ed., New York, John Wiley & Sons, Inc., 1997, pp 764-767.

[6] E. Levine, G. Malamud, S. Shtrikman, and D. Treves, “A study of microstrip array antennas with the feed network,” *IEEE Trans. Antennas & Propagation.,* vol. 37, pp. 426-433, Apr. 1989.

4 THE EXPERIMENTAL CHARACTERIZATION OF PERFORMANCE OF THE TWO-ELEMENT AND EIGHT-ELEMENT PATCH ANTENNA ARRAYS

4.1 Introduction

The data obtained from the experimental performance characterization of the two-element and eight-element planar patch antenna arrays is presented. Comparisons are made between the measured performance characteristics of the two antennas and the simulated results obtained from CST Microwave Studio. The purpose of the testing is to verify that both arrays achieve the desired performance given in Table 2-1 and Table 3-1. The overall test philosophy is also provided.

4.2 Test Philosophy

RT/duroid® 6002 substrate material from Rogers Corporation [1] is available in several panel sizes. A panel size of 18 inches by 12 inches is chosen. Because the dimensions of each array roughly form a square inch, the large panel size allows for many antennas to be fabricated on one panel. The opportunity presents itself to build not just the antennas designed in Chapters 2 and 3 but variations of these antennas as well.

4.2.1 Variation of Resonant Frequency of the Two-element Array

4.2.1.1 Variation of Patch Length

The patch length in the two-element array is 0.092 inch; however the manufacturing tolerance of the copper layer is ±0.001 inch. Hence two-element arrays

having patches of lengths 0.091 inch and 0.093 inch are also considered for fabrication. First, the final geometry for the low gain antenna of Chapter 2 is modified by reducing the length of each patch to 0.091 inch, in order to quantify the change in performance that can be expected due to tolerance variation. The geometry of this array is shown in Figure 4-1; all other parameters were held constant.

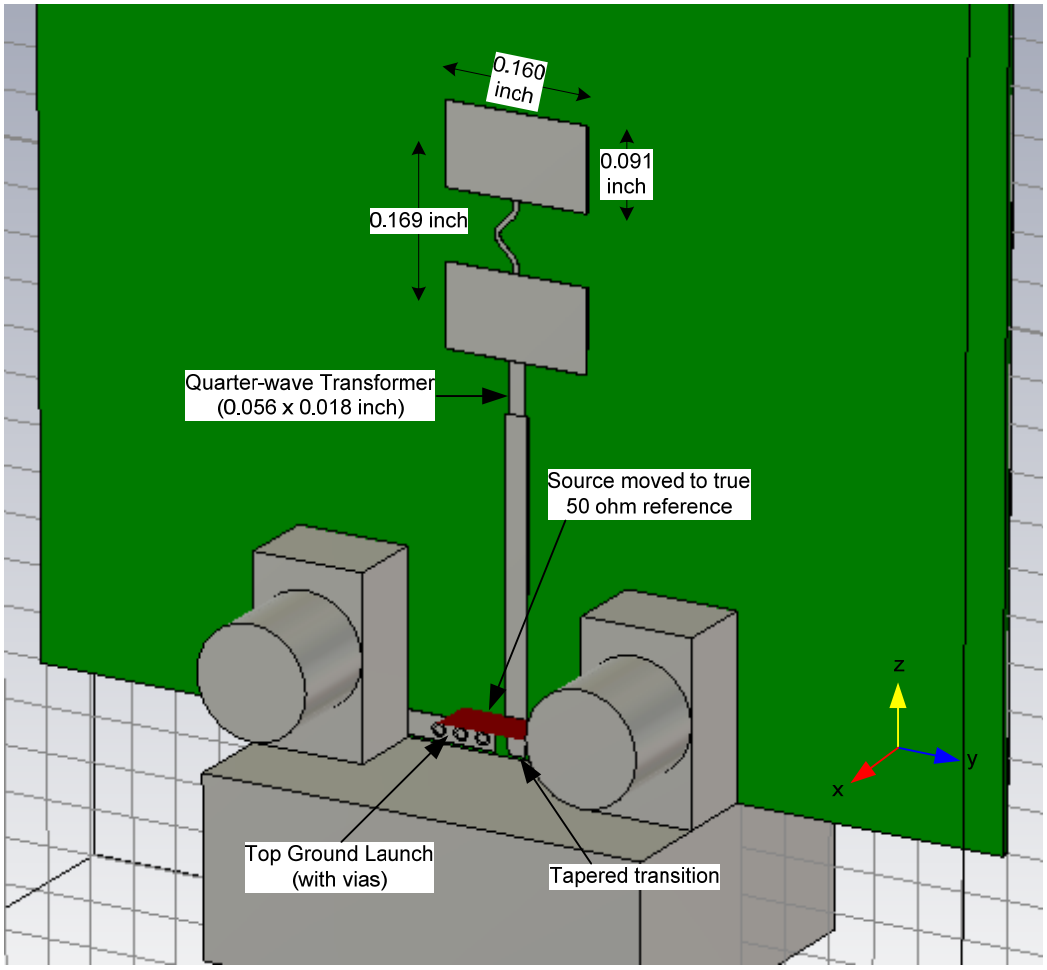

Figure 4-1. Geometry of a Two-element Array with Patches of Length 0.091 inch

This geometry is modeled and simulated in CST Microwave Studio. A plot of return loss versus frequency (Figure 4-2) indicates that the effect of reducing the length of the patches is an increase in the resonant frequency by 310 MHz.

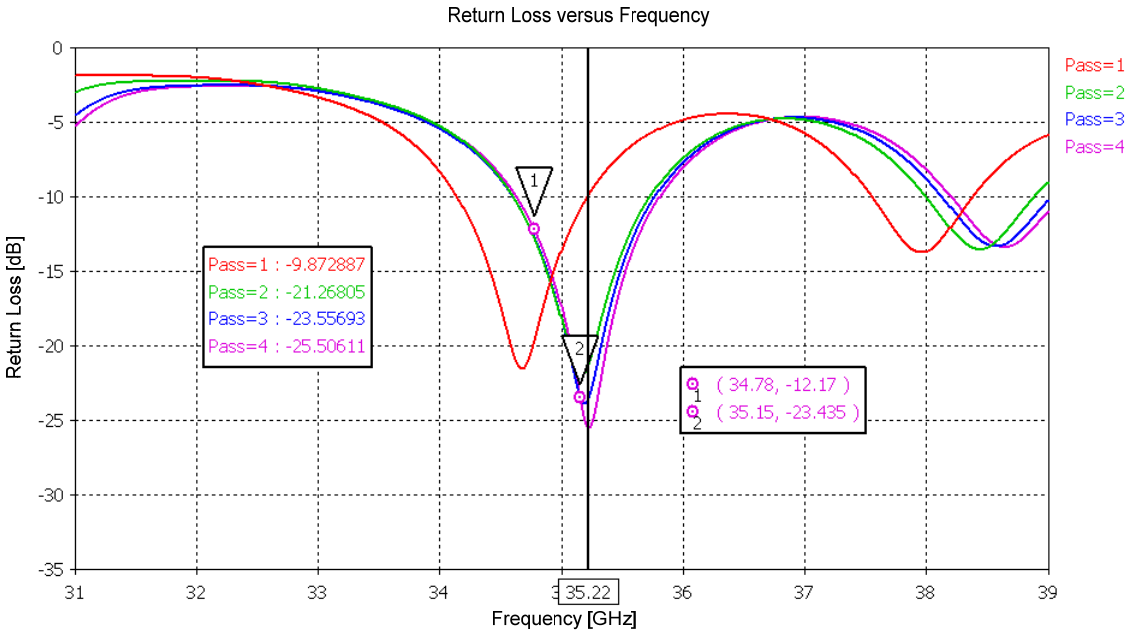

Figure 4-2. Return Loss for a Two-element Array with Patches of Length 0.091 inch

The center frequency for the array in Figure 4-1 is 35.22 GHz and the return loss magnitude is -25.5 dB. Despite the higher resonant frequency, the return loss at the design frequency of 34.965 GHz is still less than -14 dB for a VSWR of less than 1.5 to 1. Due to computer memory limitations, results for only four passes of the adaptive mesh refinement are generated.

Likewise, increasing the length of the patches results in a decrease in resonant frequency. A two-element array model with patches of length 0.093 inch is created in CST Microwave Studio (Figure 4-3). A plot of return loss versus frequency (Figure 4-4) shows that the resonant frequency decreases to 34.56 GHz, which is a shift of 405 MHz. The return loss is still less than -10 dB for the entire design bandwidth.

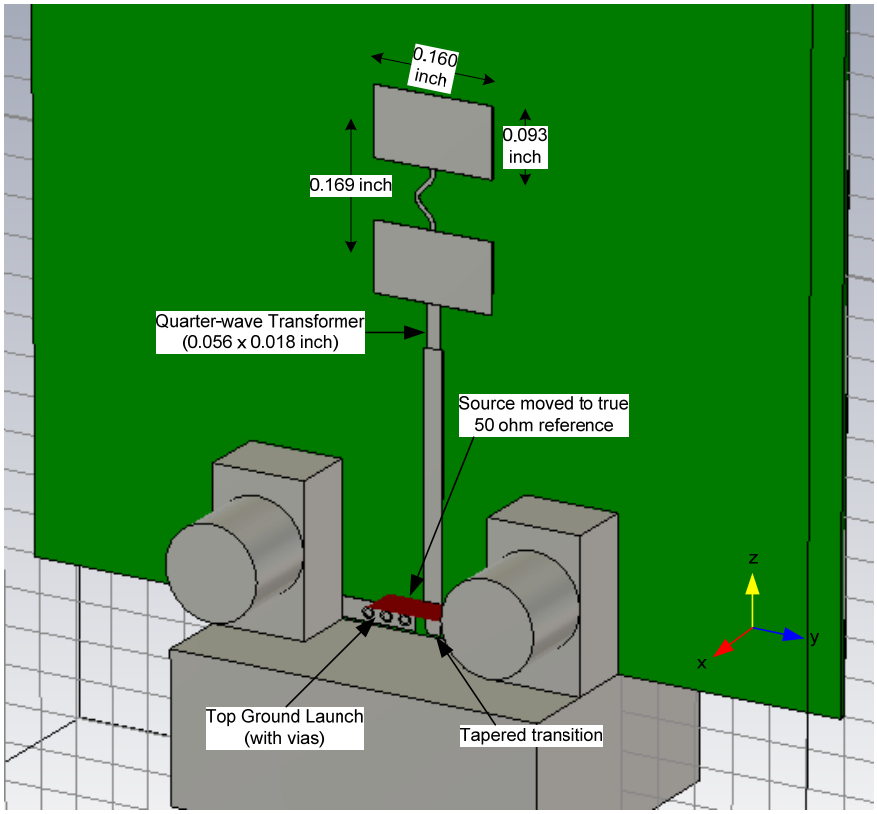

Figure 4-3. Geometry for a Two-element Array with Patches of Length 0.093 inch

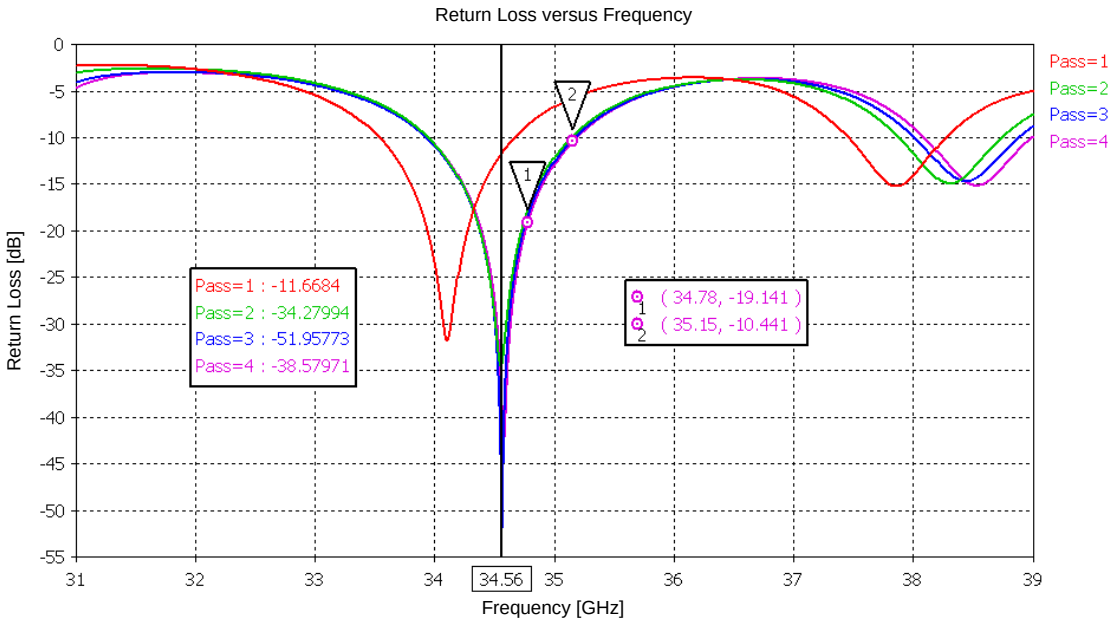

Figure 4-4. Return Loss for a Two-element Array with Patches of Length 0.093 inch

Table 4-1 summarizes the resonant frequencies for the three values of patch length.

Table 4-1. Resonant Frequency for the Two-element Array as Patch Length Varies

Patch Length (inches)	Resonant Frequency (GHz)
0.091	35.11
0.092	34.91
0.093	34.69

The far-field radiation pattern at 34.965 GHz does not change significantly as a result of variations in patch length. E- and H-plane characteristics have subtle differences as indicated by the comparisons made in Table 4-2.

Table 4-2. Radiation Pattern Characteristics at 34.965 GHz for the Two-element Array as Patch Length Varies

	0.091 inch Patches	0.092 inch Patches	0.093 inch Patches
E-plane			
Peak directivity (dBi)	10.7	10.7	10.7
Half power beamwidth	41.7º	41.9º	42.1º
Side lobe level (dB)	-27.7	-27.4	-27.2
H-plane			
Peak directivity (dBi)	10.6	10.6	10.6
Half power beamwidth	59.5º	60.5º	61.5º
Side lobe level (dB)	-31.4	-31.8	-32

4.2.1.2 Variation of Dielectric Constant

A similar analysis is done with the relative dielectric constant of the substrate material, ε_r. As mentioned in Section 2.2.2, ε_r for RT/duroid® 6002 is equal to 2.94 with a tolerance of ±0.04 [1]. The approximate shift in resonance frequency calculated from Equation (2-1) is ±240 MHz. To model the possible variation of ε_r, two additional arrays were created using CST Microwave Studio – one with the substrate material having a relative dielectric constant of 2.90 and one having a relative dielectric constant of 2.98. Figures 4-5 through 4-7 show how the resonant frequency changes as ε_r changes within its specified tolerance limits.

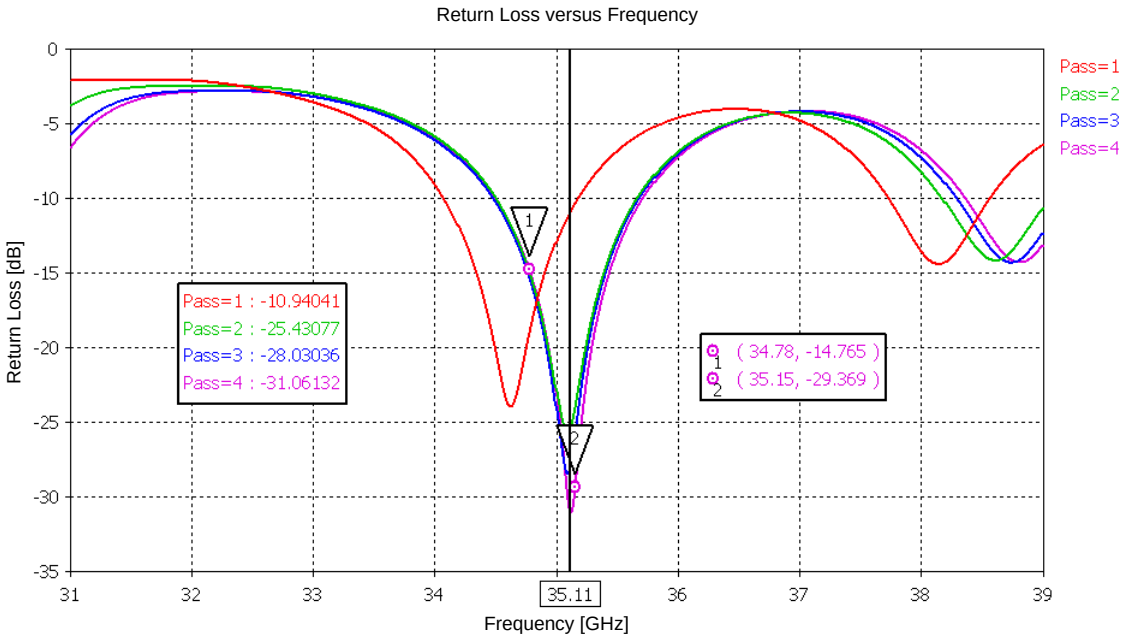

Figure 4-5. Return Loss for the Two-element Array Geometry with ε_r = 2.90

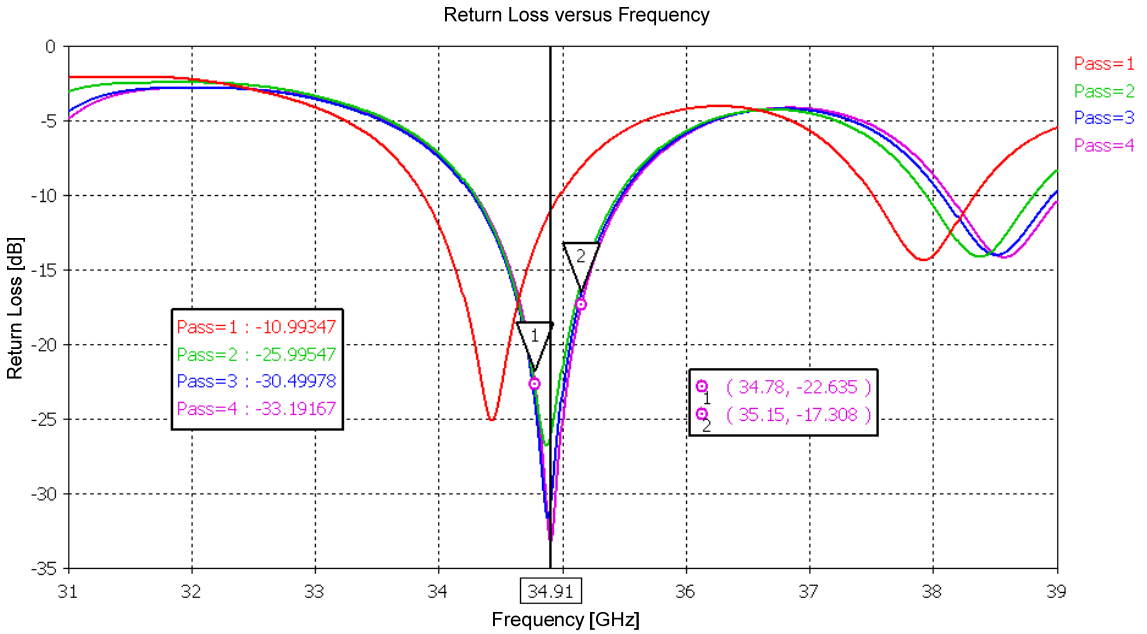

Figure 4-6. Return Loss for Final Two-element Array Geometry with ε_r = 2.94

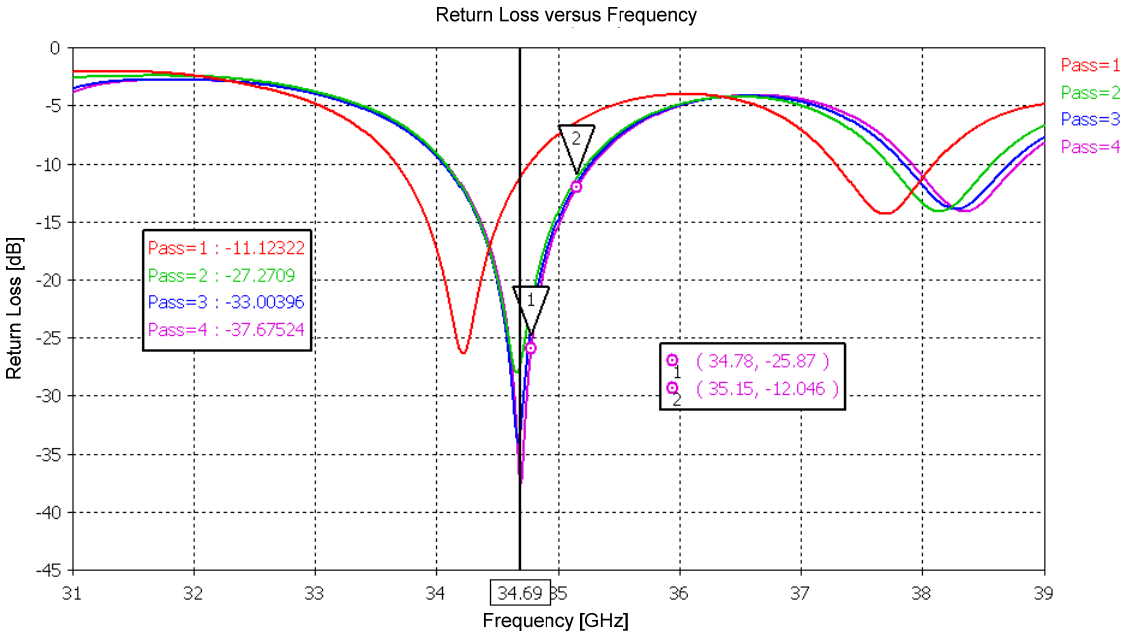

Figure 4-7. Return Loss for Final Two-element Array Geometry with ε_r = 2.98

A summary of the resonant frequencies for the low, median, and high values of ε_r is provided in Table 4-3.

Table 4-3. Two-element Array Resonant Frequencies for Low, Median, and High Values of ε_r

ε_r	Resonant Frequency (GHz)
2.90	35.11
2.94	34.91
2.98	34.69

The greatest difference in resonant frequency is ±210 MHz, 30 MHz less than the value obtained from Equation (2-1).

As in the case of patch length variation, the far-field radiation pattern at 34.965 GHz does not noticeably change with small variations in the relative dielectric constant. E- and H-plane radiation pattern characteristics summarized in Table 4-4 result in very subtle differences in half power beamwidths and SLL.

Table 4-4. Two-element Array Radiation Pattern Characteristics at 34.965 GHz for Low, Median, and High Values of ε_r

	ε_r=2.90	ε_r=2.94	ε_r=2.98
E-plane			
Peak directivity (dBi)	10.7	10.7	10.7
Half power beamwidth	42º	41.9º	41.7º
Side lobe level (dB)	-27.3	-27.4	-27.6
H-plane			
Peak directivity (dBi)	10.6	10.6	10.6
Half power beamwidth	59.2º	60.5º	61.9º
Side lobe level (dB)	-31.6	-31.8	-31.6

It is assumed that the relative dielectric constant ε_r of the material is uniform throughout the entire panel, and therefore there will be no variation in ε_r for multiple antennas built from this panel. However, the length of the patches can be varied to ensure that at least one antenna is resonant at the center frequency, despite potential tolerance variations in the fabrication. Antennas having patch lengths of 0.091, 0.092, and 0.093 inch are considered. Four instances of each antenna are fabricated to show repeatability of performance for antennas having the exact same geometries. Each antenna is given a serial number based on the length of the patches in the antenna and the instance number. A summary of the fabricated antennas is provided in Table 4-5. A total of 12 two-element arrays are considered for testing.

Table 4-5. List of Fabricated Two-element Arrays

Serial Number	Instance Number	Patch Length (inches)
91-1	1	0.091
91-2	2	0.091
91-3	3	0.091
91-4	4	0.091
92-1	1	0.092
92-2	2	0.092
92-3	3	0.092
92-4	4	0.092
93-1	1	0.093
93-2	2	0.093
93-3	3	0.093
93-4	4	0.093

4.2.2 Eight-element Array Variations

The eight-element array is susceptible to the same relative dielectric constant tolerance variations as the two-element array. Two additional models were created in CST Microwave Studio to simulate the substrate with a relative dielectric constant varying from 2.90 to 2.98. Figures 4-8 through 4-10 show how the resonant frequency changes for the eight-element array as ε_r changes within its specified tolerance limits.

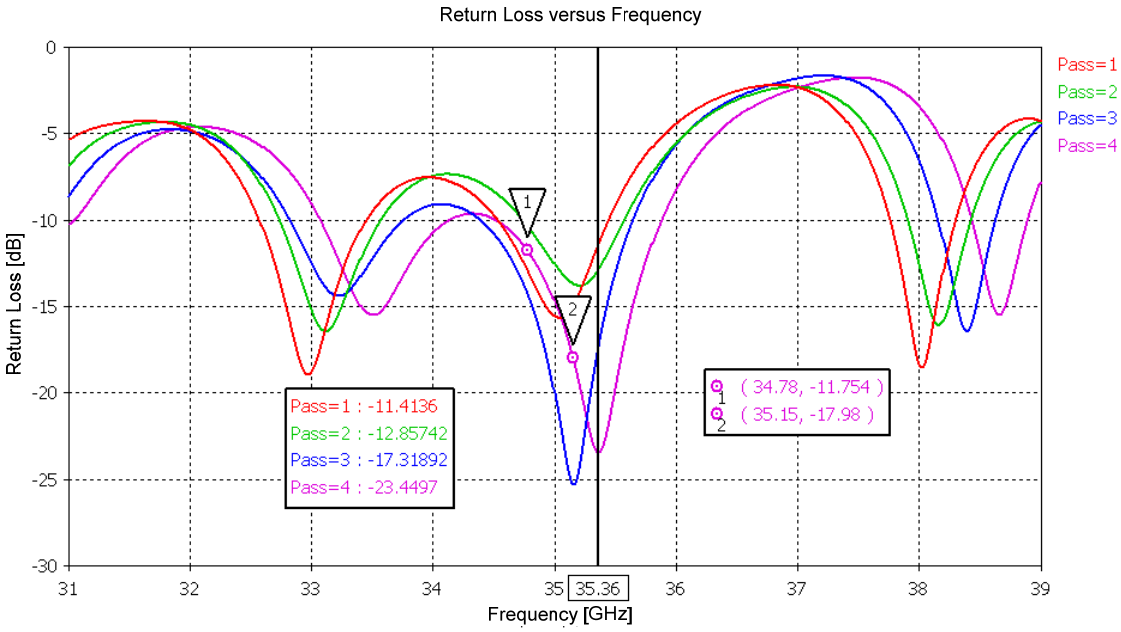

Figure 4-8. Simulated Return Loss for the Eight-element Array Geometry with ε_r = 2.90

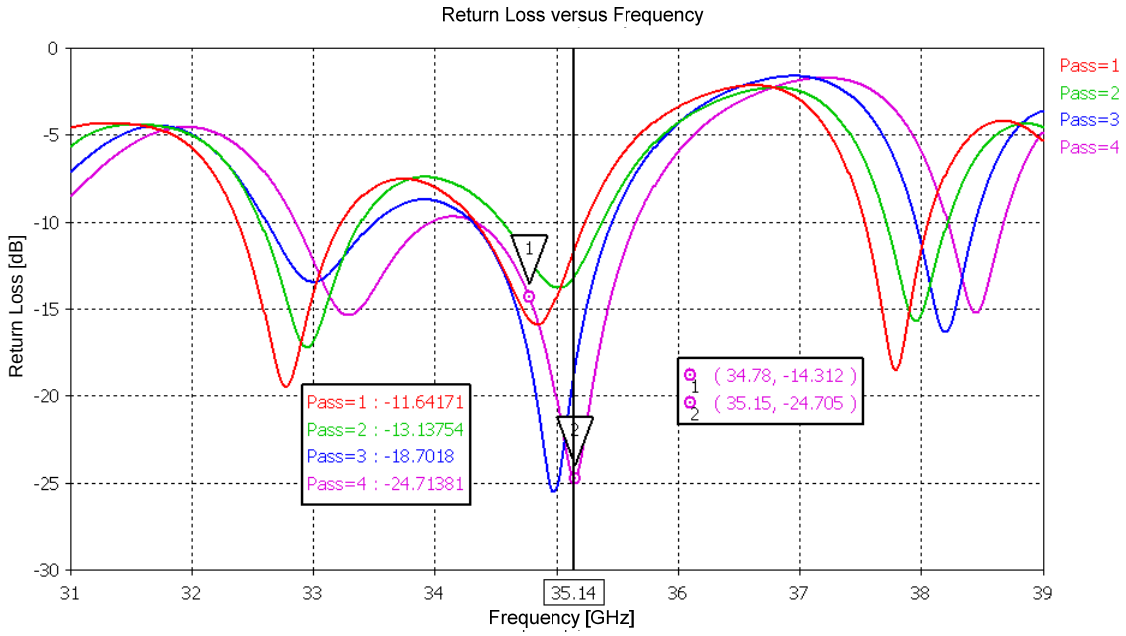

Figure 4-9. Simulated Return Loss for the Eight-element Array Geometry with ε_r = 2.94

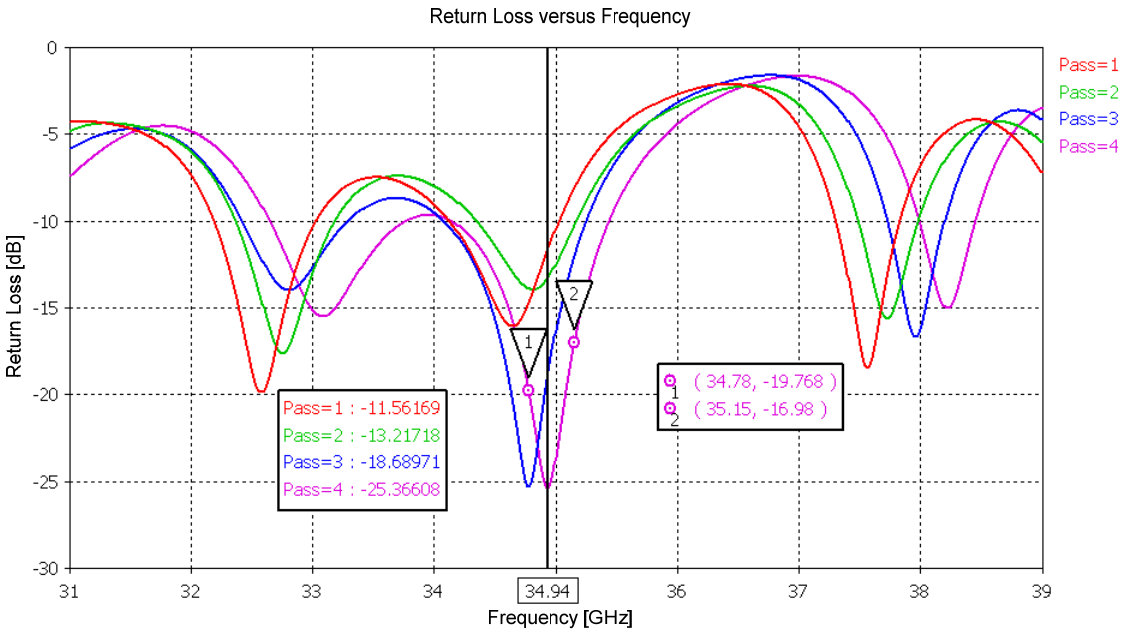

Figure 4-10. Simulated Return Loss for the Eight-element Array Geometry with ε_r = 2.98

Table 4-6 summarizes the resonant frequencies for the low, median, and high values of ε_r.

Table 4-6. Eight-element Array Resonant Frequencies for Low, Median, and High Values of ε_r

ε_r	Resonant Frequency (GHz)
2.90	35.36
2.94	35.14
2.98	34.94

The greatest difference in resonant frequency is 220 MHz for ε_r = 2.90, 20 MHz less than the value obtained from Equation (2-1).

The far-field radiation pattern characteristics at 34.965 GHz are summarized in Table 4-4. There are little differences in the pattern as ε_r varies.

Table 4-7. Eight-element Array Radiation Pattern Characteristics at 34.965 GHz for Low, Median, and High Values of ε_r

	ε_r=2.90	ε_r=2.94	ε_r=2.98
E-plane			
Peak directivity (dBi)	14.8	14.8	14.8
Half power beamwidth	26.6º	26.6º	26.7º
Side lobe level (dB)	-12.5	-12.6	-12.7
H-plane			
Peak directivity (dBi)	13.9	14.1	14.1
Half power beamwidth	45.6º	45.3º	44.9º
Side lobe level (dB)	-27.2	-27.8	-28.3

Instead of varying the length of the patches to adjust for the effects of manufacturing tolerances, the series line path lengths in the eight-element array are varied. Three different variations of the path length may provide enough options to ensure a good return loss if the curvature of the series line cannot be fabricated exactly as modeled. The path lengths are chosen to be 0.094 inch and 0.100 inch (0.097 inch is in the final geometry of Chapter 3). The geometry of the array with series line path lengths of 0.094 inch is shown in Figure 4-11.

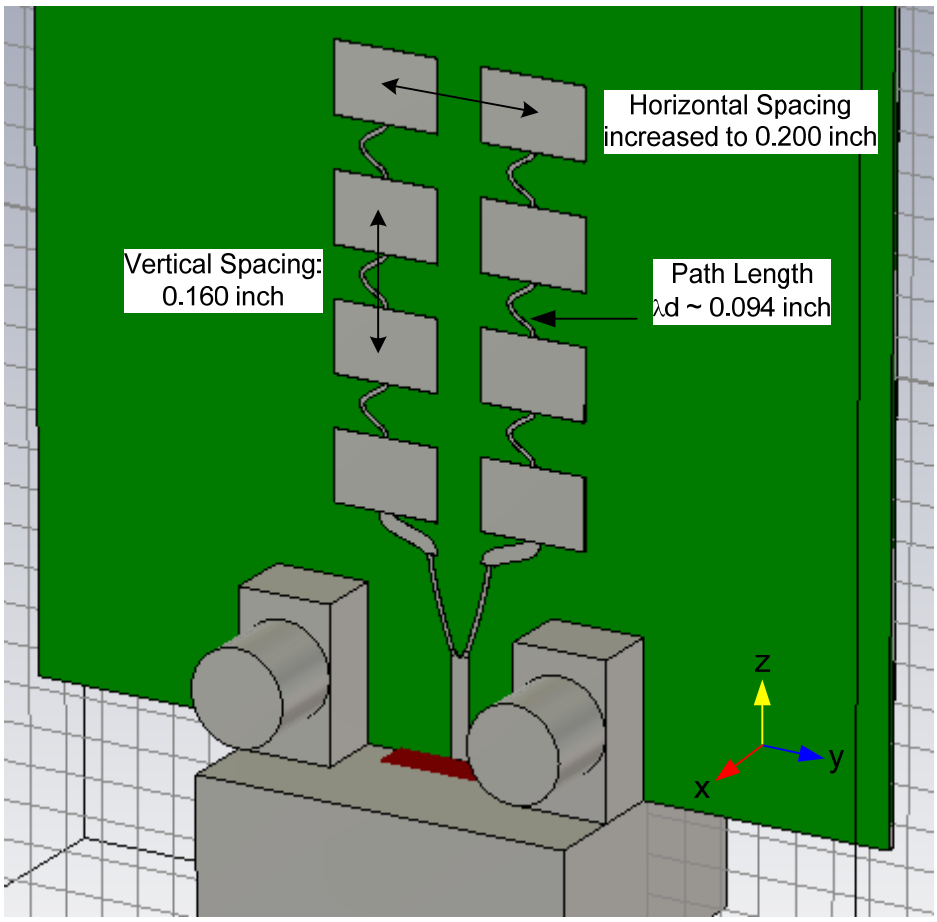

Figure 4-11. Geometry for a Planar Eight-element Array of Microstrip Patches with Series Line Path Lengths of 0.094 inch

Note that the connector board launch design is not included in the model. This is due to memory exhaustion issues in the CST Microwave Studio simulations. In order to simplify the model, the top ground launch and via structures are removed, thereby resolving the memory issue. Because of this, the results are compared to the geometry in Figure 3-31 and not the final eight-element array geometry (Figure 3-34). As shown in Figure 4-12, there is little effect on the resonance caused by such a small change in the series line path length.

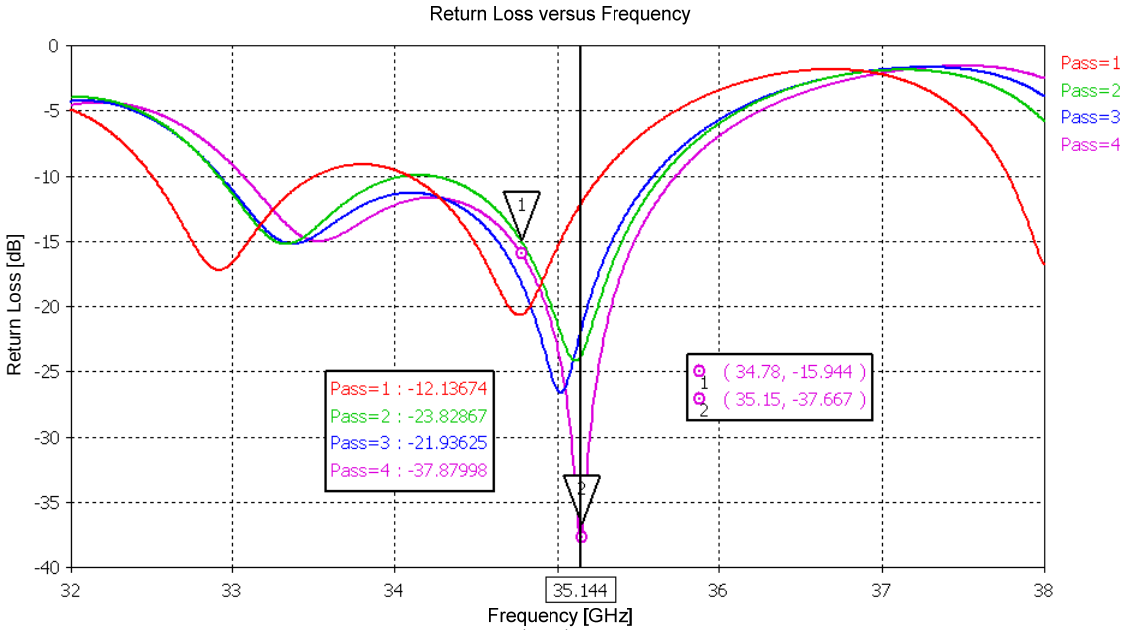

Figure 4-12. Return Loss for an Eight-element Array with Series Line Path Lengths of 0.094 inch and with the Top Ground Launch and Via Structures Removed

Increasing the path length to 0.100 inch is implemented as another variation of the antenna. All dimensions are held constant; only the path length is increased from 0.097 inch to 0.100 inch (Figure 4-13). The corresponding return loss results are shown in Figure 4-14.

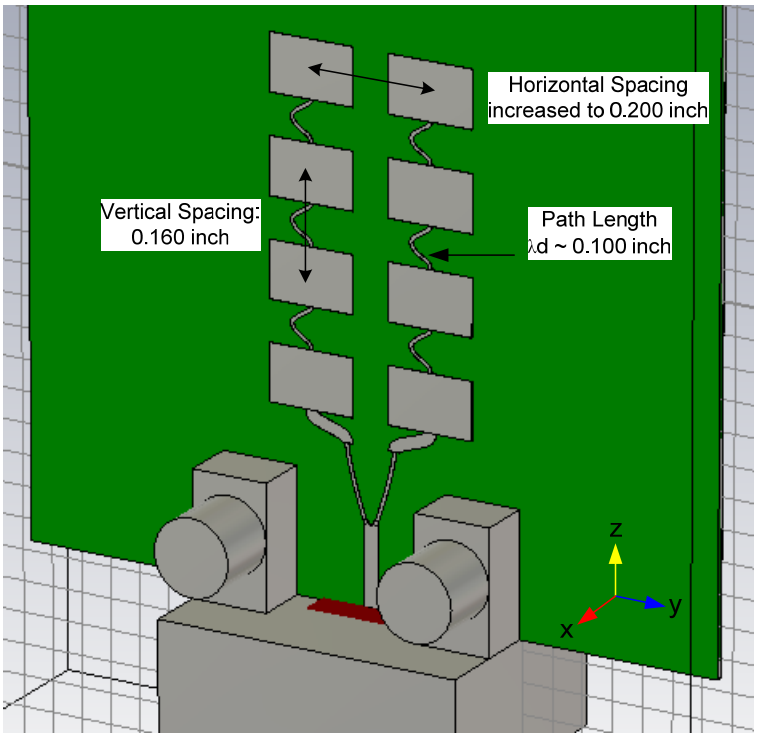

Figure 4-13. Geometry for an Eight-element Array with Series Line Path Lengths of 0.100 inch

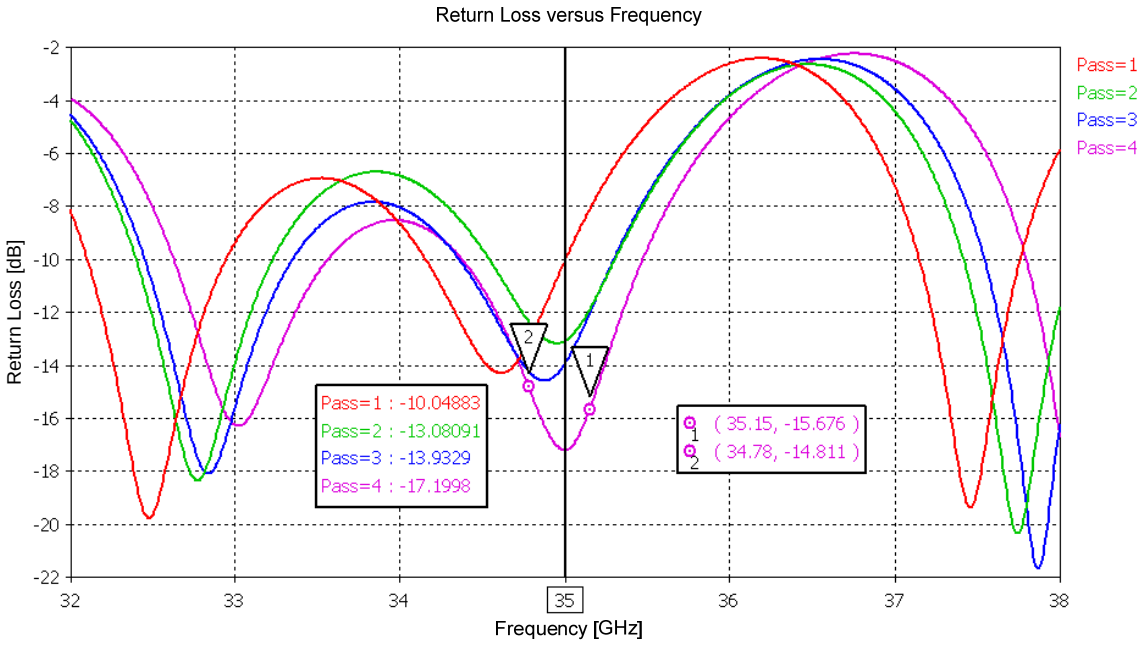

Figure 4-14. Return Loss for an Eight-element Array with Series Line Path Lengths of 0.100 inch

Though the resonance frequency moves to the left by 120 MHz, the return loss is degraded to -17 dB. However, a return loss of -17 dB yields a VSWR of 1.33, and the desired performance is still achieved over the entire band. Table 4-8 summarizes the resonant frequencies for the three variations of path length.

Table 4-8. Resonant Frequencies for the Eight-element Array as Series Line Path Length is Varied

Series Line Path Length (inches)	Resonant Frequency (GHz)	Return Loss (dB)
0.094	35.14	-37.9
0.097	35.12	-24.5
0.100	35.00	-17.2

As expected, the far-field radiation pattern at 34.965 GHz does not change significantly as a result of variations in patch length. E- and H-plane characteristics show subtle (Table 4-9) differences in the directivity, half power beamwidth, and SLL.

Table 4-9. Eight-element Array Radiation Pattern Characteristics at 34.965 GHz as Series Line Path Length Varies

Series Line Path Lengths (inches)	0.094	0.097	0.100
E-plane			
Peak directivity (dBi)	14.9	15.0	14.9
Half power beamwidth	26.2º	26.2º	26.5º
Side lobe level (dB)	-14.3	-14.3	-14.3
H-plane			
Peak directivity (dBi)	14.0	14.2	14.5
Half power beamwidth	43.6º	43.0º	43.0º
Side lobe level (dB)	-29.3	-29.1	-28.6

Four instances of each antenna are fabricated to show repeatability of performance for antennas having the exact same geometries. Each antenna is given a serial number based on the series line path length of the antenna and the instance number. A summary of the fabricated antennas is provided in Table 4-10. A total of 12 eight-element arrays are considered.

Table 4-10. List of Fabricated Eight-element Arrays

Serial Number	Instance Number	Series Line Path Length (inches)
94-1	1	0.094
94-2	2	0.094
94-3	3	0.094
97-4	4	0.094
97-1	1	0.097
97-2	2	0.097
97-3	3	0.097
97-4	4	0.097
100-1	1	0.100
100-2	2	0.100
100-3	3	0.100
100-4	4	0.100

4.2.3 Experimental Characterization of the Antennas

Two critical parameters are measured: the return loss and the far-field radiation pattern. Obtaining a full characterization of the radiation pattern is a lengthy process and it is not practical to complete this task for every antenna. However, the return loss measurement is not as lengthy and can be used in the screening process to determine which antennas get fully measured i.e. antennas with acceptable return loss results are tested further.

4.3 Fabricated Antennas and Test Equipment

Examples of the fabricated low and high gain antennas are shown adjacent to a quarter for size reference (Figure 4-15). A complete list of test equipment used for both the return loss and far-field radiation pattern measurements is given in Table 4-11.

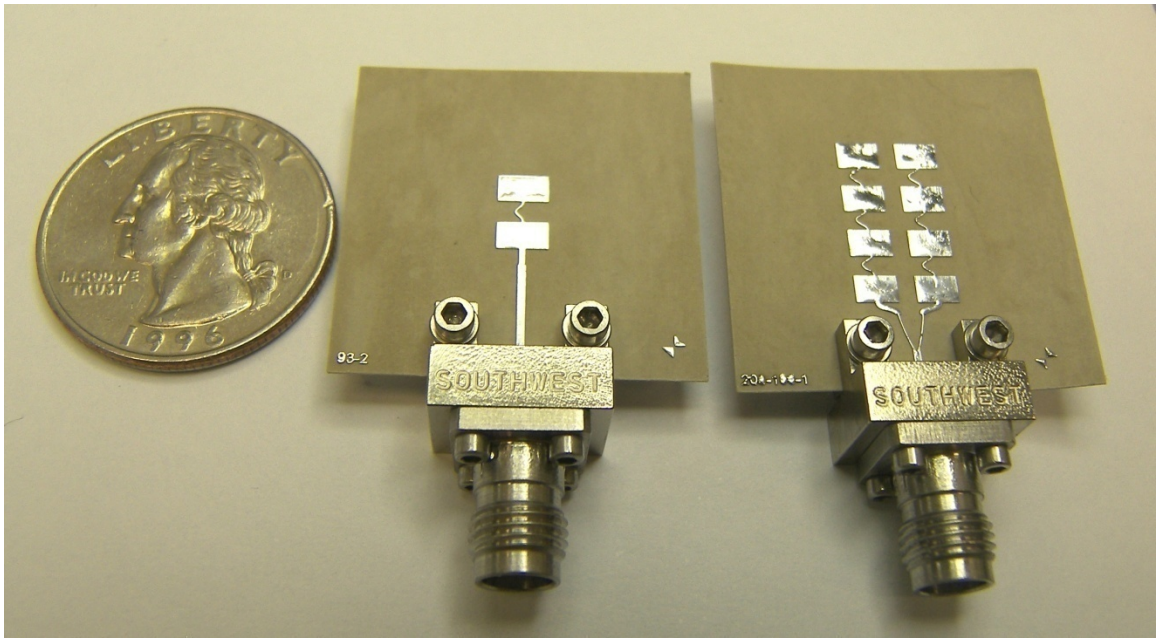

Figure 4-15. Fabricated Low and High Gain Antennas Adjacent to a Quarter

Table 4-11. Test Equipment and Software List

Model No.	Description	Manufacturer
HP 85101C	Network Analyzer	Hewlett Packard (HP)
HP 85102C	IF Detector Unit	Hewlett Packard
HP 8516A	S-Parameter Test Set	Hewlett Packard
HP 83621B	Synthesizer Sweeper	Hewlett Packard
HP 8722ES	S-Parameter Network Analyzer	Hewlett Packard
83051A	Preamp 45 MHz – 50 GHz	Agilent
AL-4370-1	Azimuth over Elevation Positioner	ORBIT/FR

Model No.	Description	Manufacturer
AL-4806-3A	Positioner Controller and PCV	ORBIT/FR
TX28-1A	Source Horn Antenna	CMT
TX28-1A	Calibration Horn Antenna	CMT
959 Spectrum	Antenna Measurement Workstation	ORBIT/FR
DataPro	Antenna Presentation and Analysis Package	ORBIT/FR

4.4 Return Loss Measurements

The HP 8722ES 50 MHz-40GHz S-Parameter Network Analyzer is used for all return loss measurements. Before data is recorded, the instrument is calibrated with the 2.4 mm calibration kit for a single port S_{11} calibration using a swept frequency span of 35.0 GHz ±2 GHz. The reference plane for the return loss measurement is where the coaxial cable from the network analyzer ends and the input connector to the antenna under test begins (Figure 4-16).

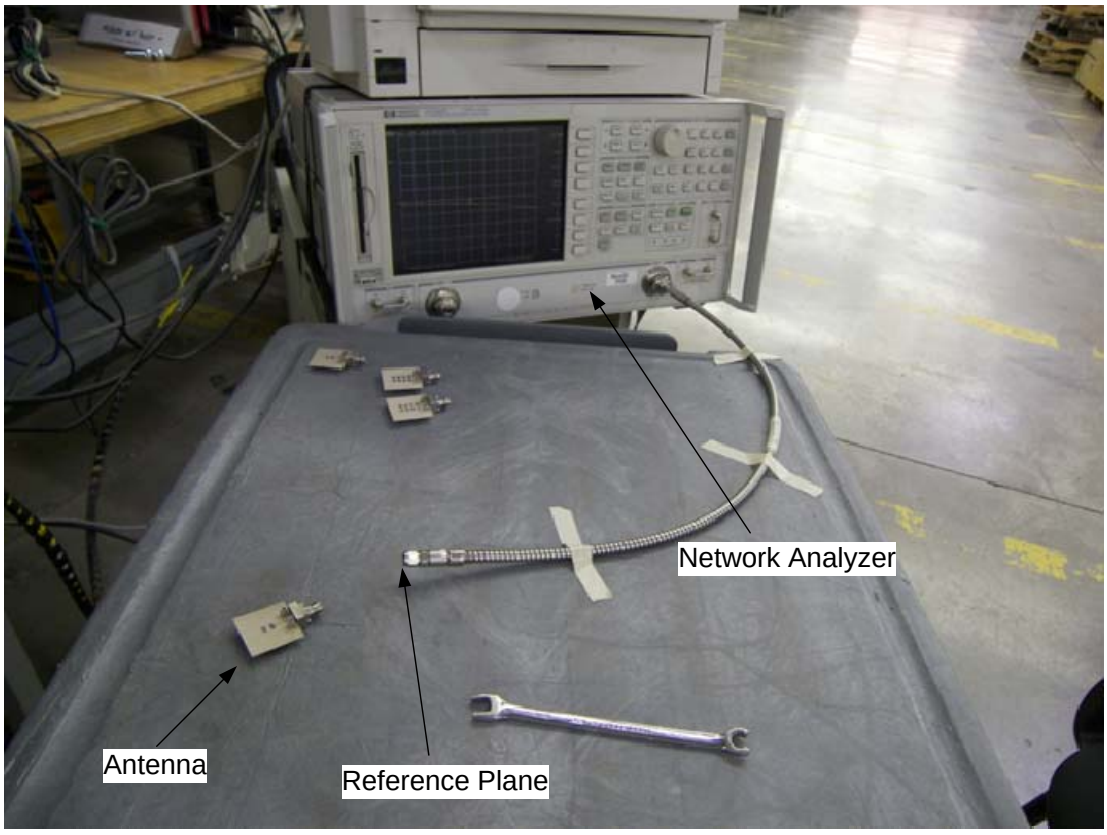

Figure 4-16. Return Loss Test Setup Showing the Network Analyzer, Coaxial Cable, and Antenna

For the first screening of antennas, the center pin of the coaxial connecter is not soldered to the input microstrip line (Figure 4-17). The reason for this is because there are fewer connectors available than there are antennas; hence each connector has to be re-used on multiple antennas every time a measurement is made.

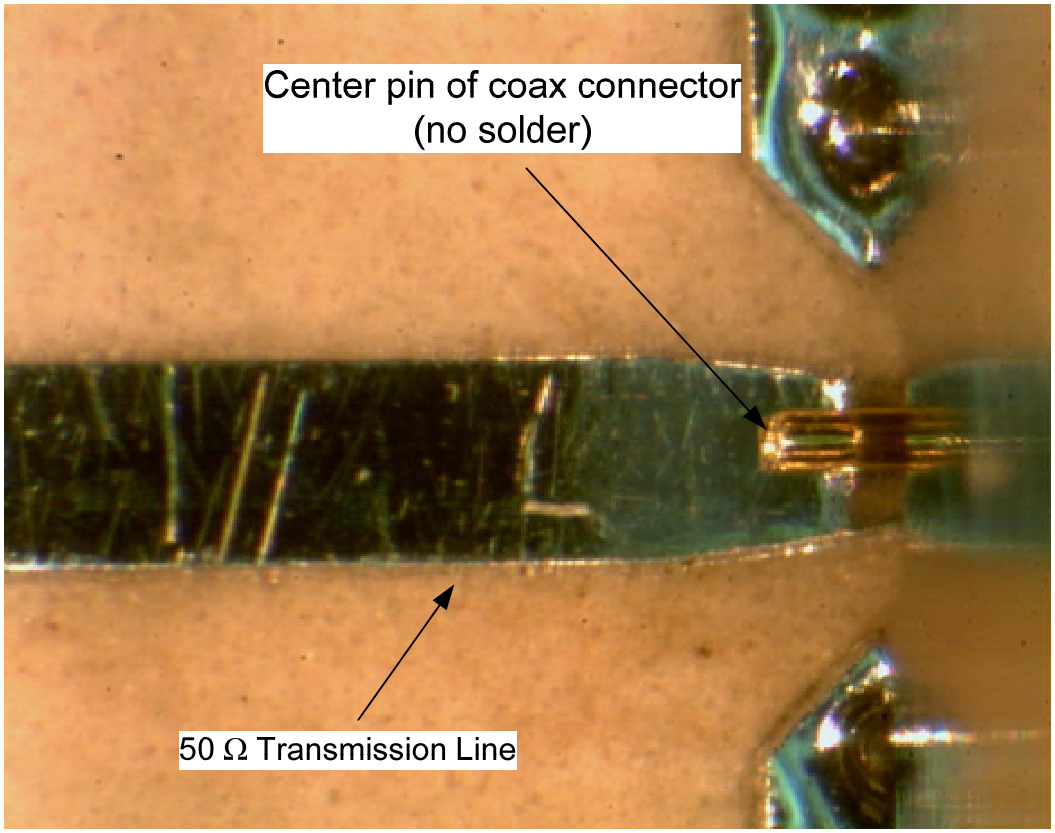

Figure 4-17. Coaxial Connecter Launch to Microstrip Line with No Solder

4.4.1 Two-element Array Return Loss Measurement (No Solder)

The return loss measured for all 12 two-element arrays listed in Table 4-5 is shown in Figure 4-18.

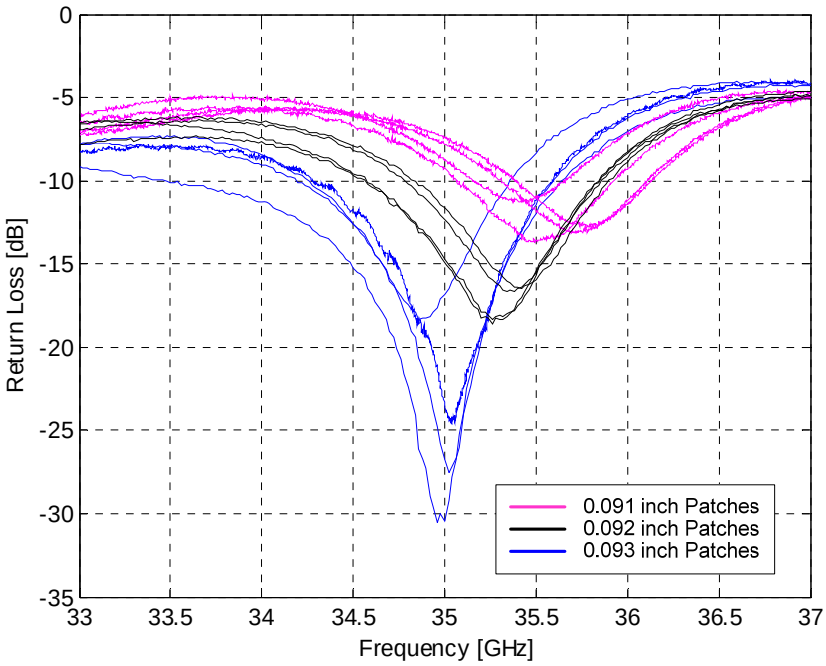

Figure 4-18. Measured Return Loss for 12 Two-element Arrays (No Solder)

The measured antennas that exhibit the best return loss (-18 dB and lower) and have a resonant frequency closest to the design frequency of 34.965 GHz consist of patches of length 0.093 inch. Antennas with patches of length 0.093 inch exhibit a resonance frequency close to that of the modeled antenna with patches of length 0.092 inch even though the antennas with patches of length 0.092 inch were expected to have a resonance frequency close to that of the modeled antenna with patches of length 0.092 inch. One explanation for the difference in resonance frequency between the simulated and measured antennas having patch lengths of 0.092 inch is that the copper layer is fabricated at the maximum allowable tolerance of ±0.001 inch, and hence the 0.092 inch version of the antenna is not truly 0.092 inch. If this is the case, then the antenna with patches of length 0.093 inch would actually consist of patches of length 0.092 inch, and this would explain the difference in resonance frequency between the simulated and

measured results. Given the capability, the length of the patches could be measured with a very accurate measurement device such as a Toolmaker Microscope and micrometer to either prove or disprove this theory. The inspection of the patch length is further discussed in Chapter 6 (Future Work). Figure 4-19 presents a comparison of the measured and simulated return loss for the 0.092 inch and 0.093 inch versions of the antennas. A difference of nearly 500 MHz in the resonance frequency exists between the measured and simulated results.

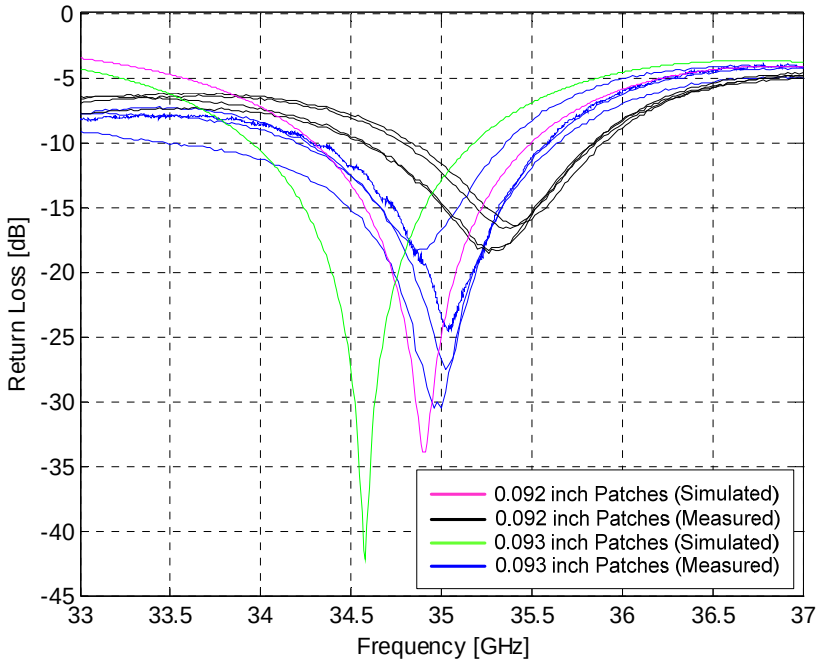

Figure 4-19. Comparison of Simulated and Measured Return Loss for Two-element Arrays (No Solder)

Another explanation for the difference between the simulated and measured results may be the relative dielectric constant tolerance value as discussed in Section 4.2.1. According to the simulated results, if ε_r is lower than its median value the resonant frequency will shift by as much as 210 MHz from the expected value. This also

partially accounts for why all 12 of the antennas have resonant frequencies almost 500 MHz higher than anticipated. The relative dielectric constant of the material can be measured if planned into the design and will be incorporated into future revisions of the antenna panel to determine if variation of ε_r is indeed a cause of the shift in resonant frequency. More details on measuring the relative dielectric constant are provided in Chapter 6.

The workmanship of the manufacturer is also noted as being a potential source of measurement deviation from the model. The substrate material on which the antennas are fabricated is very thin, and is bowed and bent possibly due to handling. This may or may not affect the return loss performance. There is also a noticeable non-uniformity in the plating of the copper layers. The boards are fabricated with a 0.0007 inch copper thickness (the same thickness modeled in CST Microwave Studio), however the antenna manufacturer applies a nickel-tin layer of plating on top of the copper. The plating on all the antennas is not uniform. An example illustrating the non-uniformity of the plating on the copper patches is shown in Figure 4-20.

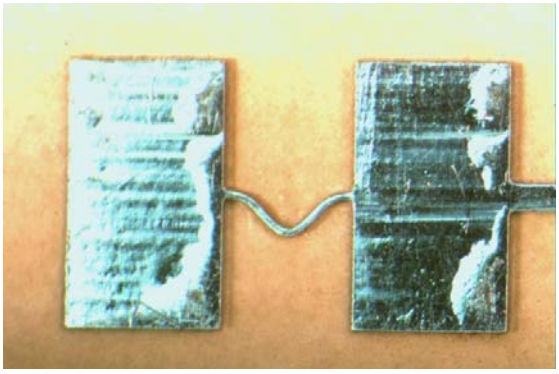

Figure 4-20. Microscope View of the Non-Uniform Plating on Top Layer Copper Structures

A larger copper thickness is implemented in CST Microwave Studio and the return loss results are compared to those from a model with the designed 0.0007 inch thickness of copper. The return loss for a geometry with 0.0014 inch thick copper and patches of length 0.093 inch is shown in Figure 4-21.

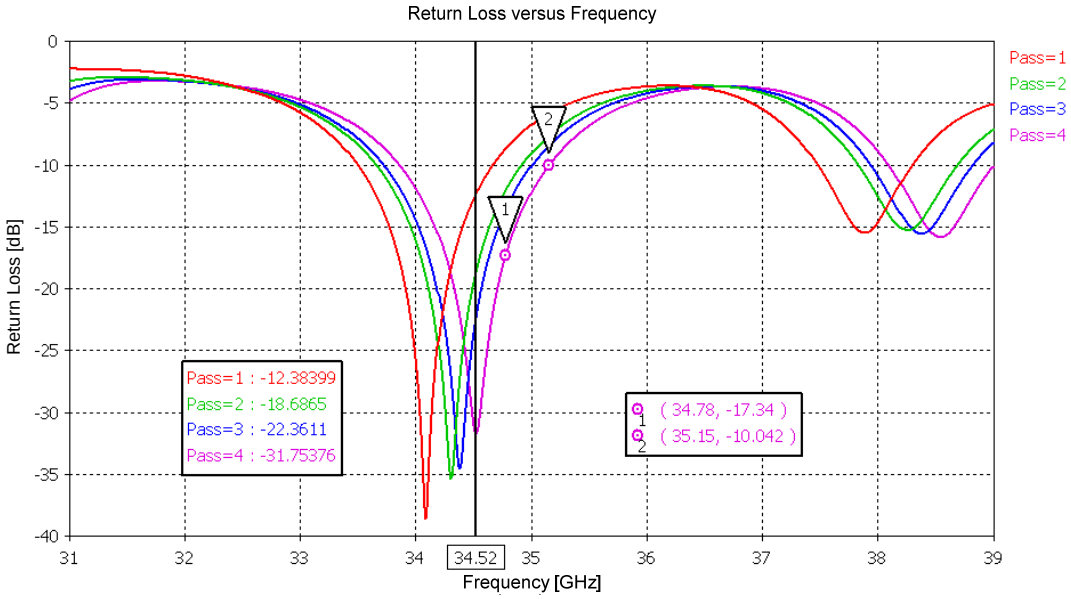

Figure 4-21. Return Loss for a Two-element Array with Thicker Copper (0.0014 inch) Layers and Patches of Length 0.093 inch

The resonance frequency changes slightly from 34.56 GHz (Figure 4-4) to 34.52 GHz in the case of thicker copper. In addition to the small change (only 40 MHz), the shift in resonance is also in the opposite direction to that observed in the measurements. Based on this, it is unlikely that the non-uniform plating is the reason that the resonant frequency is off the mark.

The antennas having patches of length 0.093 inch are used for further testing as they show the best return loss results. Figure 4-22 shows the measured return loss for the 4 two-element array instances. The resonant frequencies are all to within 250 MHz

(0.7%) of each other. Antennas 93-1 and 93-2 are chosen for full radiation pattern characterization.

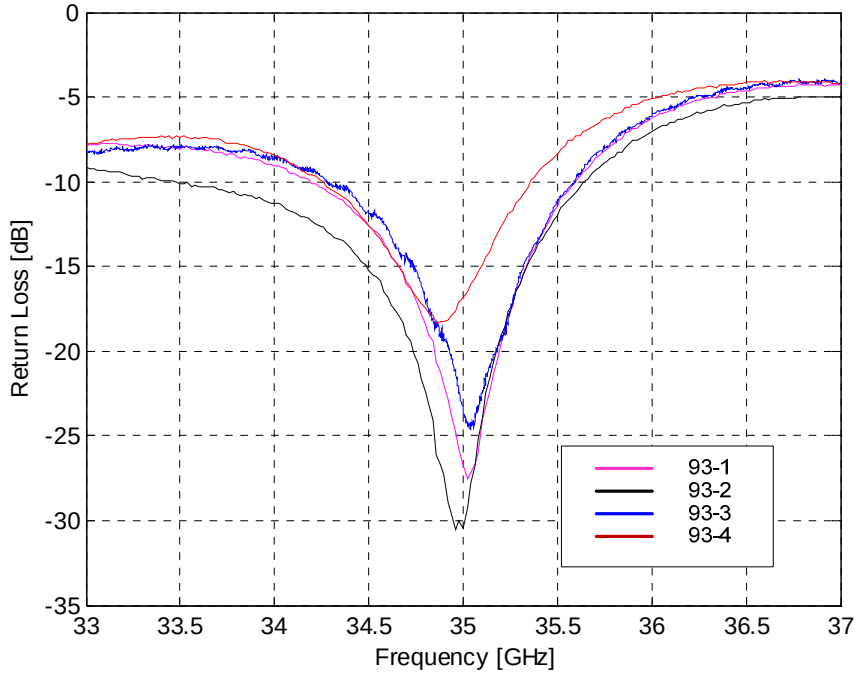

Figure 4-22. Measured Return Loss for 4 Instances of Two-element Arrays with Patches of Length 0.093 inch (No Solder)

4.4.2 Eight-element Array Return Loss Measurement (No Solder)

The return loss measured for the 12 eight-element arrays is shown in Figure 4-23.

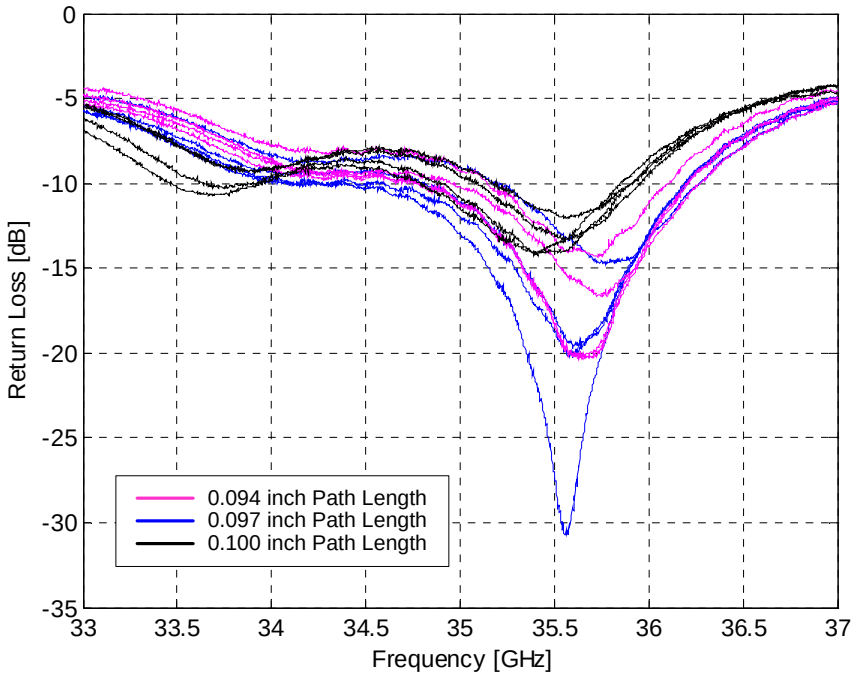

Figure 4-23. Measured Return Loss for Eight-element Arrays (No Solder)

The antennas with the best return loss consist of those with series line path lengths of 0.097 inch; however, these antennas are resonant at a frequency 500 MHz higher than the design frequency of 34.965 GHz. The same shift in resonance seen in the two-element array is also observed in the case of the eight-element array. The simulated data is compared to the measured data of 4 of the antennas (Figure 4-24). The simulated and measured differences in resonance frequency may be evidence of a manufacturing feature. Comparing only the measured 0.097 inch path length arrays to one another shows a variation to within 0.7% of resonance (250 MHz).

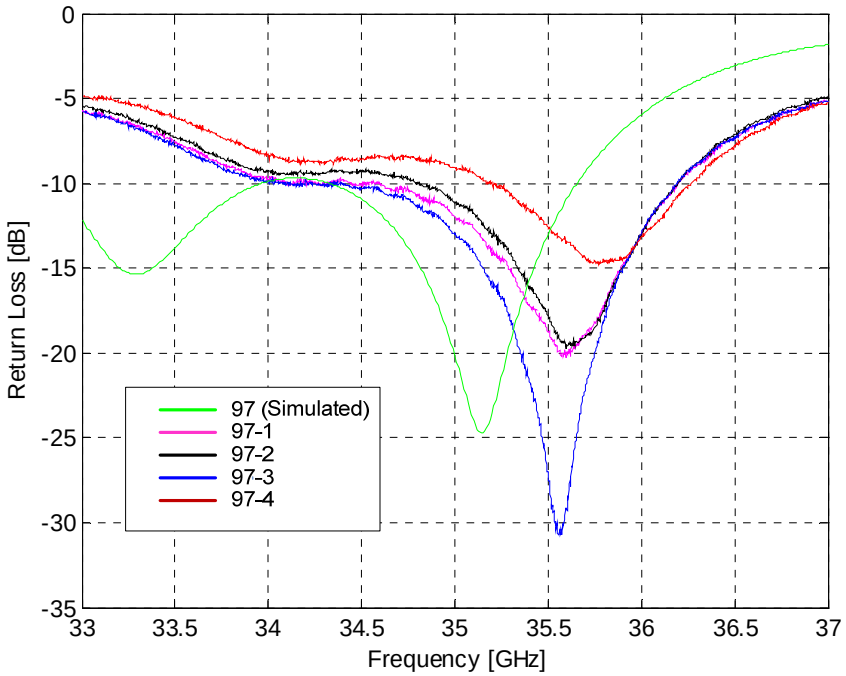

Figure 4-24. Measured Return Loss for 4 Instances of Eight-element Arrays (No Solder) Compared with Simulated Results

Two of the antennas having series line path lengths of 0.097 inch are used for further measurements, as they showed the best return loss results (-20 dB and -30 dB). Antennas 97-1 and 97-3 are used for full pattern characterizations.

4.5 Far-field Radiation Pattern Measurements

Azimuth cuts (two-dimensional patterns sweeping ϕ) are obtained at elevation angles θ ranging from -40° to +80°. The antenna under test is mounted on the AL-4370-1 Antenna Positioner (Figure 4-25). The source antenna, model number TX28-1A, is positioned along a wooden arch to set the elevation to the desired angle (Figure 4-26). When initiated, the source antenna begins transmission at the programmed frequencies and rotates the antenna under test 360º in the azimuth direction (Figure 4-27). A software

package consisting of both measurement software (959 Spectrum) and analysis software (DataPro) is provided with the Antenna Positioner from ORBIT/FR and records the relative gain from the antenna under test as a function of the azimuth position.

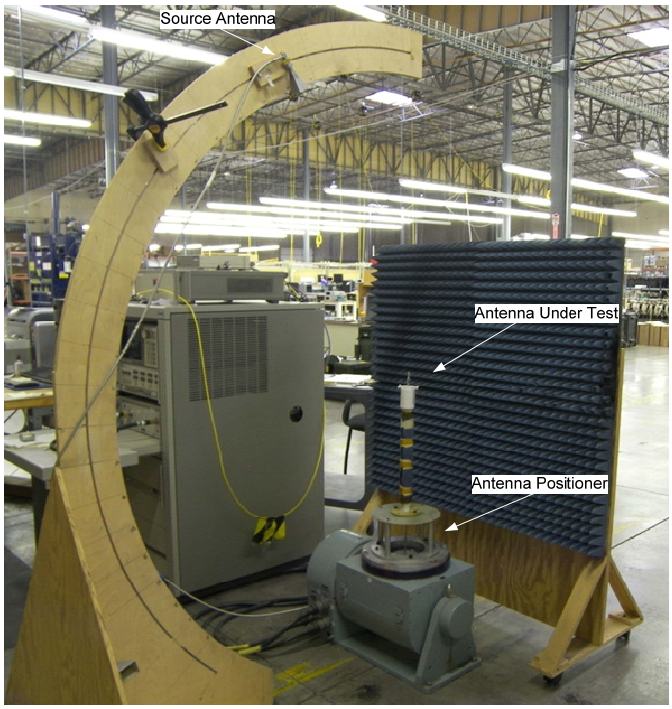

Figure 4-25. Radiation Pattern Test Setup Showing the Source Antenna, Antenna Under Test, and Antenna Positioner

Figure 4-26. Source Antenna Mounted on the Wooden Arch at $\theta = 60^{o}$

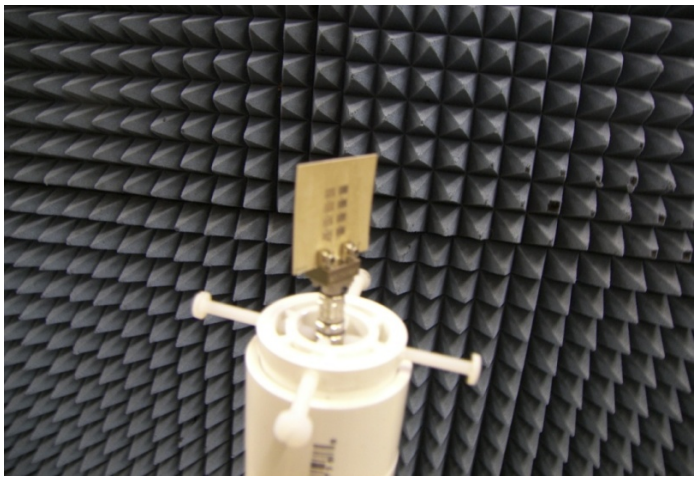

Figure 4-27. Antenna Under Test Held in Position by the Antenna Mounting Fixture

A block diagram of all the test equipment is shown in Figure 4-28.

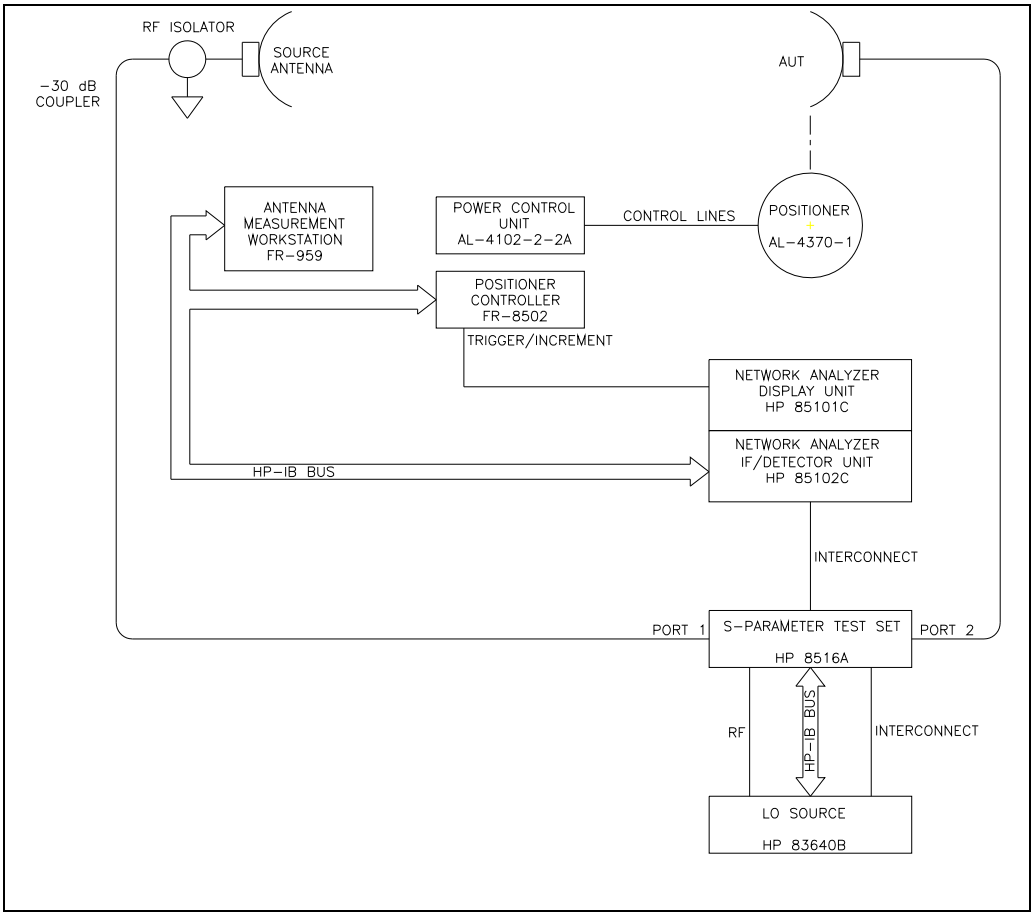

Figure 4-28. Radiation Pattern Test Block Diagram

4.5.1 Calculation of the Far-field

The far-field is the distance at which the magnitude of the field varies by $\frac{1}{r}$, where r is the radial distance from the source to an observation point [1]. An approximate formula for the far-field is given by:

$$r_{ff} = \frac{2D^2}{\lambda} \tag{4-1}$$

where D is the maximum dimension of the antenna and λ is the wavelength in free space. The high gain antenna has the greatest maximum dimension (0.667 inch) and is therefore used in the far-field calculation (Figure 4-29). The far-field, r_{ff} is calculated to be 2.65 inches.

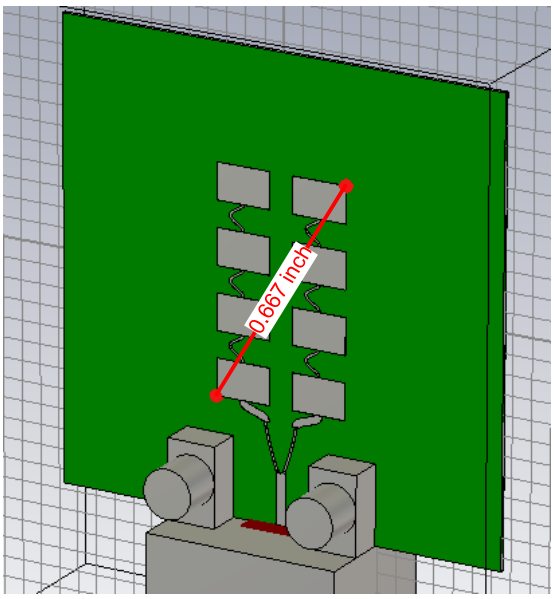

Figure 4-29. Maximum Dimension Used in Far-field Calculation

The distance between the source and test antennas is 41 inches which is also much greater than the free space wavelength and the antenna dimensions; hence the far-field conditions are satisfied.

4.5.2 Two-element Array Far-field Radiation Pattern Measurement

The simulated and measured (Antennas 93-1 and 93-2) three-dimensional radiation patterns at 35.0 GHz are compared for the low gain antenna case with patches of length 0.093 inch (Figure 4-30 and Figure 4-31).

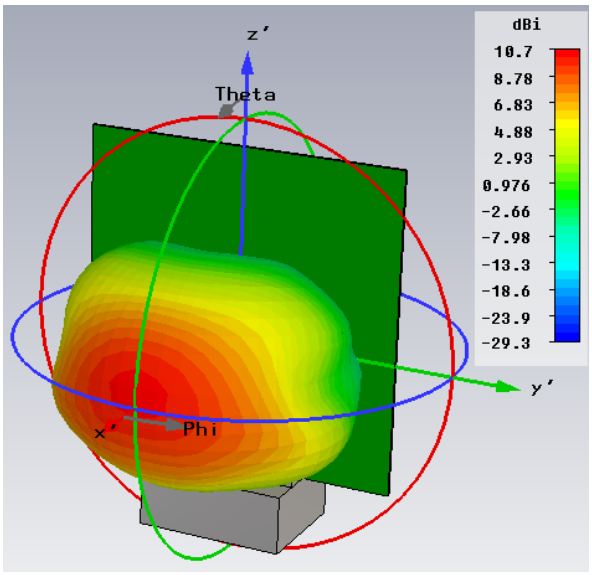

Figure 4-30. Simulated 3-D Far-field Radiation Pattern at 35.0 GHz for the Two-element Array with Patches of Length 0.093 inch

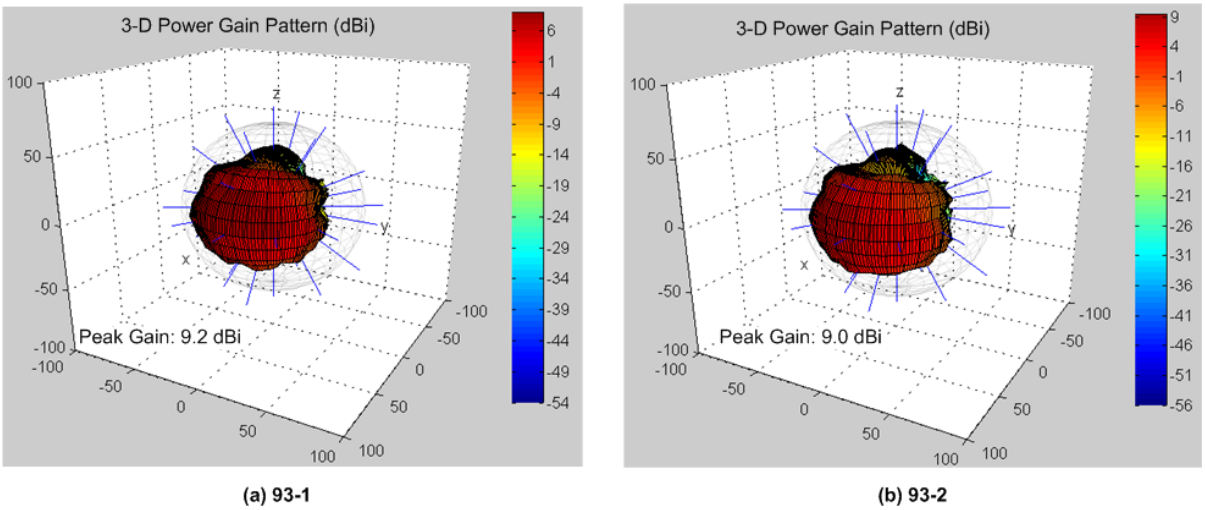

(a) 93-1 (b) 93-2

Figure 4-31. Measured 3-D Far-field Radiation Patterns at 35.0 GHz for the Two-element Arrays with Patches of Length 0.093 inch

The simulated and measured patterns have similar overall shapes. However, one clear difference is the peak gain value. The peak directivity obtained in CST Microwave Studio is 10.7 dBi; however copper loss is not taken into account in the modeling. The peak gains (which include all of the losses in the antennas) for the measured antennas are 9.2 dBi and 9.0 dBi, respectively. In order to more closely compare the simulated and measured radiation patterns, the E- and H-plane principal patterns are plotted (Figure 4-32 and Figure 4-33).

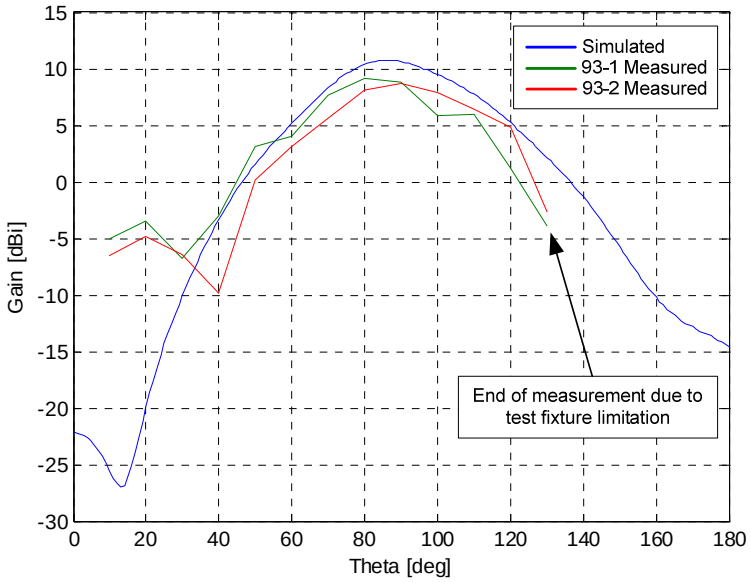

Figure 4-32. Simulated versus Measured E-plane Pattern at 35 GHz for the Two-element Arrays with Patches of Length 0.093 inch

$0° < \theta < 180°$

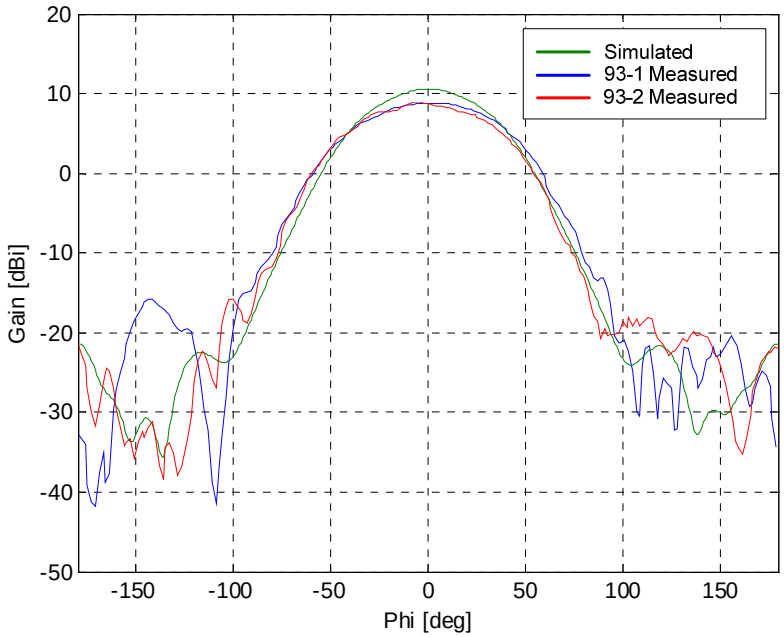

Figure 4-33. Simulated versus Measured H-plane Pattern at 35 GHz for the Two-element Array with Patches of Length 0.093 inch

-180° < ϕ < 180°

For the E-plane patterns in Figure 4-32, it is difficult to make a full comparison because of testing limitations. The range of elevation angles tested is limited by the capability of the test fixture. The E-plane data for the measured antennas can only be obtained within the range of angles θ from 10º to 130º, whereas the full range of θ is 0º to 180º. Also, the test fixture and setup do not accommodate a continuous sweep of θ, but instead pattern information is obtained at discrete points of θ (10º increments in the case of the low gain antenna). The measured results follow the beam shape of the simulated E-plane pattern until the θ = 40º point where a small lobe (SLL = -13 dB) begins to appear in the measured pattern of Antenna 93-1. This same lobe begins to appear at the θ = 30º point for the 93-2 antenna. The side lobe may be the result of the antenna board being slightly bent, as this lobe is not present in the simulated results.

Because of the coarse resolution of the measured E-plane pattern, the half power beamwidths for the 93-1 and 93-2 antennas are approximately measured to be 45º and 43º, respectively.

The H-plane pattern (Figure 4-33) shows very good agreement between the simulated and measured results. Besides the gain being slightly lower (most likely due to losses not included in the model), the pattern shape of the measured antennas follows that of the modeled antenna almost exactly. The 3 dB points for antennas 93-1 and 93-2 occur at about ±37º and ±35º, respectively. Table 4-12 below is a comparison of the half power beamwidths for each antenna.

Table 4-12. Simulated and Measured Half Power Beamwidths at 35.0 GHz for the Low Gain Antenna

	Half Power Beamwidth	
	E-plane	H-plane
Simulated Model	41.8º	60.6º
Antenna 93-1	45º	74º
Antenna 93-2	43º	70º

Though the measured half power beamwidths are greater than those for the modeled antennas, the desired performance of a half power beamwidth greater than 60º is attained.

4.5.3 Eight-element Array Far-field Radiation Pattern Measurement

The eight-element array is characterized in a similar manner to the two-element array and three-dimensional patterns at 35 GHz are obtained for a comparison of the measured resulted to the simulated results. Figure 4-34 and Figure 4-35 show the far-

field radiation patterns for the modeled and two measured high gain antennas, respectively.

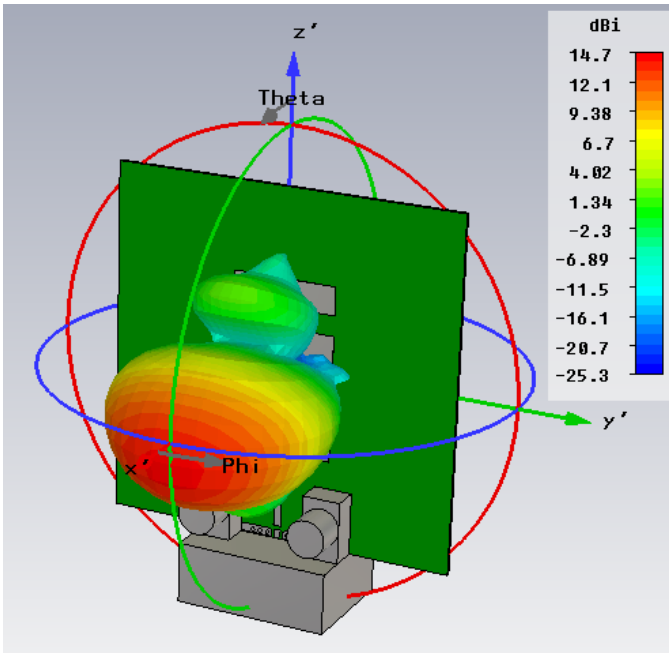

Figure 4-34. Simulated 3-D Far-field Radiation Pattern at 35 GHz for the Eight-element Array with Series Line Path Lengths of 0.097 inch

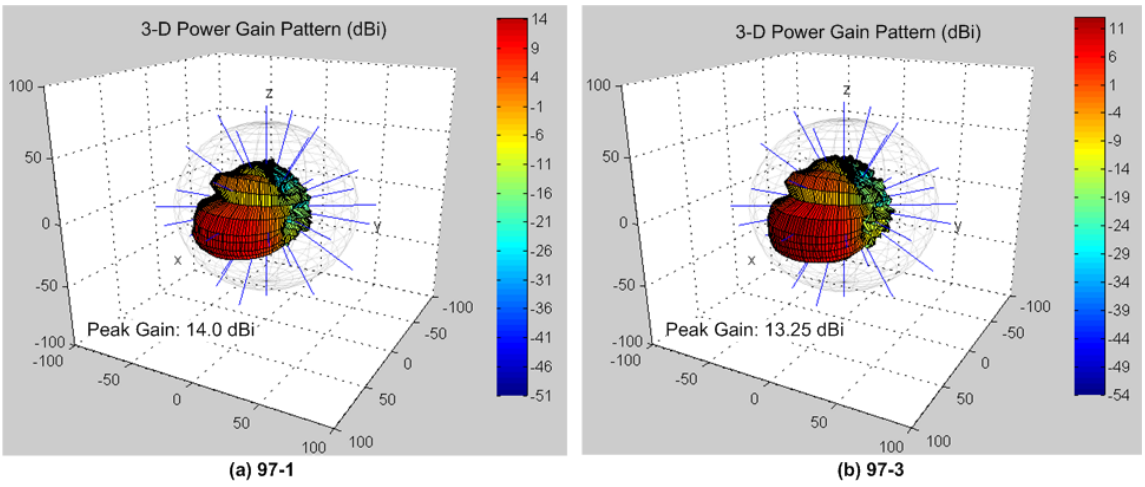

Figure 4-35. Measured 3-D Far-field Radiation Patterns at 35 GHz for the Eight-element Array with Series Line Path Lengths of 0.097 inch

Similar to the low gain antenna, the measured peak gains of Antennas 97-1 and 97-3 (14.0 dBi and 13.25 dBi) are slightly lower than the peak directivity (14.7 dBi) obtained from the simulation. However beam shapes and side lobe locations at approximately θ = 50º to 60º agree. The E- and H-plane patterns are provided in Figure 4-36 and Figure 4-37, respectively.

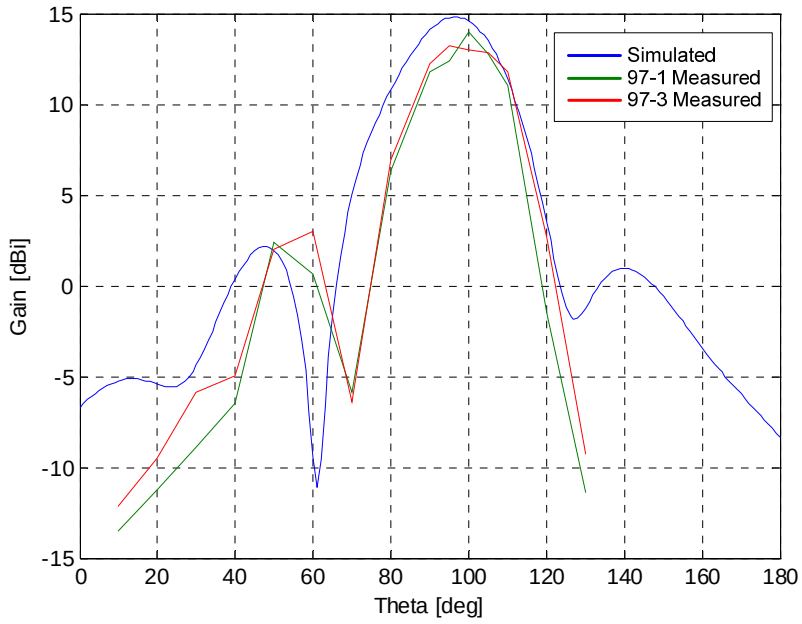

Figure 4-36. Simulated versus Measured E-plane Pattern at 35 GHz for the Eight-element Array with Series Line Path Lengths of 0.097 inch

0° <θ < 180°

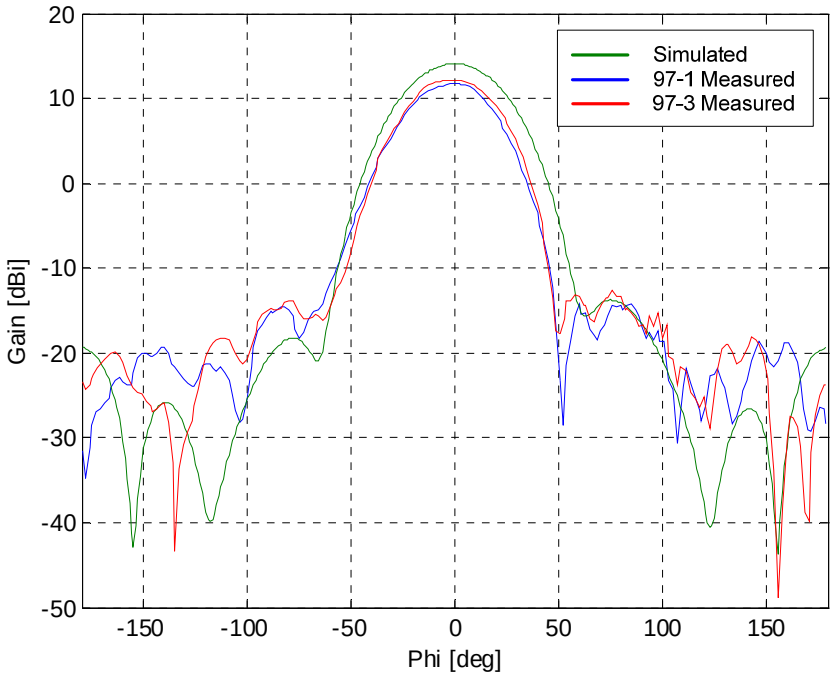

Figure 4-37. Simulated versus Measured H-plane Pattern at 35 GHz for the Eight-element Array with Series Line Path Lengths of 0.097 inch

-180° < ϕ < 180°

The peak gain of the measured E-plane pattern is shifted by about 10º from that of the simulated results. The shift could easily be a consequence of the test fixture because of the way the source antenna mounts on the wooden arch. Small angle deviations can easily result each time the source antenna is moved to a different angle θ. However, the simulated and measured SLLs of the lobe centered near θ = 50º are to within 1 dB. Also, the results for the two measured antennas are very similar, which is a sign that the performance is consistent and repeatable. The half power beamwidth in the E-plane of the antennas measured is approximately 23º and 25º. These values are very close to the half power beamwidth of 26.7º obtained from the simulation.

The H-plane patterns of the measured eight-element arrays also show very good agreement with the simulated results. Again the measured gain is slightly less than expected, but the pattern shape of the measured antennas agrees with that of the modeled antenna almost exactly. The 3 dB points for antennas 97-1 and 97-3 occur at about ±20º and ±20.5º, respectively. Table 4-13 below is a comparison of the half power beamwidths for each antenna.

Table 4-13. Simulated and Measured Half Power Beamwidths for the High Gain Antenna

	Half Power Beamwidth	
	E-plane	H-plane
Simulated Model	26.7º	45.2º
Antenna 97-1	23º	40º
Antenna 97-3	25º	41º

The measured half power beamwidths are less than the simulated values; however the values meet the desired performance characteristics.

4.6 The Effects of Solder on Return Loss Measurements

Once return loss measurements are made on all 24 antennas, and full pattern characterizations are completed on the selected antennas, the center tab of the coaxial end launch connector is soldered to the input microstrip line as shown in Figure 4-38. This is completed on the 4 antennas used for the pattern measurements in order to see if soldering the connector to the microstrip improves, degrades, or has no effect on the return loss measurement.

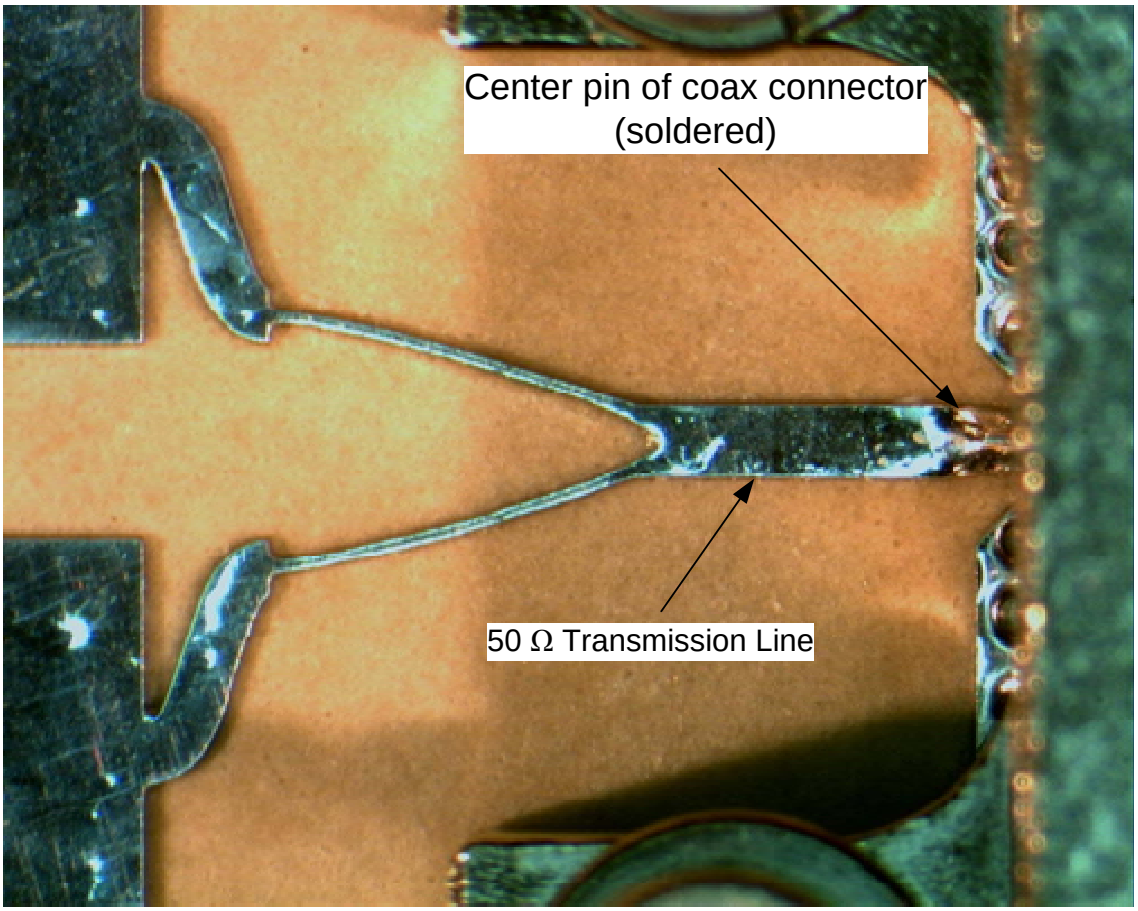

Figure 4-38. Antenna with Center Tab Soldered to the Input Feed Line

Figures 4-39 through 4-42 illustrate the measured return loss before and after soldering for the two low gain arrays and the two high gain arrays. The minimum return loss is increased with solder for the 93-1 antenna, though the results still indicated a good match (less than -20 dB at 35 GHz). The return loss for the 93-2 antenna shows a small decrease in the resonant frequency of about 150 MHz, with no change in magnitude. Overall however, there is no effect on return loss resulting from soldering the connector to the feed line.

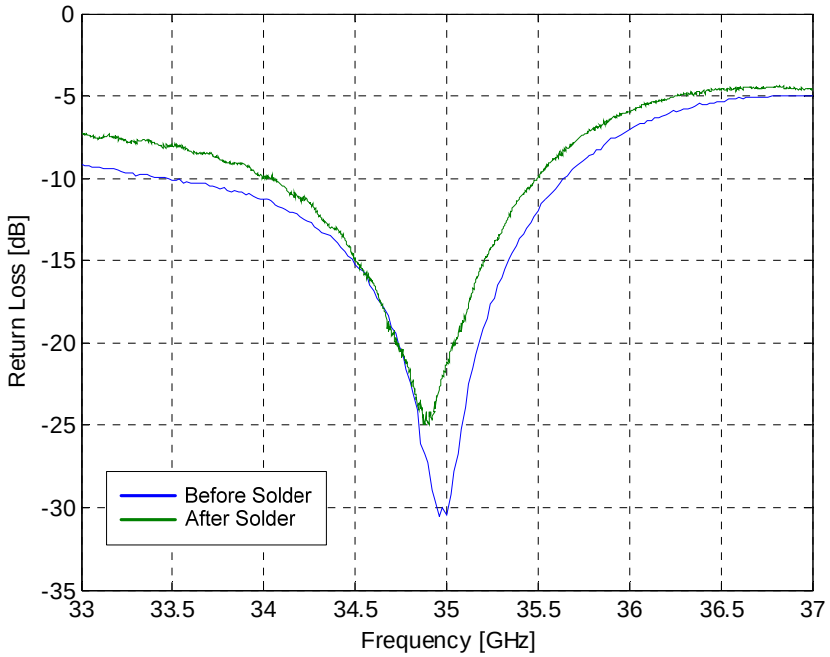

Figure 4-39. Measured Return Loss for the 93-1 Two-element Array (Before and After Soldering of the Connector to the Feed Line)

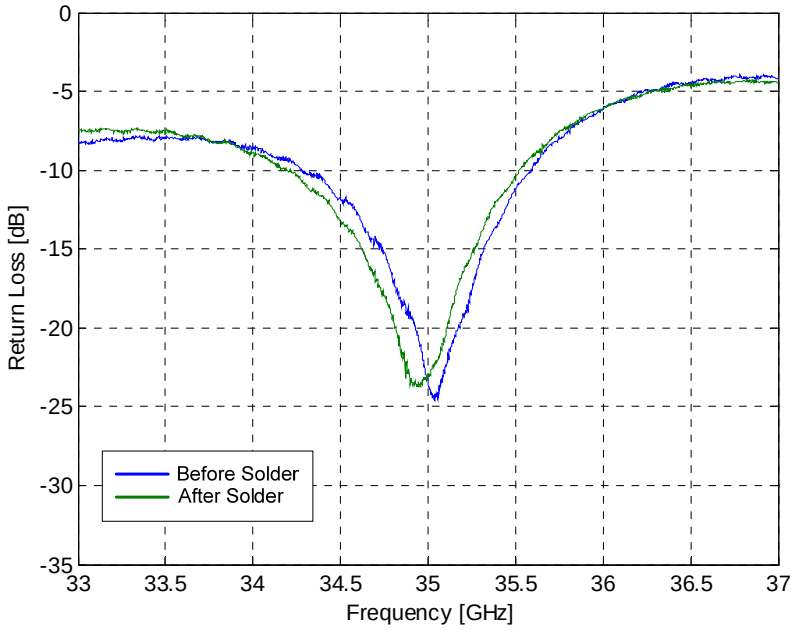

Figure 4-40. Measured Return Loss for the 93-2 Two-element Array (Before and After Soldering of the Connector to the Feed Line)

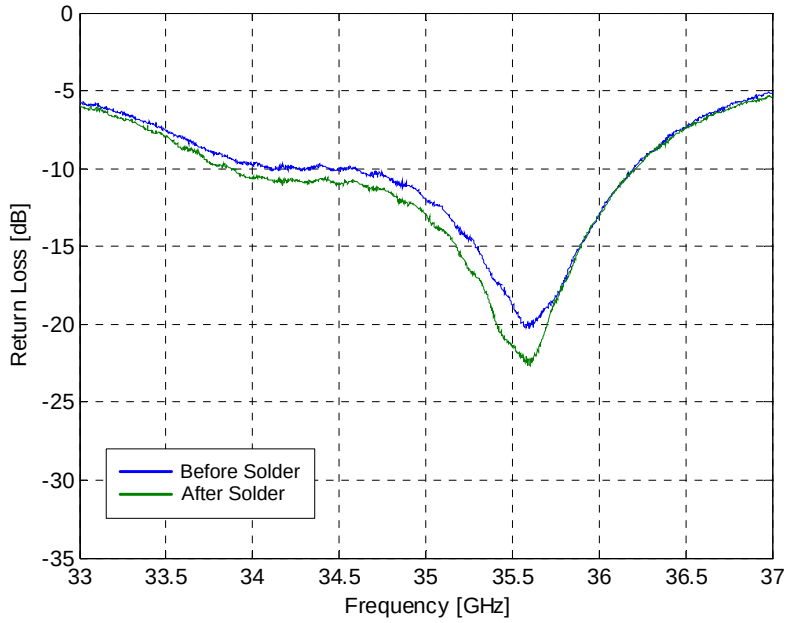

Figure 4-41. Measured Return Loss for the 97-1 Eight-element Array (Before and After Soldering of the Connector to the Feed Line)

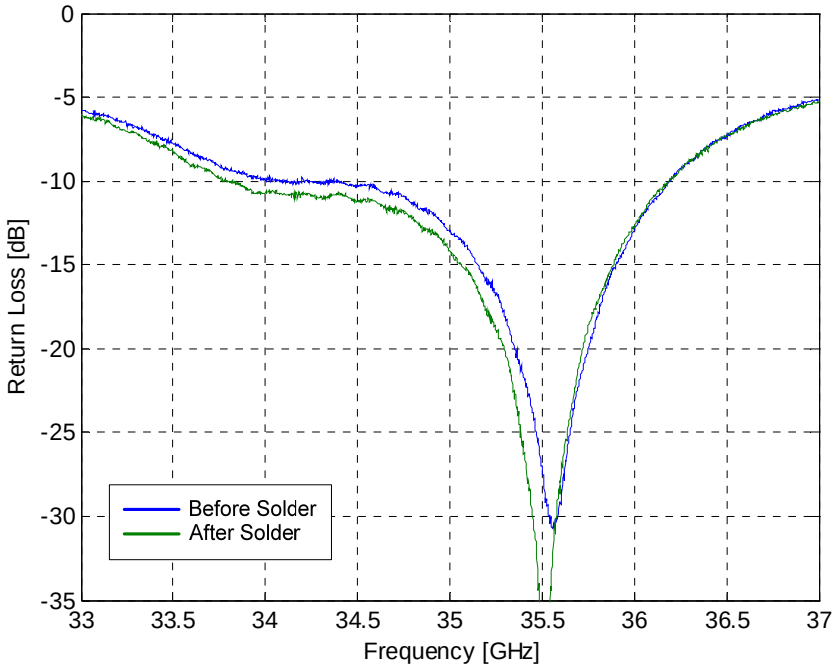

Figure 4-42. Measured Return Loss for the 97-3 Eight-element Array (Before and After Soldering of the Connector to the Feed Line)

Soldering the connector to the feed line actually improved the return loss for both high gain antennas; however there is little effect on the resonant frequency. Although the connector manufacturer states that the use of solder is optional, it does provide a more permanent solution when the antennas are installed on the aircraft and guarantees contact with the feed lines even if the connector is accidentally loosened.

4.7 Conclusion

The simulated two-element and eight-element arrays are fabricated and characterized. In addition to the designed geometries, variations of each array have also been manufactured in order to account for manufacturing tolerance limitations. For the low gain antenna, the two-element array with patches of length 0.093 inch produces the best return loss measured results, although it is a variation of the original design geometry. For the high gain antenna, the originally designed eight-element array with series line path lengths of 0.097 inch yields the best return loss measurements.

Two instances of each antenna type are used for the complete characterization of the far-field radiation pattern. A comparison of the simulated versus measured 3-D and principal plane radiation patterns is completed. Other than gain (or directivity in the case of the model) the measured performance of the antenna is in good agreement with the simulated results.

After all pattern data is obtained, the connectors of the four antennas used for measurements are soldered permanently to the input feed line and the effects on return loss are observed. Though not required by the manufacturer, the use of solder on the connector launch may not necessarily improve return loss performance but it will

eliminate risk of the center tab breaking contact with the feed line if the connector is accidentally loosened.

4.8 References

[1] Roger's Corporation. "RT/duroid®6002 High Frequency Laminates." http://www.rogerscorp.com/acm/products/12/RT-duroid-6002-6202-6006-6010-PTFE-Ceramic-Laminates.aspx.

[2] W.L. Stutzman and G.A. Thiele, *Antenna Theory & Design*, 2nd Ed. John Wiley & Sons, Inc., 1998, pp 28-31.

5 CONCLUSIONS

The detailed design, modeling, and experimental characterization of two types of microstrip patch antenna arrays have been described. Design equations for the microstrip patches and array theory are used to calculate the geometry of the patch array and radiation pattern performance, and a 3-dimensional electromagnetic simulator is used to model, simulate, and optimize the performance of the antennas. Comparisons are made between the calculated and simulated results as well as between the simulated and measured results.

5.1 Low Gain Antenna

The low gain antenna is accomplished using a two-element array of microstrip patches. Initial designs show pattern distortion caused by the corporate feed network. A series feed network is used in the final design to achieve an improved radiation pattern. A 2.40 mm end launch connector is used to feed the array and is proven to have minimal effects on the radiation pattern. Design iterations are modeled using CST Microwave Studio until acceptable results are obtained.

Due to manufacturing tolerance, multiple variations of the final geometry with varying patch length are fabricated. The two-element array with patches of length 0.093 inch yields the best return loss performance and is used for full pattern characterization testing. The testing of two instances is completed, and Table 5-1 compares the measured results to the original desired performance characteristics.

Table 5-1. Low Gain Array Measured Results

	Desired Performance	93-1	93-2
Center frequency, f_r (GHz):	34.965	34.875	34.935
Bandwidth (MHz):	370	805	738
Gain at 0° azimuth, 0° elevation (dBi):	> 4	9.2	9.0
H-plane half power beamwidth:	> 60º	74º	70º
E-plane half power beamwidth:	$30º \leq \theta \leq 60º$	45º	43º
SLL (dB):	< -20	-12.7	-13.8
RF feed VSWR (at 34.965 GHz):	1.5:1 max	1.158	1.143

The resonant frequencies are to within 0.26% and 0.08% of the design center frequency, for the 93-1 and 93-2 antennas, respectively. The bandwidth and gain for both antennas are more than double the specified value. The E- and H-plane half power beamwidths also exceed the specifications. The SLL does not meet the required performance and will be addressed in future work. The VSWR results are well below the maximum allowable value.

5.2 High Gain Antenna

The high gain antenna is accomplished using an eight-element array of microstrip patches. The horizontal spacing between the patch elements is increased from one-half wavelength to approximately 0.6λ in order to increase directivity and the vertical spacing is less than half-wavelength (0.47λ) in order to reduce SLL. A meandered quarter-wave transformer is also implemented to reduce the SLL. Due to manufacturing tolerance uncertainties, multiple variations of the final geometry with different series line path lengths are fabricated. The eight-element array with series line path lengths of 0.093 inch

yields the best return loss performance and is used for full pattern characterization testing. The testing of two instances is completed, and Table 5-2 compares the results of the measured antennas to the original desired performance characteristics.

Table 5-2. High Gain Array Measured Results

	Desired Performance	97-1	97-3
Center frequency, f_r (GHz):	34.965	35.595	35.515
Bandwidth (MHz):	370	842	937
Gain at 0° azimuth, 0° elevation (dBi):	> 14.0	12.21	11.74
H-plane half power beamwidth:	$40^o \leq \phi \leq 50^o$	40º	41º
E-plane half power beamwidth:	$20^o \leq \theta \leq 40^o$	23º	25º
SLL (dB):	< -13	-11.6	-10.25
RF feed VSWR (at 34.965 GHz):	1.5:1 max	1.621	1.536

For the eight-element planar array the measured resonance frequency is shifted higher than the simulated value by 630 MHz (1.8%) and 550 MHz (1.6%) for the 97-1 and 97-3 antennas, respectively. Although this difference is rather high, possibly due to a manufacturing tolerance uncertainty, the tested antennas have a much wider bandwidth than required by the design specification. This results in the measured VSWR at the design center frequency being within 10% of the desired value even with the large shift in resonance. The gain for each antenna is less than the required value and is to be improved in future iterations of the design. The desired E- and H-plane half power beamwidths are achieved. And finally, similar to the low gain antenna, the SLLs are higher than the specified value.

6 FUTURE WORK

6.1 Introduction

A main goal of this project was to determine whether prototype microstip patch antenna arrays would achieve the desired performance to allow for use in radar-based autonomous landing systems. Although many of the performance characteristics are either met or exceeded by the designs described in this thesis, more research, numerical modeling, and experimental testing are required before a production-ready solution is achieved. The work needed to improve the design of the antennas as well as address issues such as production yields and the integration into VTOL aircraft is outlined.

6.2 Patch Length Tolerance Verification

A measurement can be made with a Toolmaker Microscope and micrometer to determine the dimensions of the patches to within an accuracy of ±0.0001 inch. This would eliminate one parameter of uncertainty in the copper layer manufacturing tolerance. Knowing exactly what the reasons are for the difference between the simulated and measured results will allow for design changes that guarantee acceptable performance for all variations of tolerance when the antennas are in full production.

6.3 Dielectric Permittivity Measurement Capability

In the models of both the low and high gain antennas, the relative dielectric constant is a fixed value of 2.94, whereas in the actual antennas, this value can vary from 2.90 to 2.98 because of manufacturing tolerance uncertainty. Measuring the ε_r of each antenna would give insight as to whether the shift in the resonant frequency of the antenna is

caused by variations of ε_r. Accurate measurements can be made using open resonators; however this effort is more expensive than the antennas themselves. Another option is to design future iterations with increased bandwidth so that effects of manufacturing tolerance uncertainties do not impact the return loss over the entire band of operation.

6.4 Method of Board Stiffening

Because the board material is a soft substrate, bending and bowing of the antennas while handling may alter performance and be a cause for the differences between the simulated and measured results. The next revision of the design will increase the rigidity of the board by either adhering the antenna into an aluminum housing or by creating a multi-layer board that provides a rigid backing.

6.5 Integration into the Aircraft

More analysis is required before the antennas can be installed on a VTOL aircraft. Specifically, the mechanical packaging of the antennas and radome enclosures must be defined.